Development of a large scale rooftop PV potential assessment tool

Case study: Municipality of Delft

Josu Etxebarria Azanza

Technische Universiteit Delft

TU Delft

Development of a large scale rooftop PV potential assessment tool

by

Josu Etxebarria Azanza

to obtain the degree of Master of Science

Sustainable Energy Technology

at the Delft University of Technology,

to be defended publicly on Thursday December 12, 2019 at 10:00 AM.

Student number: 4749340

Project duration: March, 2019 – December, 2019

Thesis committee:

Dr. ir. O. Isabella,	TU Delft, ESE - PVMD	Supervisor
Dr. ir. H. Ziar,	TU Delft, ESE - PVMD	Daily supervisor
Prof. Dr. ir. A. Smets,	TU Delft, ESE - PVMD	Internal committee member
Dr. ir. M. Cvetković,	TU Delft, ESE - IEPG	External committee member
Dr. ir. G. Agugiaro,	TU Delft, BK-3DGEO	External committee member

An electronic version of this thesis is available at `http://repository.tudelft.nl/`.

TU Delft

Abstract

Recently, climate action has become a priority in the agendas of every government, and the Netherlands was no exception. Almost 6 months ago, the so-called Klimaatakkord was released. This climate agreement sets ambitious goals to reduce greenhouse gas emissions, such as ensuring that 70% of the electricity comes from renewable sources by 2030 (only 13% does today). Considering that the Netherlands is the 2nd most densely populated country in the EU and that by 2050 95% of the population will live in urban areas it can be predicted that rooftop PV will play a major role, since it occupies no extra space and generates energy next to the consumption points. This project aims to develop a large scale rooftop PV potential assessment tool which can help urban planners, grid operators and homeowners stimulate the uptake of clean solar energy.

In order to build such a tool, the first step was to extract the information of the rooftop surfaces. To do so, a model that uses openly available height point cloud data (AHN3) and cadastral data (BAG) was developed in-house. This model can extract the tilt, orientation, and area of every roof surface on a building. It can do it with an average estimation deviation of -0.02° for tilts and -0.66° for orientations. The area estimation percentage is 80.5% of the total area of the roof, mainly due to data quality issues, while the model takes an average of 5 seconds to extract the roof information of a building.

The second step was to develop a PV yield calculation tool for estimating the potential of the extracted roof surfaces. As computational time is a constraint for large scale PV potential assessment, the Simplified skyline-based method was used. This method was improved by implementing two correction factors, optical airmass and angle of incidence, which can now be applied to surfaces with any tilt and orientation. Consequently, the PV yield calculation tool estimates the energy potential with an average estimation deviation of -6.64% and takes 2.7 seconds on average per building.

In an effort to prove the application of the developed tool a PV potential assessment was done for the municipality of Delft. The results show that if every rooftop in the city would be covered with the state of the art PV module technology (SunPOWER MAXEON 3 | 400 W), 437.38 GWh could be generated, which represents 81% of the total electricity consumption in 2018. In the case of only suitable rooftops being covered, those with a yield of over 650 kWh/kW and payback time of less than 10 years, 384.81 GWh could be yielded, which could cover up to the 72% of the electricity demand in 2018.

The research made in this project together with the positive findings hope to support in accelerating the transition towards a more sustainable world.

Acknowledgements

After two years and a few months it is time to end up my time as a student of the TU Delft. This period has been by far the most exciting period of my life, in which I have learned so much and made amazing friends from all around the World. My cousin, Julen, was one of the main reasons why I am here today, so I would like to thank him in the first place for encouraging me to come and helping me in whatever I needed.

Secondly, I would like to share my gratitude with my supervisors. Olindo was the one that convinced me to take this project and has provided as much help as I have required, while Hesan has been supporting me every week and pushing me to go that extra mile. Furthermore, I would like to thank Giorgio Agugiaro, Miloš Cvetković and Arno Smets for accepting to join my thesis committee.

My family made this happen and I cannot be more grateful for their love and ever-lasting support.

Finally, a thesis could be compared to a roller coaster, with many ups and downs. These would have not been dealt as well without a strong social circle, this is why I would like to say thanks to the Heineken group and Zamarrans football team for the fun evenings we have spent. But I am specially thankful for having had Carlotta, Leo, Eliora, Marianne, Emilio, Rayen, Senja and Patrycja as office mates, it has been a pleasure! Last but not least, I cannot forget about Mónica, I feel very lucky of having her by my side.

Now, I look forward to starting a job and making an impact in accelerating the energy transition.

Josu Etxebarria Azanza
Delft, December 2019

Contents

List of Figures

List of Tables

1 Introduction

The goal of this chapter is to firstly introduce the motivation of the research project and explain the relevance of PV potential mapping in the energy transition. Secondly, the current market landscape is studied. Finally, the thesis project objectives and outline are stated.

1.1. Motivation

In the past few years, things have changed for good. Finally, Climate Change has been considered a fact rather than a debatable topic. World leaders have agreed that fighting global warming is a top priority and therefore, have gathered to set targets in order to limit the planet temperature increase. The most recent convention is the Paris agreement in 2015, where most of the countries on earth committed to "holding the increase in the global average temperature to well below 2 °C above pre-industrial levels and pursuing efforts to limit the temperature increase to 1.5 °C above pre-industrial levels, recognizing that this would significantly reduce the risks and impacts of climate change" [1].

In an effort to meet those goals, each and every country presented their plans of action to reduce their national greenhouse effect gas emissions. The Netherlands was no exception, the western European country presented its "Klimaatakkord" on the 28th of June of 2019 [2]. This agreement focuses on five main sectors: electricity, built environment, industry, mobility and agriculture & land use. The goals of the four most relevant for this project are stated below:

- **Electricity**: In 2030, 70 % of all electricity will come from renewable sources. This will be done with wind turbines at sea, on land and with solar panels on roofs and in solar parks [2].
- **Built environment**: By 2050, 7 million homes and 1 million buildings will eliminate their natural gas dependence. Thus, insulating and using sustainable heat and electricity. As a first step, the first 1.5 million existing homes must be made more sustainable by 2030 [2].
- **Industry**: By 2050, the industry will be circular and will virtually no longer emit any greenhouse gas. The factories will run on sustainable electricity from the Sun and wind or energy from geothermal energy, hydrogen and biogas. The raw materials will come from biomass, residual flows and gases [2].
- **Mobility**: Mobility in 2050 will be emission-free and of high quality. Electric driving will be important [2].

It can be concluded that electrification is the main strategy towards a carbon neutral country. However, the Dutch energy mix is far from reaching a 70 % renewable electricity. In fact, only 13 % of the electricity consumed in the Netherlands today comes from renewable energy sources [3]. Figure 1.1 shows the energy sources of the Dutch electricity mix.

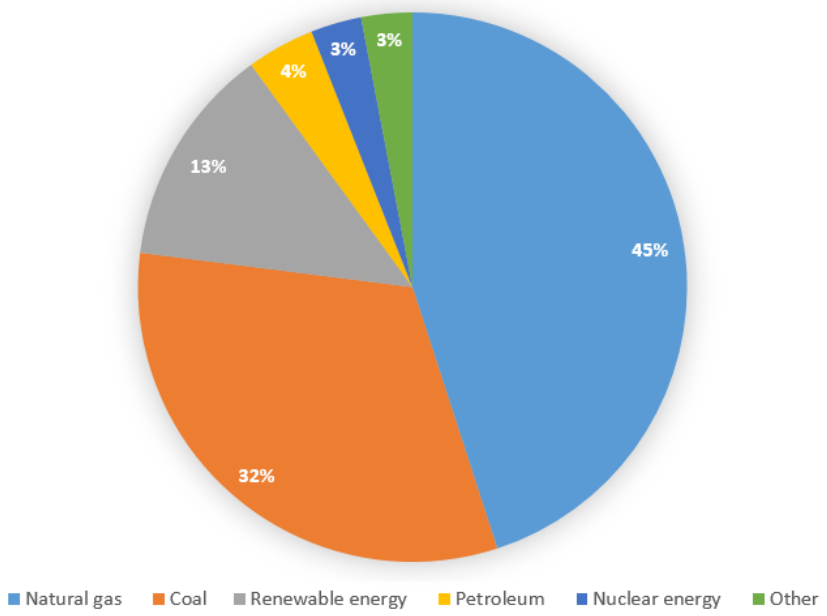

Figure 1.1: Dutch Electricity Mix in 2019 [3].

In order to reach the proposed goals, the Netherlands needs to invest heavily in wind and solar plants. Nevertheless, the Netherlands is a small country with the 2nd highest population density in the EU, only after Malta [4]. Therefore, land use is a delicate matter since energy plants compete with other important sectors, such as agriculture or industry. For this reason, the Dutch government has made clear its intentions to develop off-shore energy plants. A roadmap to reach 11.5 GW of off-shore wind capacity by 2030 was revealed in 2018 [5], while there are still no concrete plans for solar development.

Nonetheless, the government of the Netherlands is aware of the great potential of solar energy. Hence, there is a program for stimulating the growth of this renewable energy source, which offers tax cuts and investment grants to the people that install PV panels, learn more in [6].

Furthermore, the global urbanisation trend is also a reality in the Netherlands. As it can be observed in Figure 1.2, by 2050 over 95% of the population will live in urban areas. This means that the electricity consumption will also shift towards densely populated cities, where it will double due to the electrification of mobility and heating, according to [7].

This highlights the importance of urban energy generation and specifically of roof-top PV, since it is the most appropriate solution.

Urban planners (municipalities) and DSOs (Distributed System Operators) will increasingly require to keep track of the potential PV generation in the built environment, which arises the need of having quality PV potential assessment services.

Future energy systems will be more sustainable but also more complex. Thus, information about the potential energy generation in the different neighbourhoods of the city will become crucial, specially for electricity grid planning. PV potential studies combined with grid infrastructure data

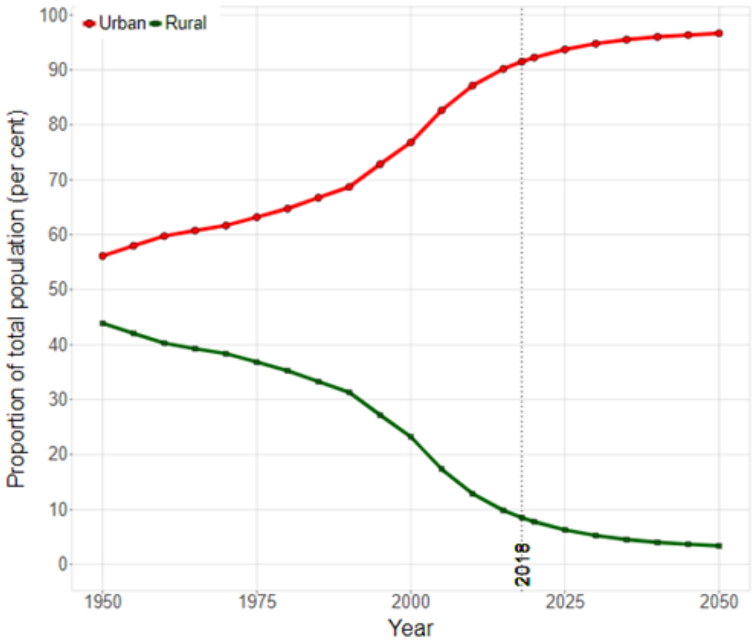

Figure 1.2: Urban and rural population in The Netherlands as a percentage of the total population, 1950 to 2050 [8].

will enable decision makers to see if the hosting capacity of the grid allows further PV installations or if the grid might require upgrades.

Finally, on the consumer side, some of the barriers that slow down the adoption of PV could be taken away by facilitating yield prediction in a quick and user-friendly manner. Consumers would have fewer concerns about the suitability of their rooftop for a PV system. A so-called "quick-scan" algorithm could quickly provide them with a first estimate on these matters, which will bring awareness and incentivise green energy generation.

1.2. Market landscape

In order to determine the uniqueness and relevance of the PV potential assessment tool presented in this report it is important to study the similar solutions available in the market. Two different categories will be analysed, firstly, online yield prediction platforms and secondly, GIS softwares that can calculate the potential of solar energy in the built environment.

1.2.1. Online yield prediction platforms

This subsection introduces the two most similar online yield prediction platforms, both are national open source platforms that predict the yield of buildings using the same data sources as the tool presented in this report.

Zonatlas

This openly available online platform is probably the most complete one. It offers three different maps, the first one shares the PV suitability of each building, the second one illustrates the irradiation impinging in each roof segment of the building and the last one shows the suitable roof surfaces. The maps make use of the highly detailed height data, Actueel Hoogtebestand Nederland

(AHN3), and land register data [9]. With these files a 3D model is made for every municipality in the Netherlands. Then the irradiation and yield are calculated. However, this important part is not explained in their website, which makes it a considerable downside, since the user does not know how the shown values have been calculated.

Regarding the first map, Zonatlas makes a distinction between very suitable roofs (colored green), suitable roofs (colored yellow) and less suitable roofs (colored red) for generating solar energy. Figure 1.3 shows a screenshot of the map. The suitability classification is explained below.

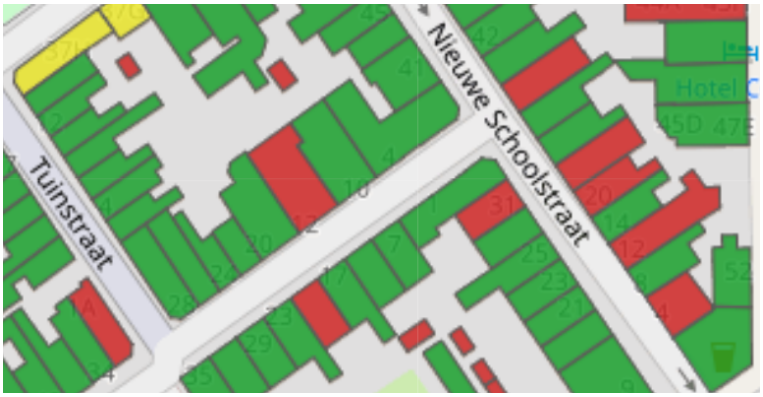

Figure 1.3: Screenshot of Zonatlas website, showing the PV suitability map.

- Green roof: very suitable roof surface. A highly suitable roof surface is at least 11 m² (good for 1.25 kW_p) and has significant annual solar irradiation (at least 85% of the highest irradiation of the region).
- Yellow roof: suitable roof surface. A suitable roof surface is at least 11 m² (good for 1.25 kW_p) and has good annual solar radiation (at least 70% of the highest radiation of the region).
- Red roof: buildings on which - according to the automated calculation based on the available data - less than 11 m² (good for 1.25 kW_p) can be installed or where the solar irradiation is very low, are considered less suitable (less than 70% of the highest radiation of the region). Solar panels on these roofs can have a relatively long financial payback period. It may also be that there is not enough (accurate) data available for the roof, as a result of which a reliable determination of suitability has not been able to be made.

If you click on one specific building you are able to see which parts of the roof receive more irradiation (exactly what is shown in their second map, Figure 1.4) and also learn about the payback period of a potential PV system. Zonatlas only allows 5 building requests from a same computer IP address.

As seen in Figure 1.4, the roof segmentation appears to be quite accurate, nevertheless, the values of irradiation are shown in a scale of low to high, not specifying any values, which is yet another significant drawback.

Lastly, their third map, Figure 1.5, only illustrates the roof surfaces with enough potential, and then within those it differentiates two categories: high sunshine and little sunshine. This map appears to be of little use due to the fact that it does not specify which values correspond to the threshold to consider if a surface is suitable or receives high/little sunshine.

Pico Geodan

This online platform follows the same input data as Zonatlas and the tool presented in this thesis.

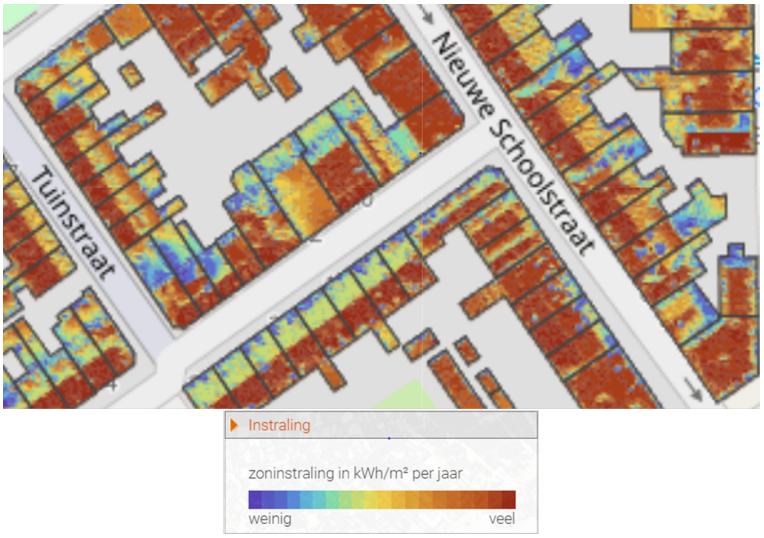

Figure 1.4: Screenshot of Zonatlas website, showing the irradiation map.

Figure 1.5: Screenshot of Zonatlas website, showing the suitable roof surfaces.

Thus, height point cloud and land register data. Nevertheless, Pico Geodan uses AHN2 version of the elevation point cloud data, which is already outdated since it was taken in between 2007 and 2012, compared to AHN3 that was taken in between 2014 and 2019. Regarding the explanation behind their calculations, it is stated that the yield is determined on the basis of the average incoming solar radiation between 1990 and 2010 from weather station De Bilt. This data comes from the KNMI (Koninklijk Nederlands Meteorologisch Instituut). The efficiency of solar panels is set to 16% with a performance ratio of the entire PV system of 85% [10].

Figure 1.6 represents a screenshot of the offered map. It colours buildings in different tones depending on how high their potential PV yield is and it specifies the value of their potential energy generation.

There is no specification of which roof surfaces are the most suitable ones, which together with the outdated height data make this platform less appealing.

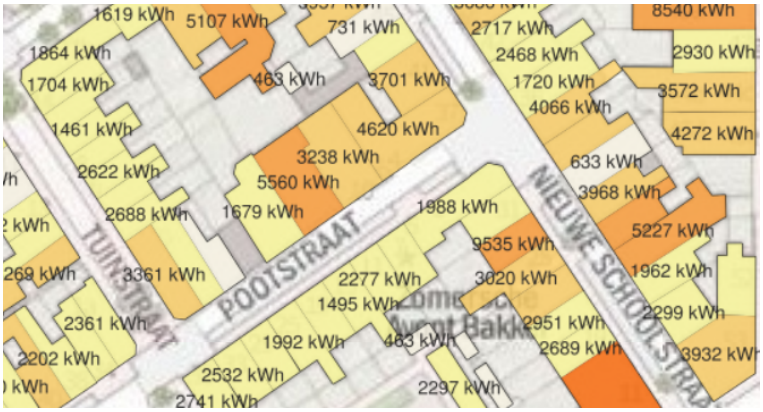

Figure 1.6: Screenshot of Pico Geodan website, showing the PV yield potential of each building.

1.2.2. GIS Softwares

Two of the main GIS softwares capable of calculating the solar irradiation are introduced in this subsection. Their irradiation calculation approach and model are analysed.

GrassGIS-r.sun

When comparing open-source GIS software, GRASS GIS, or Geographic Resources Analysis Support System, is considered to be the best for research [11], but does have a steep learning curve. Tools, with their parameters, need to be inserted in a text format style, which means its not intuitive and requires detailed research for each parameter. With this tool, in Mode 1, a local time can be specified to compute solar irradiance raster maps [W/m2]. In Mode 2, the r.sun tool computes direct (beam), diffuse and reflected solar irradiation for given day [Wh/m^2/day], by integrating the irradiance between sunrise and sunset with a default time step of 0.5 hours. The yield over a longer range of days can be obtained from the r.sun.daily tool. The prefix "r." means the tool can only work with raster data, opposed to vector. In total there are 29 parameters that can be altered across the two modes.

The r.sun tool works within the GRASS GIS environment, so user experience is required. Many parameters need to be determined to provide accurate results. Having obtained these, results are automatically exported into raster maps and can be visualized inside the program.

In the documentation page of [12] it is mentioned that the sky model of r.sun is based on the formulas suggested by Kittler and Mikler (1986). Although this exact work could not be retrieved, Kittler has been linked to the CIE standard sky model [13]. By default, a standard clear sky is considered, but using real-sky radiation (beam, diffuse) coefficients that define the fraction of the reduction by atmospheric factors (e.g. cloudiness). Usually these coefficients can be obtained from meteorological measurement provided as raster maps [12].

The error of r.sun is considered to be below 10% in clear sky conditions, but grows larger in cloudy conditions. Its irradiance model is ranked as the 8th most accurate clear-sky direct irradiance estimation model among the 18 studied radiative models in [14].

ArcGIS-Solar radiation tool

ArcGIS includes a solar radiation tool in its Spatial analyst toolbox. The tool, as most of the features

in this GIS software, is very user friendly. In order to estimate the irradiation, it only needs the digital elevation model (DEM); optionally the sky resolution, the time configuration, topographic parameters and radiation parameters can be configured.

The irradiation calculation methodology consists of firstly a viewshed calculation, which is a raster representation of the entire sky that is visible or obstructed when viewed from a particular location. Secondly, a sun map is calculated, which is a raster representation that displays the position of the Sun as it moves through the hours of the day and through the days of the year. This map is used to later calculate the direct irradiation. Thirdly, a sky map is calculated to represent the diffuse irradiation in every sky sector.

Consequently, both the Sun map and the sky map are overlayed with the viewshed, to estimate the direct and diffuse irradiance respectively. This process is repeated for every location of interest [15].

Reflected irradiation is not included in the calculation of total irradiation. Thus, the total irradiation of the solar radiation tool is calculated as the sum of the direct and diffuse irradiation.

The irradiation model used by this tool is based on methods from the hemispherical viewshed algorithm developed by Rich et al. ([16]) and further developed by Fu and Rich ([17]) [18].

The Fu and Rich model is ranked as the worst one among the 18 radiative models in terms of clear-sky direct irradiation estimation, which is generally proportional to the global irradiance calculation. Moreover, in words of the author of the study "the solar radiation tool of ArcGIS should not be used for serious work, since it is far from accurate" [14].

1.2.3. Conclusions of the market research

In this market research mainly two aspects have been studied, mapping features (online platforms) and irradiation calculation approach and model (GIS softwares).

The online platforms follow a similar approach to one that will be used to extract the roof surfaces in this project. Zonatlas does not show any clearance on how the calculations have been done or if any validation has been carried out. Furthermore, their maps do not show specific values for yield or irradiation. Regarding PicoGeodan, it uses an old version of height point cloud data and does not segment the roofs, it just shows a yield prediction for the whole roof.

r.sun from GRASSGIS is considered an accurate tool to estimate the irradiation but requires a steep learning curve to be able to use it. However, the solar radiation tool of ArcGIS is a user friendly tool but its irradiation model is far from accurate and cannot be considered for serious work.

The computational time of the GIS irradiation tools has not been assessed and therefore conclusions cannot be drawn.

1.3. Research objectives

After introducing the motivation of this thesis and analysing the market landscape, the main thesis objective can be formulated as well as the research questions that must be addressed in order to accomplish it.

The main research objective is:

Development and proof of application of a large scale rooftop PV potential assessment tool with roof segment resolution.

The following research questions will be evaluated in order to accomplish the main objective:

Research question I: How can the information of the potential surfaces for PV be extracted from open source data?

This sub-objective deals with the question of what and how data sources could be used to extract the information of the roofs where potentially PV panels could be installed.

Research question II: How can the existing tool be evolved to calculate a high resolution PV yield in large scale urban areas?

This research question will address how to evolve and improve an existing irradiation and DC yield model (developed by [19] and [20] and adapt it to be able to use it for large urban areas.

Research question III: How can the application of the developed model be proved?

In order to prove the application of the developed model it will be applied for studying the PV potential of the municipality of Delft. Thus, the results of potential PV energy generation can be analysed and compared to the existing electricity consumption.

1.4. Report outline

Subsequent to introducing the thesis motivation, market landscape and project research questions Chapter2 focuses on explaining the theoretical background to enable the reader to follow the report. Starting from describing the relevant parameters for solar irradiation calculation to outlining the procedure of measuring and calculating them, finally it introduces the PV system modelling methods.

Chapter 3 shares the methodology used to tackle research question I, describing the data sources used, the approach and the output data from the in-house built model.

Chapter 4 analyses the model used for estimating the solar irradiation and yield as well as describing the improvements made to accomplish a more accurate tool.

Chapter 5 summarises the most relevant results of the developed tool, showing the validation of both the surface information extraction tool and the PV potential calculation tool. Lastly, the case study of the municipality of Delft is discussed.

Conclusions are drawn in Chapter 6 and the possible upgrades to the model and future work are presented in Chapter 7.

2

Theoretical background

This chapter provides the reader with all the theoretical background that will be required for following the rest of the report. First, relevant parameters for calculating the solar irradiation are introduced. Secondly, the procedure to calculate these parameters is described. Section 2.3 explains how these are extracted in a faster manner, in order to be applied in a quick scan algorithm. Finally, section 2.4 analyses the conventional modelling techniques and the one used for developing the tool presented in this project, the Simplified skyline method.

2.1. Relevant parameters for solar irradiation calculation

In order to understand all the terminology used throughout the report it is important to become familiar with certain parameters. These parameters are used for the calculation of irradiation and yield.

2.1.1. Solar and module position parameters

Firstly, the parameters describing the positions of the sun and the PV modules are introduced.

Figure 2.1a describes the altitude (a_s) and azimuth (A_s) of the sun. The altitude, as the name states, describes how high the sun is with respect with the horizontal surface, therefore, when sun is located completely above the observer, the value of (a_s) will be 90° whereas when the sun is positioned at the horizon for the observer, the value equals 0°. Regarding the azimuth, it is defined as the horizontal angle measured clockwise starting at 0° in the Northern direction, going up to 360°.

Figure 2.1b also shows the tilt of the module. Similarly, the azimuth of the module (A_M) is the horizontal angle between the origin (North) and the horizontal projection of the normal vector of the module POA. The altitude of the module (a_M) is 90° when the panel is placed flat on the surface, whereas the tilt (θ_M) is then 0°, since the sum of a_M and θ_M is always 90°.

2.1.2. Solar irradiation indicators

Furthermore, understanding the terms "skyline profile", "SVF" and "SCF" and their influence will be crucial to properly follow the explanations written in this report.

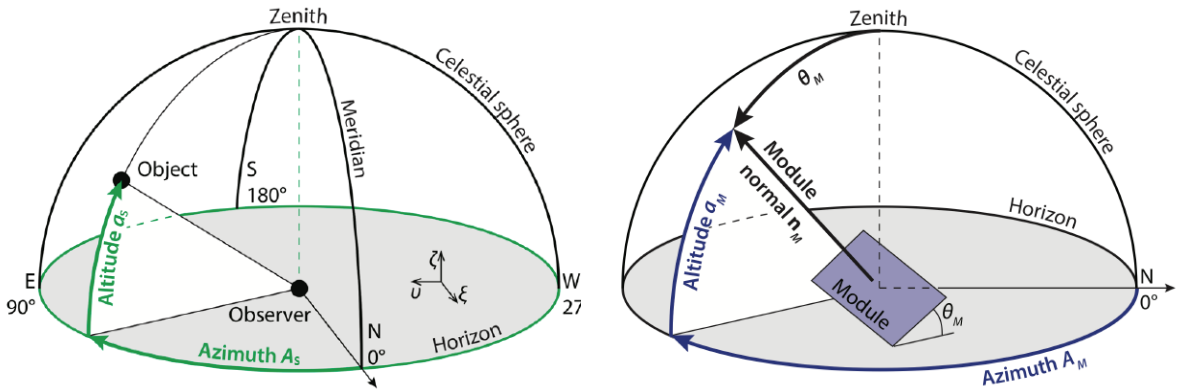

(a) Solar position.

(b) Module tilt and orientation.

Figure 2.1: Definition of altitude and azimuth in the horizontal coordinate system. Adapted from [21]

Skyline profile

The skyline profile is a 2D projection of the 3D surrounding landscape calculated at the central point of a PV module and it is required to precisely calculate the yield of a PV system. Figure 2.7b shows the skyline profile from the centre of the main square in Delft.

Sky View factor (SVF)

The Sky View Factor (SVF) is a parameter that can be extracted from the skyline profile. It describes the ratio of visible sky with respect to the whole sky dome. When there is a completely free skyline profile the value of SVF is 1, whereas when it is completely obstructed, its value equals 0. For instance, the SVF of the skyline showed in Figure 2.7b is equal to 0.9167.

Regarding the calculation of SVF, in a condition of free horizon, the SVF only depends on the tilt angle of the module (θ_M). The more tilted the module the lower SVF, since the part of the sky laying behind the POA of the panel will become bigger and therefore a smaller fraction of sun rays will get to the active surface. This is explained in Equation 2.1 and illustrated in Figure 2.2.

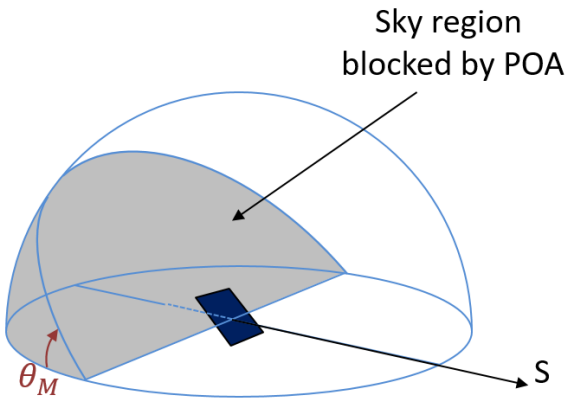

Figure 2.2: SVF is only dependent on the θ_M in a free horizon condition, courtesy of A. Calcabrini

$$SVF_{fh}(\theta_M) = \frac{1 + cos(\theta_M)}{2} \tag{2.1}$$

However, most of the PV locations have a raised horizon, specially in urban environments. In that case, the SVF has to be calculated by numerical integration. The sky dome must be discretised in small sky sectors as shown in Figure 2.3. The SVF can then be calculated according to Equation 2.2, where VF_{ij} is the view factor of each of the sky sectors that are visible for the PV module and is calculated according to Equation 2.3.

$$SVF = \sum_i \sum_j VF_{ij} \tag{2.2}$$

$$VF_{ij} = \frac{n_1 \cdot n_{ij}}{\pi} \cdot cos(a_S^{ij}) \cdot \Delta A_S \cdot \Delta a_S \tag{2.3}$$

Where n_{ij} stands for the normal vector of the sky sector *ij*, n_1 represents the normal vector of the PV module surface and ΔA_s, and Δa_s describe the area of the sky sector.

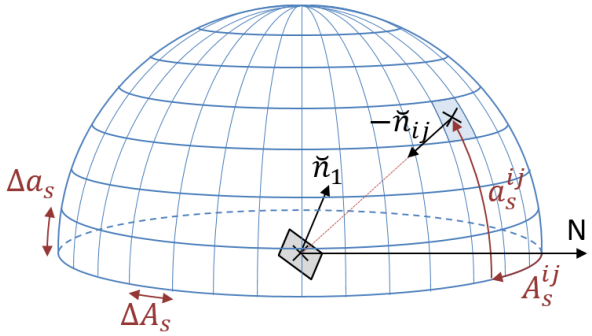

Figure 2.3: Sky dome discretized into sky sectors of width ΔA_s and height Δa_s, courtesy of A. Calcabrini

Sun Coverage factor (SCF)

The Sun Coverage Factor (SVF) is also a crucial parameter to estimate the irradiation in the Simplified skyline-based method, which is further analysed in subsection 2.4.2. It describes the ratio between the hours that the sun is behind the module or obstructed by an obstacle and the total amount of time the sun shines per year at the same location with a free horizon.

$$SCF = \frac{\sum_{year} \chi_{sp}(A_S(t), a_S(t))}{\sum_{year} \chi_{fh}(a_S(t))} \tag{2.4}$$

where

$$\begin{aligned} \chi_{sp}(A_S(t), a_S(t)) &= 1 \quad \text{if} \quad 0 < a_S(t) \leq a_{sp}(A_S(t)) \\ &= 0 \quad \text{otherwise} \end{aligned} \tag{2.5}$$

$$\begin{aligned} \chi_{fh}(a_S(t)) &= 1 \quad \text{if} \quad a_S(t) > 0 \\ &= 0 \quad \text{otherwise} \end{aligned} \tag{2.6}$$

2.2. Standard procedure to measure module parameters

The first step prior to installing a PV system in your roof is usually estimating what the potential yield of the system would be. Depending on the result, people assess if it is worth it for them or not.

In order to calculate the potential energy generation a few parameters need to be known. As previously introduced, the tilt and orientation of the modules and the skyline profile of the surroundings of the roof.

For estimating the roof tilt, and therefore, usually the tilt of the future PV panels, the standard procedure is time consuming. Someone would generally need to step on the roof and measure the slope with a Digital level meter. An example of one of them can be seen in Figure 2.5.

Figure 2.4: Digital level meter to measure tilt, from [22].

Similarly, the typical procedure for calculating the orientation your roof is facing is by measuring it with a compass. Figure 2.5 shows an example.

Figure 2.5: Digital compass to measure orientation, from [23].

Finally, the skyline profile to learn about the potential shading losses your system would have can be calculated with a HORIcatcher tool. This device will take a 360° view of the obstacles around your roof. Figure 2.6 illustrates how this tool looks like.

2.3. Quick procedure to calculate module parameters

However, if a large scale estimation of rooftop PV potential is the aim, the above-mentioned procedure is no longer feasible. An alternative approach must be followed to speed up the process. In order to achieve the main goal of this project, developing a quick rooftop PV potential calculation tool a height point cloud and cadastral data have been used to estimate the tilt, orientation and skyline profile.

Chapter 3 further explains the characteristics of the used data sets as well as the procedure followed to obtain the tilt and orientation of any roof surface in a fast way. Regarding the skyline profile calculation, firstly Sonmez and then Keijzer developed an algorithm to extract it from the previously

Figure 2.6: HORIcatcher tool to calculate the skyline profile, from [24].

mentioned height point cloud data. Please refer to [25] & [26] to learn more about it. This process is also quick and ideal for large scale calculations. The results are shown in Figure 2.7.

This algorithm has been combined with the Simplified skyline-method, introduced in subsection 2.4.2 and further analysed in Chapter 4, to later estimate the irradiation and yield of roof surfaces in a quick way.

2.4. PV system modelling methods

In the last decades, the PV industry has grown exponentially and so the simulation tools to estimate the potential irradiation/energy generation of different systems are becoming more important. Many softwares and tools are being developed, such as, rsun from GRASSGIS and solar radiation tool from ArcGIS (introduced in subsection 1.2.2).

Most of these softwares/tools estimate the irradiance impinging on the plane of array (POA) on a hourly basis, considering the surface characteristics (tilt and orientation), the radiation intensity and the weather conditions. Then, in order to calculate the annual irradiation or yield all the hourly values are integrated. These tools are named irradiance-based approaches, further explained in subsection 2.4.1.

Nevertheless, if the objective is to only estimate the annual PV potential of different surfaces for seeing if they would be suitable for PV purposes (like in this project), then the intermediate hourly values would not be useful. They would just make the calculations highly computationally demanding, due to the repetitive calculation process. As a solution to this, [19] came up with a new method to estimate the annual irradiation and yield called the "Simplified skyline-based" method, which is the one used for this project and further explained in subsection 2.4.2.

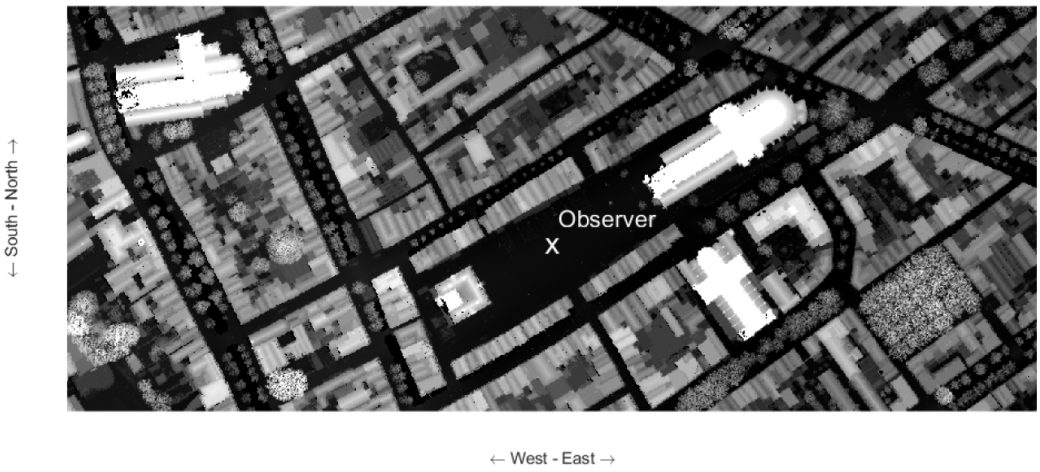

(a) LiDAR plot representing the main square in Delft.

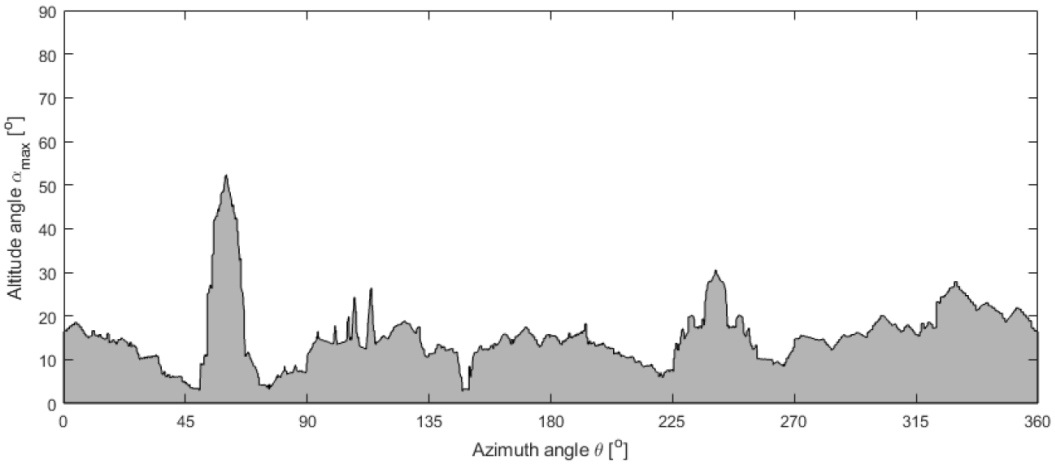

(b) Skyline profile using LiDAR data.

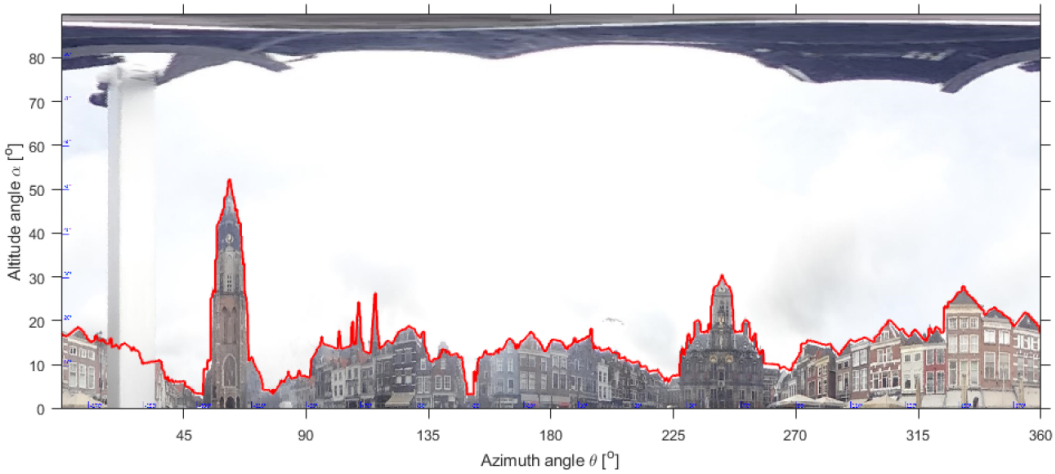

(c) Skyline profile obtained with LiDAR data represented as a read line over the Horicatcher image.

Figure 2.7: Skyline profile obtained from LiDAR data compared to the one obtained with a Horicatcher tool [26].

2.4.1. Irradiance-based approach

The majority of irradiance-based approaches combine irradiance, thermal and electrical models to calculate the annual irradiation and energy yield of a PV panel. As described at Figure 2.8, such models require three different inputs to calculate the instantaneous irradiance on the plane of array and the electric power generated:

- **Meteorological data**: Data that is usually retrieved from weather stations, like irradiance measurements, ambient and ground temperature, wind speed and cloud cover.
- **Location specifications**: Geographical coordinates and the obstacle view surrounding your system. GIS softwares require the Digital Elevation Model, from which the two above-mentioned parameters can be extracted.
- **PV module data**: The mechanical, electrical, optical and thermal parameters of the PV panel as well as its dimensions.

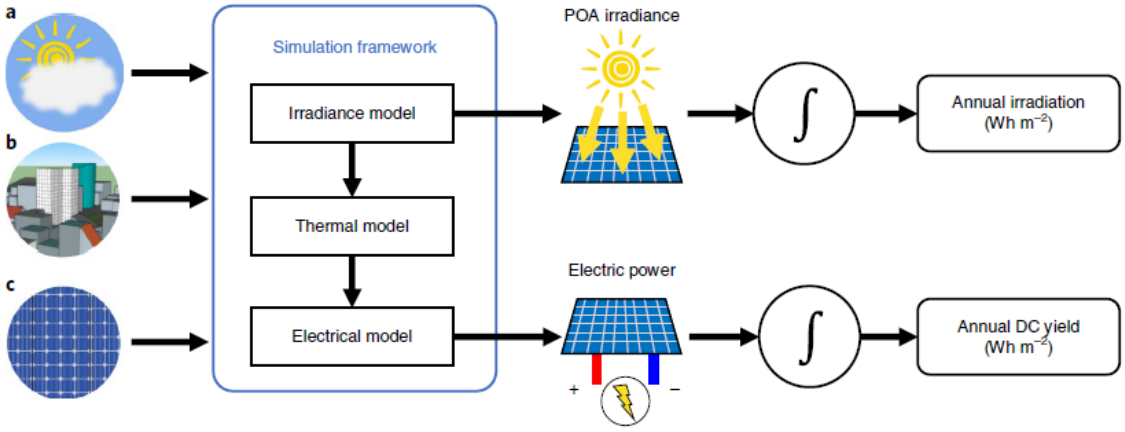

Figure 2.8: Irradiance based approach flowchart, from [19]

The total irradiance impinging on POA, or global irradiance ($G_M{}^{tot}$), is calculated as the sum of three components, as described in Equation 2.7 and illustrated in Figure 2.9. These components are the direct, diffuse and reflected irradiance.

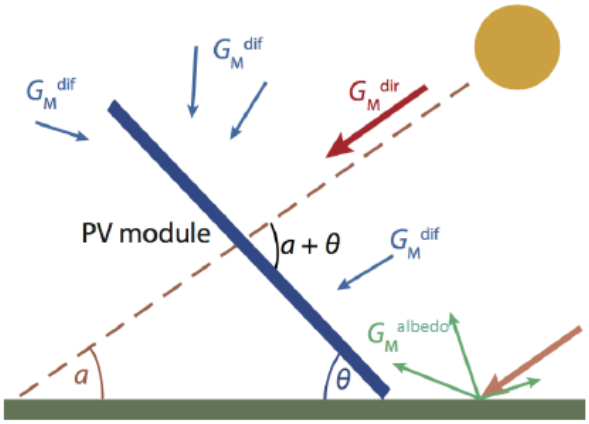

Figure 2.9: Irradiance components, from [21]

$$G_M^{tot} = G_M^{dir} + G_M^{dif} + G_M^{albedo} \tag{2.7}$$

The direct irradiance is calculated from the DNI, the angle of incidence (AoI) and a shading factor (SF), as shown in Equation 2.8. DNI stands for Direct Normal Irradiance (DNI) and refers to the direct light that is incident on the plane that is perpendicular to the sun. The AoI is dependent on the altitude and azimuth of the Sun and on the module tilt and azimuth, described in Equation 2.9. On the other hand, the shading factor (SF) takes the surrounding obstacles into consideration and varies from 0 when the sun is completely shaded to 1 when there is a free horizon.

$$G_M^{dir} = DNI \cdot \cos(AoI) \cdot SF \tag{2.8}$$

$$\cos(AoI) = \cos(\theta_M) \cdot \sin(a_S) + \sin(\theta_M) \cdot \cos(a_S) \cdot \cos(A_M - A_S) \tag{2.9}$$

It is important to highlight that only positive values must be considered for $\cos(AoI)$ unless the modules are bi-facial. Negative values happen when the angle of incidence is larger than 90°, which means that the Sun is located behind the module.

Diffuse irradiance is due to photon scattering throughout the atmosphere, which can be explained as direct irradiance undergoing multiple reflections while bouncing against air and water particles (clouds for instance) in the air, thereby changing direction. As it could be expected, this component will become more important in cloudy days.

There are many models that describe the diffuse irradiation calculation, however, since the simplified version of the anisotropic Perez model [27] is used in subsection 2.4.2, this method is shown. It divides the diffuse irradiance into three sub-components: isotropic, circumsolar and horizontal ribbon, each of them corresponding to the terms in Equation 2.10.

$$G_M^{dif} = DHI \left[(1 - F_1) SVF + F_1 \frac{a}{b} + F_2 \sin(\theta_M) \right] \tag{2.10}$$

where F_1 and F_2 are empirical coefficients, respectively corresponding to the circumsolar and horizontal ribbon components and a and b are geometrical coefficients that depend on the sun position.

The third component is the reflected irradiance or albedo irradiance, which is the irradiance that was originally direct or diffuse, but reached the module via the ground or other surfaces. Equation 2.11 describes its calculation.

$$G_M^{alb} = GHI \cdot \alpha \cdot (1 - SVF_M) \tag{2.11}$$

where α is the albedo value or reflectivity of the ground or surface and the GHI is the global horizontal irradiance.

Once the global irradiation impinging on POA is calculated, the value becomes the input of the thermal model. This model takes into account variables such as the wind speed, ambient and ground temperatures, the cloud cover and the mounting to obtain the operating temperature of the PV module, which together with the computed irradiance, are the inputs to the electrical model to calculate the instantaneous power generated by the PV module.

The instantaneous power is calculated for every time step and then integrated to get the total value. This modelling approach consists in repetitive expensive calculations, which require a high amount of meteorological data. Furthermore, the larger the area of study the more input data becomes

necessary for the model. Hence, for the purpose of this thesis (large scale rooftop PV assessment), this modelling approach does not seem to be appropriate.

2.4.2. Simplified skyline method

As introduced previously, Calcabrini developed this modelling approach in an effort to simplify the irradiation and energy yield estimation [19]. For doing so, the first assumption is based on using climate data as an input, contrary to the above mentioned irradiance-based approaches which rely on meteorological data. Climate data is obtained by evaluating the weather conditions of several years.

It has been proved that using this data together with two indicators that quantify the landscape it is possible to estimate the annual irradiation at a certain location. The first used indicator is the Sky View Factor (SVF), which has already been introduced in subsection 2.1.2. This indicator represents the ratio of sky that is visible from the central point of a PV panel. The SVF is used because the previously mentioned diffuse isotropic and ground reflected components of the Perez model depend (almost) linearly on it. The main advantage of using SVF compared to SF, is that SVF is not dependent on the time and the position of the Sun but only on the geometry of the skyline.

Nonetheless, the direct and diffuse circumsolar irradiance are not linked to this parameter. Therefore, the need of a new indicator for representing all the irradiation components is required. This new indicator is the Sun Coverage Factor (SCF), which can be described as the fraction of time the Sun is behind the panel or blocked by an obstacle in the skyline per year compared with the total amount of hours the sun shines at the same location with a free horizon. As it can be expected, this parameter is not irradiance-weighted but can be quickly calculated combining the skyline and the sun path.

The total POA irradiance is divided in two parts in [19], one related to the SVF and the other related to the SCF, represented in Equation 2.12.

$$I_Y = I_Y^{SCF} + I_Y^{SVF} \tag{2.12}$$

where

$$I_Y^{SCF} = \sum_{k=1}^{3} c_k(1 - SCF^k) \tag{2.13}$$

$$I_Y^{SVF} = (c_4 + c_5 \cdot \alpha_{gnd})SVF \tag{2.14}$$

$I_y{}^{SCF}$ represents the direct and diffuse circumsolar components of the irradiation due to the fact that both are directly influenced by the Sun being obstructed, whereas $I_y{}^{SVF}$ represents the reflected and diffuse isotropic irradiation.

Simulations were done by using a set of 161 synthetic and 12 real skyline profiles to find the correlation between the annual irradiation and the SCF and SVF indicators. It was found that there was a strong linear correlation between with SVF and the sum of the simulated isotropic diffuse and albedo components $I_y{}^{SVF}$ and a cubic correlation between the SCF and the sum of the simulated direct and circumsolar components.

The fitting coefficients ($c_1 ... c_5$) are dependent on the orientation and tilt angle of a module and also the region climate. The model is independent from the ground albedo (α), however, it can be changed in Equation 2.14. Once the 5 fitting coefficients are known and the albedo value is introduced, the total irradiance on a PV panel can be calculated only by using the SCF and SVF.

Nevertheless, if the horizon is free, the irradiation received by a horizontal surface can be described with 4 coefficients like shown in Equation 2.15.

$$I_{Y(max)} = \sum_{k=1}^{4} c_k \tag{2.15}$$

Once the annual irradiation is known for a specific PV system, the operative efficiency of the panel needs to be calculated in order to convert the irradiation into DC yield. The operative efficiency is mainly dependent on the module temperature and irradiance level. The author in [19] claims that "Despite the fact that the ambient temperature and the solar irradiance levels, which affect the operative efficiency, vary substantially from month to month, the relative variations in the monthly performance ratios of a PV system are generally lower than 10%", which implies that the irradiation model can be extended to estimate the energy generation of a PV module. Equations 2.16, 2.17 and 2.18 describe the calculations.

$$E_Y = E_Y^{SCF} + E_Y^{SVF} \tag{2.16}$$

where

$$E_Y = \sum_{k=1}^{3} d_k(1 - SCF^k) \tag{2.17}$$

$$E_Y = (d_4 + d_5 \cdot \alpha_{gnd})SVF \tag{2.18}$$

Finally, a flowchart has been made to summarise the Simplified skyline-based method approach, which can be seen in Figure 2.10.

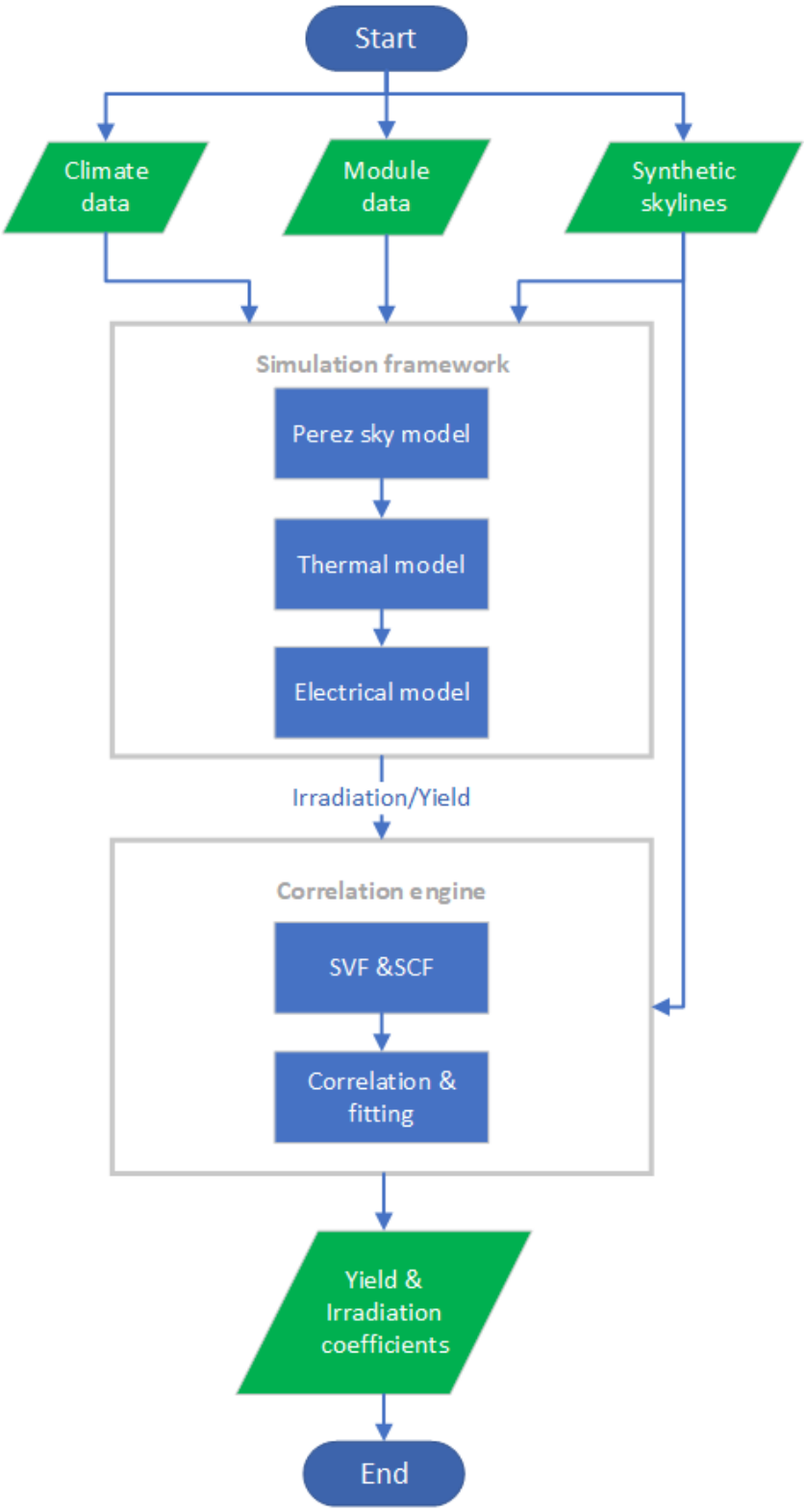

Figure 2.10: Irradiation & yield coefficients generation flowchart

3

Roof segment extraction

The goal of this chapter is to explain the approach followed in this thesis to extract the roof segments from a point cloud and the relevance of it in the project. In section 3.1 the algorithm is introduced. Section 3.2 describes the needed input data and its characteristics. The approach itself is analysed in section 3.3. Finally, section 3.4 describes what and how output data is extracted and section 3.5 summarises the chapter.

3.1. Introduction to the roof segment extraction algorithm

The main goal of this thesis project is to develop a quick rooftop PV potential calculation tool. In order to achieve this, the Simplified skyline-based method developed by A. Calcabrini [19] is followed, which is explained in Chapter 2 and further analysed in chapter 4. This method requires certain inputs that are not openly available in any database, such as tilt, orientation or coordinates of the roof segments. Therefore, a "Roof Segment Detection Algorithm" turned out to be crucial for the success of the project.

As explained previously in section 2.1, there are companies that have already developed such an algorithm. However, they are not open source. Thus, in an effort to make this project independent from external stakeholders, the algorithm has been developed in-house using MATLAB and freely available data sources, introduced in section 3.2.

The roof segment detection algorithm extracts the different planes that coexist on the same roof, from a height point cloud. It saves each roof segment and extracts its tilt, orientation or azimuth and area.

3.2. Input data

In order to extract the roof segments of a built environment, two openly available data sources have been used: Actueel Hoogtebestand Nederland (AHN) and Basisregistraties Adressen en Gebouwen (BAG).

3.2.1. Actueel Hoogtebestand Nederland (AHN)

The elevation model of the entire Netherlands, or Actueel Hoogtebestand Nederland (AHN), is provided in an online open source website (pdok.nl). This dataset is generated with a measurement

system called LiDAR (Light Detecting and Ranging), introduced in section 2.3.

LiDAR is an optical remote-sensing technique which implements laser light beam to sample the surface of Earth, collecting x,y,z measurements. As shown in Figure 3.1, the measurement is performed by a moving vehicle (usually an aircraft or a helicopter) where a scanner system, a GPS and an inertial navigation system (INS) are incorporated. The latter is used to measure roll, pitch, and heading of the LiDAR system.

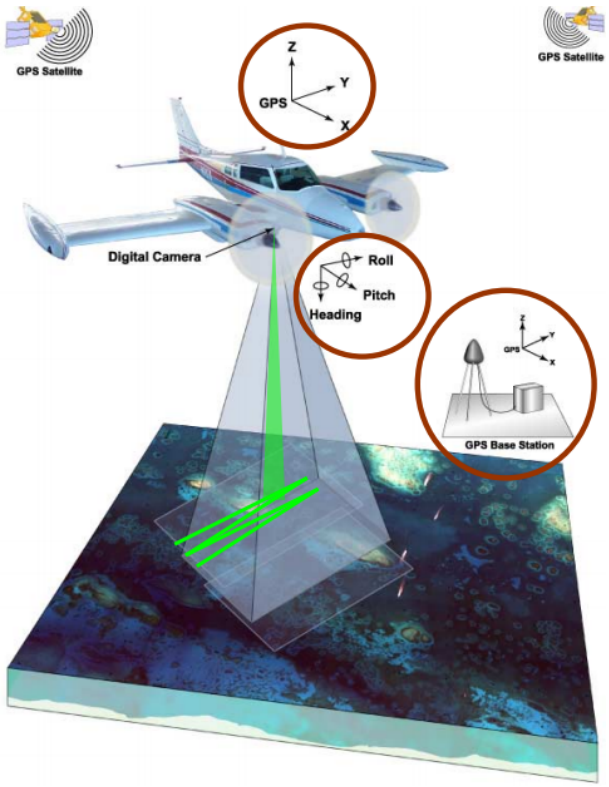

Figure 3.1: Airborne LiDAR System Components [28].

Laser pulses are emitted from the scanner system, they reach the Earth surface and are reflected back to the flying object where they are collected. The time of return of the emitted beams is then converted into a height model of the scanned area. For a more detailed information about how LiDAR data works, refer to [29].

The current data set is AHN3, the third version (collected from 2014 to 2019). For disseminating the AHN efficiently, the area of the Netherlands is split into 1377 tiles. In this project only the 2 tiles that contain the Municipality of Delft have been used. Furthermore, pdok.nl offers different download formats for the height point cloud, such as GeoTIFF grid and LAZ point cloud, and within GeoTIFF: DSM or DTM and 5 or 0.5 meter grid.

The LAZ file is a compressed version of LAS, which is a point cloud that applies a classification to the individual points. Each point is assigned to one of the following classes: ground level, buildings, water, artwork or other. While GeoTIFF is a grid of height points that can be either DSM or DTM. DSM stands for Digital Surface Model and represents the natural and built features on Earth's surface. On the other hand, as Figure 3.2 shows, DTM or Digital Terrain Model only includes bare Earth elevation data.

In an attempt to keep a consistent density of analysed points throughout the studied areas, GeoTIFF was the chosen format. As the height points come in a grid, one point every 0.5 or 5 m (pixels of 0.5

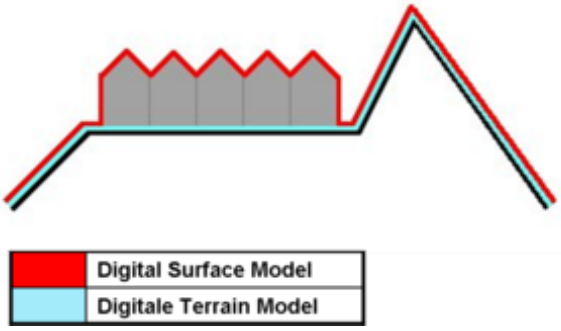

Figure 3.2: Digital Surface Model vs Digital Terrain Model [30].

x 0.5 m^2 were chosen to have a higher accuracy) rather than in uneven densities like in a LAS file. Moreover, GeoTIFF files are almost 30 times lighter than LAS files (0.5 MB vs 13.9 MB for a tile)[31]. Finally, DSM was the used format since the built environment is crucial for the project and the Earth elevation in the studied area can be considered as flat and 0 m over the sea level. However, if such a study would be done in an area with an uneven landscape, a normalisation of the point cloud should be carried out, this is further elaborated in chapter 7.

The height map of the Netherlands is represented in Figure 3.3, areas under the sea level can be noticed in the middle-west part of the country. Such a map is made possible due to a collaboration between the central government and the provinces.

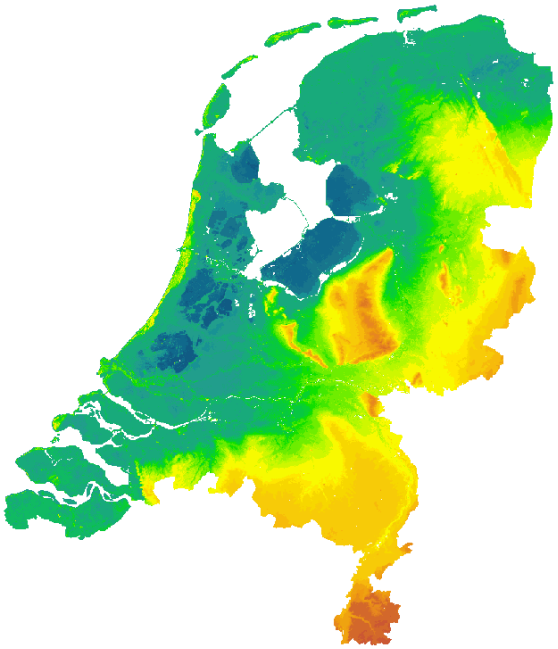

Figure 3.3: Actueel Hoogtebestand Nederland - Height map of the Netherlands [32].

Limitations

Although LiDAR data is known for its high 3D positional accuracy and high point density for mapping it has some limitations. First of all, part of the data is likely to be outdated. While the mea-

surements are conducted every certain years, the built environment and rural areas are constantly changing. Therefore, it is common that for instance, some of the newest buildings or parks are not part of the data set. Additionally, a scan of the entire national area takes more than one year. Thus, data of different regions are also dated differently.

Secondly, in the case of boundary detection, LiDAR may have a limitation in providing sharp and straight roof edges, as LiDAR points, generally do not hit the exact building edges. This usually leads to a detection of a roof area smaller than the actual one.

Finally, LiDAR data presents some intrinsic errors. Highly reflective surfaces such as waterways or windows are often represented by remarkably high height values, which distort the image and need to be filtered out. Moreover, since measurements are only taken from above LiDAR data is unable to properly detect the shape of objects like trees, bridges or electricity lines. The laser pulses detect the top part but are not able to penetrate and detect the bottom part. Therefore, such objects are usually represented as walls. This can affect the irradiation estimation for rooftops placed close to them, the shading during the year becomes higher and the solar potential is underestimated. Figure 3.4 shows an example of a row of trees being represented as a wall, the picture at the bottom (c) shows the zoomed in view of the row of trees, it can be seen that there are gaps in between the trees that LiDAR is not able to represent.

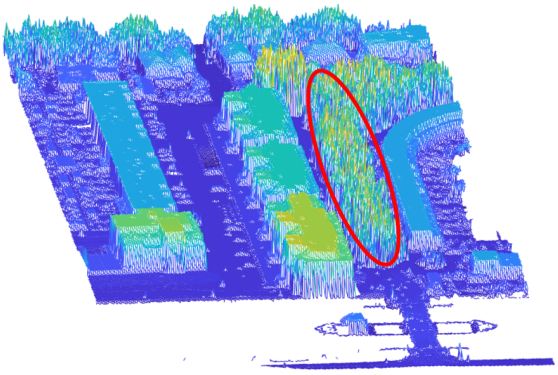

(a) LiDAR plot.

(b) Satellite photo.

(c) Street view from the X shown in (b).

Figure 3.4: (a) highlights in red the tree row represented as a "wall". The X in (b) represents the street view location shown in (c).

3.2.2. Basisregistraties Adressen en Gebouwen (BAG)

This project makes use of the geopackage (.gpkg) prepared by the 3D Geoinformation group of the Technical University of Delft [33], which combines both BAG and AHN (introduced in 3.2.1) to pro-

vide all the information needed about the built environment. The file contains every registered building in the Netherlands, Figure 3.5 shows its overview.

The Basisregistraties Adressen en Gebouwen (BAG) is the most detailed, openly available data set on buildings and addresses in the Netherlands. It contains information about each address in a building, such as its current use, construction date or registration status. The polygons in the BAG represent the footprint of the building as the projection of the roof's outline. The data set is regularly updated as new buildings are registered, built or demolished. The project NLExtract prepares a monthly PostgreSQL backup of the BAG, which is then used as basis for the 3D BAG [34].

Figure 3.5: Map containing every registered building in the Netherlands.

Limitations
As mentioned previously, the BAG data is high quality and up-to-date. However, there are some examples in which it can be seen that the contours of the buildings do not match the building edges but describe the cadastral parcel, where for instance, an elevated playground is also included as part of the building. In Figure 3.6 it can be noticed that three different buildings (Figure 3.6b) are represented as one polygon in the BAG data (Figure 3.6a), this happens because they have an elevated playground connecting all three blocks. Luckily, these errors are not seen often and therefore barely affect the results.

3.3. Methodology

The aim of this section is to explain the steps taken to extract the information of the different roof segments in each building. In order to accomplish that objective two software programs have been used: MATLAB and ArcGIS. The following subsections further analyse their use.

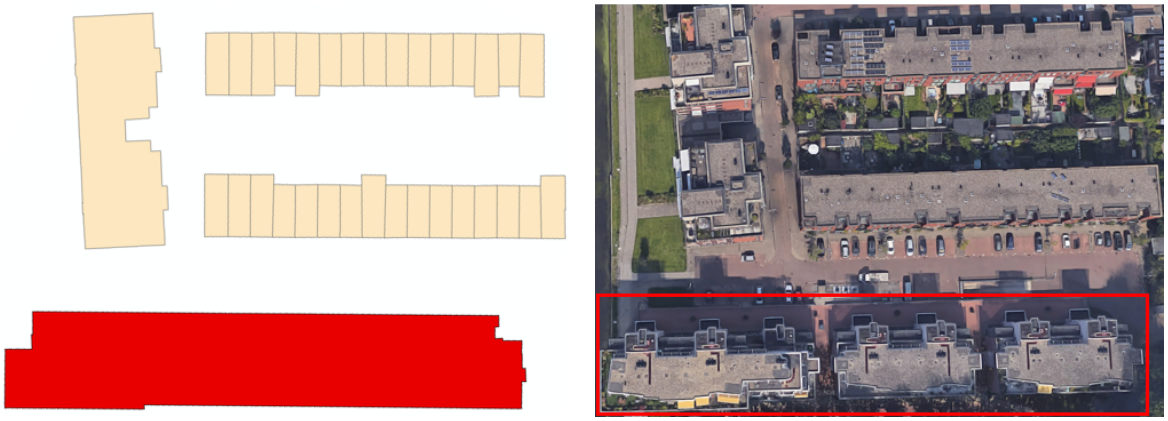

(a) BAG representation.

(b) Satellite photo of the area described in (a).

Figure 3.6: Example of BAG data limitation: The building in red in the top picture (BAG) describes the three buildings shown in the bottom picture.

3.3.1. Combination of data sets

The first step is to combine both data sets, BAG and AHN. The former is imported as a geopackage (.gpkg) file to ArcGIS, whereas the latter is directly loaded in MATLAB as a GeoTIFF image file.

Secondly, the geopackage containing the information of the built environment of the entire Netherlands is converted in ArcGIS into a shapefile (.shp) that only includes the area of interest of this project, thus, the municipality of Delft. Shapefiles are supported and readable by MATLAB. This approach is further explained in Appendix A.

Thirdly, the shapefile is imported into MATLAB, where the coordinates of the contour of the buildings are extracted, these are then used to cut the LiDAR data. Consequently, any height point outside the roof of a building, such as trees or electricity posts is filtered out.

3.3.2. Plane detection

The second step, rooftop plane detection, is necessary for the roof segment extraction. The normal vector of the detected plane will be an input for the MSAC algorithm that extracts all the planes of the building, further explained in section 3.3.3.

This method focuses on analysing buildings individually. The starting point is having the height point cloud cut by the contours of the buildings. Thus, the points within the matrix that are lying on the roof of the selected edifice have a height value whereas the points outside the roof but within the same bounding box are set to 0 m.

The approach to detect a plane is as follows: to begin with 3 points are chosen, Figure 3.7a shows an example of a building close to the TU Delft campus in Delft. Then, 2 vectors are calculated from the 3 chosen points, see Figure 3.7b. After doing the cross product of the 2 vectors the normal vector is obtained, Figure 3.7c, the normal vector to the plane formed by the 3 points.

In order to confirm that those 3 points are lying on a valid plane, the procedure is repeated with other 3 points located close to the previously chosen ones. If the normal vector of the plane where the 3 new points are lying forms an angle smaller than 1° with the normal vector of the 3 old points, a plane can be considered. The angle between the two normal vectors is calculated by doing the dot product of both vectors. The answer is equal to the arcosine of the angle theta (θ), Figure 3.8

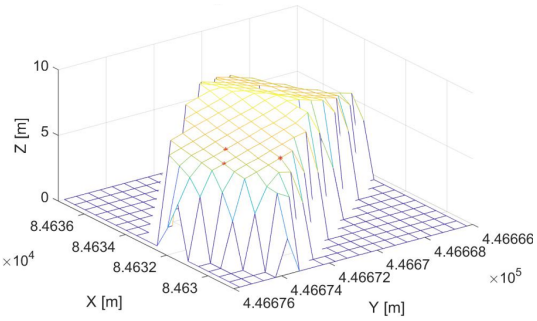

(a) 3 points lying on the plane

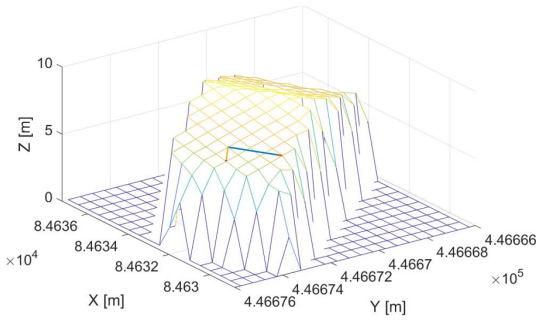

(b) 2 vectors out of the 3 points

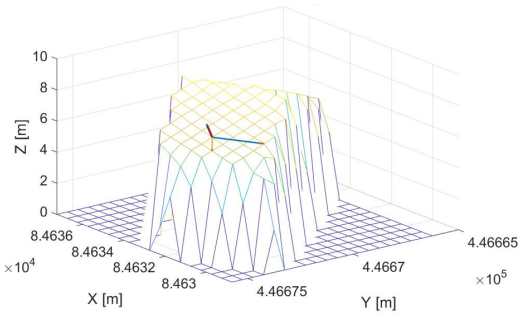

(c) Normal vector, cross product of the 2 vectors

Figure 3.7: Procedure to detect a plane. The X and Y axis of the plots show the "Amersfoort / RD New" coordinates of the building in meters, the Z axis describes the height of the points also in meters.

illustrates it, being "a" and "b" the normal vectors. The considered plane in the showed example is represented in Figure 3.9.

A 1° angle difference was chosen after empirically checking that with larger angle differences some faulty or minor planes would be detected. In case the angle difference is larger than the set boundary, new points are chosen and the procedure is repeated until finding the 6 points lying on the same plane.

3.3.3. Roof plane extraction

The third step is to extract the roof planes. For this, as previously mentioned, a methodology called MSAC is used. It stands for M-estimator SAmple Consensus, which is a variant of RANSAC (Random Sample Consensus), an iterative method for estimating a mathematical model from a data set. The algorithm fits a model into the selected point cloud and calculates the outliers, the data points that are not contained in the model. In this case, the program fits a plane to the points lying on it and calculates the points that are located outside that plane, the outliers.

The code uses the normal vector of the detected plane, previously explained in 3.3.2, as a reference vector for the fit plane. Furthermore, a maximum distance from an inlier point to the plane is defined. Consequently, the algorithm considers the points within that range from the detected plane to be inliers, those will form the roof segment. The remaining points of the data set, the outliers, become an input for the calculation of the next planes. In this project a distance of 20 cm between inlier and plane has been selected, which is a good trade-off in between ensuring the points do lie on the plane and avoiding selecting too little points out of the total points that belong to the plane. Figure 3.10 illustrates the first extracted plane of the building shown in 3.3.2.

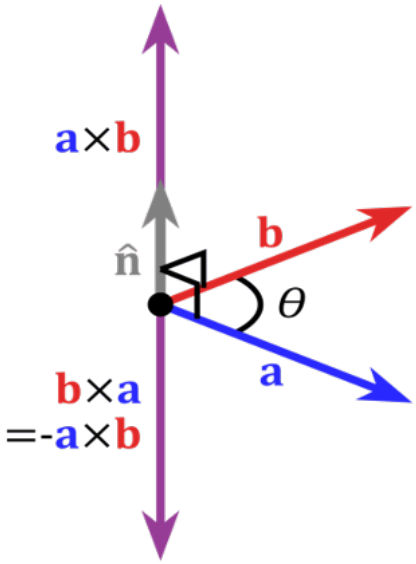

Figure 3.8: Theta (θ), the angle between the two normal vectors

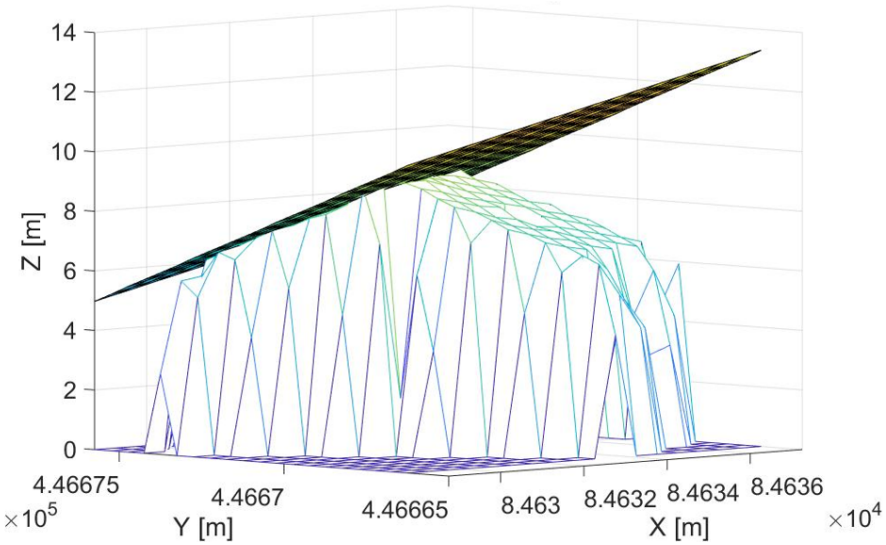

Figure 3.9: Plane considered if theta is smaller than 1°.

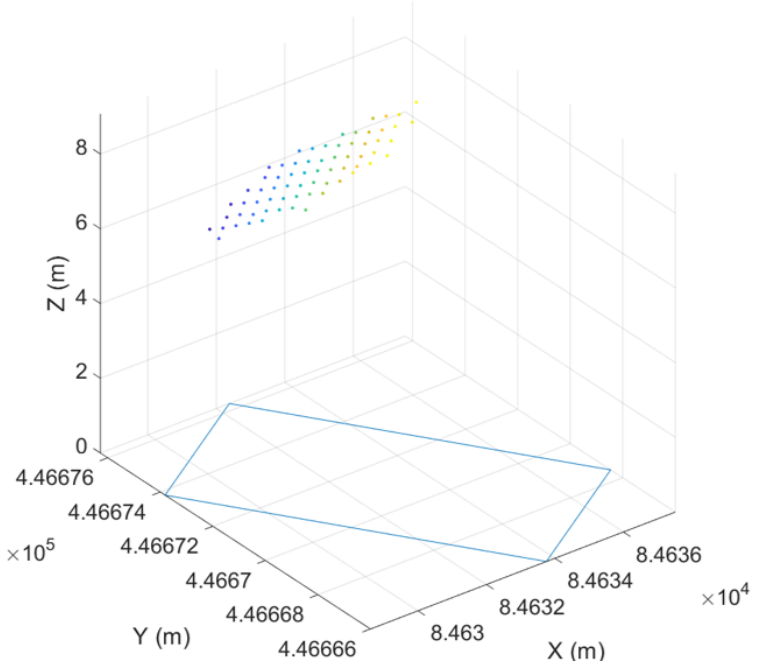

Figure 3.10: Plane 1 is composed by the points lying on the fit plane.

For extracting the following roof segments there is no need to define a reference vector for the fit plane, the algorithm itself detects the points that are lying on a same plane. Once there are no more planes to extract from the building the program stops. Figure 3.11 represents the 2nd extracted plane of the house presented in the previous subsection.

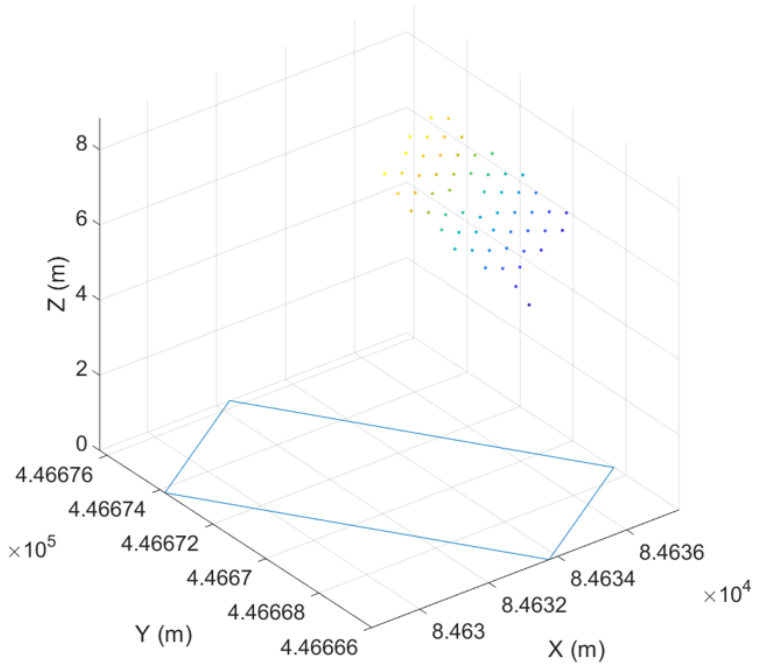

Figure 3.11: Plane 2, extracted from the outliers of the 1st plane.

3.4. Output data

Once the roof segments have been extracted, a few calculations are carried out in order to obtain the following parameters from each plane: Tilt, orientation and area. These parameters are relevant for the calculation of the irradiation and yield, which is further explained in Chapter 4.

In order to calculate the tilt and orientation of a roof segment, the normal vector to the plane is used.

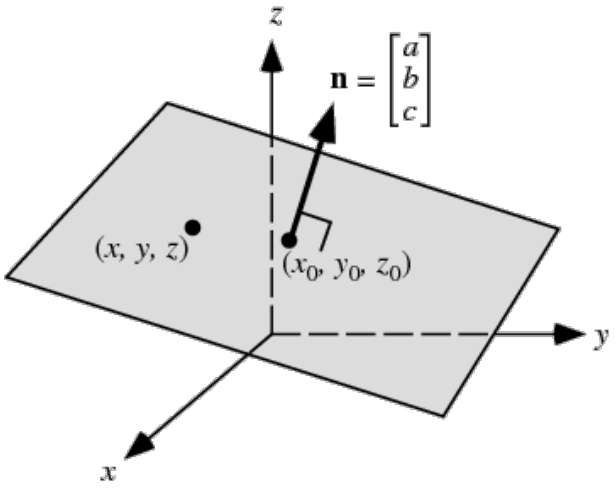

Figure 3.12: The decomposed normal vector of a plane [35].

The tilt of a plane is the inverse cosine of the absolute value of the z component of the normal vector. The absolute value is taken to ensure the angle is in between 0 and 90°. In Figure 3.12 the z component of the normal vector shown as c. Equation 3.1 describes how the formula would look like for that plane.

$$Tilt = \arccos(|c|) \tag{3.1}$$

Secondly, the orientation or azimuth of a roof segment is determined by taking the projection of the normal vector onto the horizontal plane. This is calculated with the Four-quadrant inverse tangent of the y component of the normal vector of the plane divided by the x one, as shown in Equation 3.2. The range of the result is in between -180° and 180°, which is then converted into a 0° to 360° by adding 360° to the negative azimuth values.

$$Orientation = \arctan 2\left(\frac{b}{a}\right) \tag{3.2}$$

Finally, the area is estimated based on the amount of points the plane contains. Each height point is taken every 0.5 m in the x and y axis and therefore each point represents a surface of 0.25 m^2 on the horizontal surface in the case of a flat building. Nevertheless, if the roof is tilted the surface covered by a point is inversely proportional to the cosine of the angle of the roof as described in Equation 3.3.

$$Area = \frac{n_{points} \cdot 0.25}{\cos(Tilt)} \tag{3.3}$$

3.5. Summary

The goal of this chapter was describing the methodology to extract roof segments from a height point cloud and prove its accuracy. Firstly, the reasoning behind needing such an algorithm has been introduced. In section 3.2 the input data needed has been explained. Both Actueel Hoogtebestand Nederland (AHN) and Basisregistraties Adressen en Gebouwen (BAG) are open source data sets. Although the data sets are accurate they have certain limitations. Section 3.3 addresses the methodology, Figure 3.13 summarises it. The BAG data contains the building contour coordinates, which are used to cut the LiDAR data. Thus, the buildings can be analysed individually. The plane detection is the first step to then extract the roof segments using the MSAC algorithm. The next section, 3.4, explains what parameters are extracted and how they are calculated. Finally, in section 5.1 the validation of this algorithm is carried out, where the accuracy of the code is evaluated.

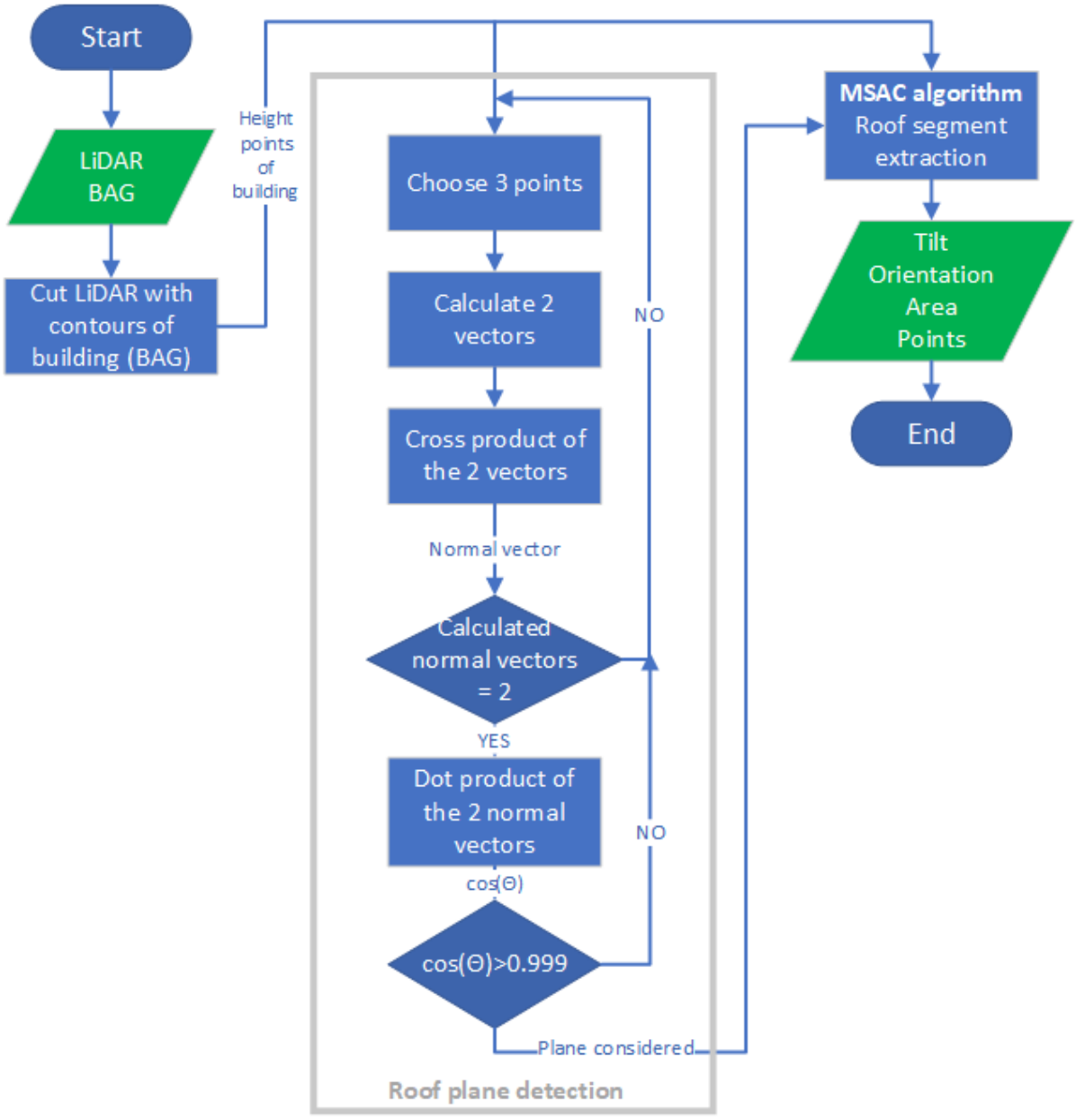

Figure 3.13: Roof segment extraction methodology flowchart.

4

POA irradiation and yield model improvement

Chapter 4 introduces the improvements applied to the Simplified skyline-based method and explains the steps taken in order to calculate the yield and irradiation of the rooftops in Delft. Section 4.1 focuses on the improvements made for flat and tilted surfaces. Section 4.2 describes the followed procedure to calculate the potential irradiation and yield. Finally, 4.3 summarises the chapter.

4.1. Improvements to the Simplified skyline-based method

This section addresses the improvements made to the Simplified skyline-based method presented in [19] and summarised in subsection 2.4.2. In that paper, the author states the following: "the SCF is not an irradiance-weighted parameter - that is, blocking the Sun one hour in the morning and blocking the Sun one hour at midday contribute in the same amount to reduce the SCF value". The Simplified skyline-based method relies on the SVF and SCF to estimate the irradiation, hence, making a stronger correlation between SCF and the irradiance would improve the method.

In an effort to do so, [20] came up with two correction factors, the air mass and angle of incidence correction factors. Thus, the irradiation and yield estimations become more accurate. However, the AoI factor worked only for the case of a 0° tilted module. Now, thanks to the work carried out in this thesis project this correction factor can be applied to any surface, no matter its tilt or orientation.

In order to represent the Sun path during the year and the effects of the correction factors a so-called analemma is used. It shows the position of the Sun (altitude and azimuth) at a same hour every day of the year. Figure 4.1 illustrates it, the colours represent the amount of hours the Sun is at each position. Such an analemma shows no difference in between, for instance, having the Sun at an azimuth of 180° and altitude of 50° or having it at an azimuth of 80° and 10°. However, the irradiance received by the PV panel will be way higher in the first case. The Simplified skyline-based method used to take this analemma as a reference.

4.1.1. Air mass correction factor

As introduced previously, the first proposed correction factor to improve the correlation of SCF with the irradiance is based on the optical air mass (AM), measured in [kg/m^2]. The air mass is defined

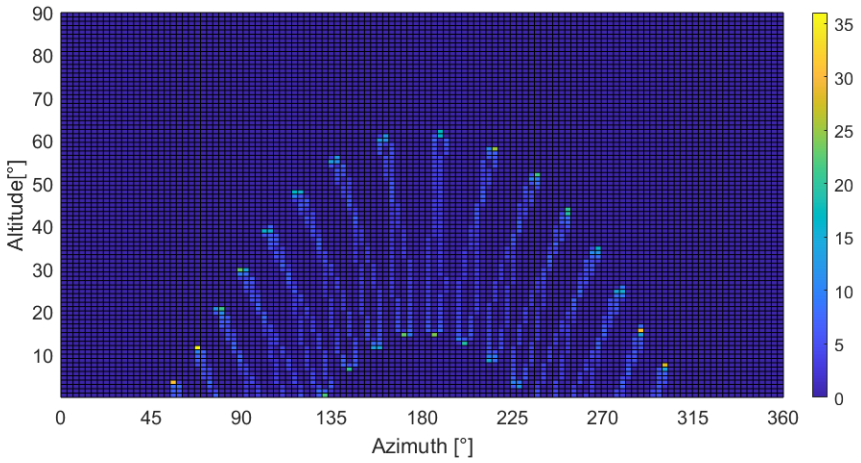

Figure 4.1: Sun path during the year, the colours describe the amount of hours the Sun has been in each position, adapted from [20]

as the ratio of an actual path length that the Sun has to travel through the Earth atmosphere to the minimal possible distance, which is the case of the Sunlight passing the atmosphere when the Sun is at its zenith [21]. The optical air mass is equal to one when the Sun is at its zenith, then the spectrum is named air mass 1 spectrum (AM1).

In order to calculate the air mass precisely for different Sun zenith angles the following formula (Equation 4.1) proposed by Gueymard in [36] is used.

$$AM(\theta_z) = \left[\cos(\theta_z) + \frac{0.48353 \cdot \theta_z^{0.095846}}{(96.7412 - \theta_z)^{1.754}}\right]^{-1} \tag{4.1}$$

The higher the AM the longer the path the photons take to reach the Earth's surface and the longer the light needs to travel the more photons will be scattered or absorbed before hitting the PV panel. Therefore, when the Sun is at a low altitude is when the most photons energy will be lost before reaching the module.

4.2 describes the relation between the Sun altitude, the direct irradiation component and the elevation of the studied location, adapted from [37].

$$I_d(AM(t), h) = I_0 \cdot (1 - 1.14 \cdot h) \cdot e^{-0.357 \cdot AM(t)^{0.678}} \tag{4.2}$$

Where I_0, the solar constant, equals 1361 [W/m^2] and h is the height of the location in [km].

The correction factor applied in the model is described in 4.3, it calculates the ratio of the actual direct beam at a specific *AM* and h compared to the direct beam at *AM1* (the shortest path from the Sun to the surface of the Earth).

$$f_{AM} = \frac{I_d(AM(t))}{I_d(AM1)} \tag{4.3}$$

As shown in Figure 4.2 the f_{AM} factor has a major influence when the Sun is in an altitude of 0-15°. Therefore, PV systems located within the built environment will rarely be affected by it since most

of the times the skyline will be blocked by other buildings or trees at those low altitudes. However, this correction factor will be useful for systems in a free horizon condition.

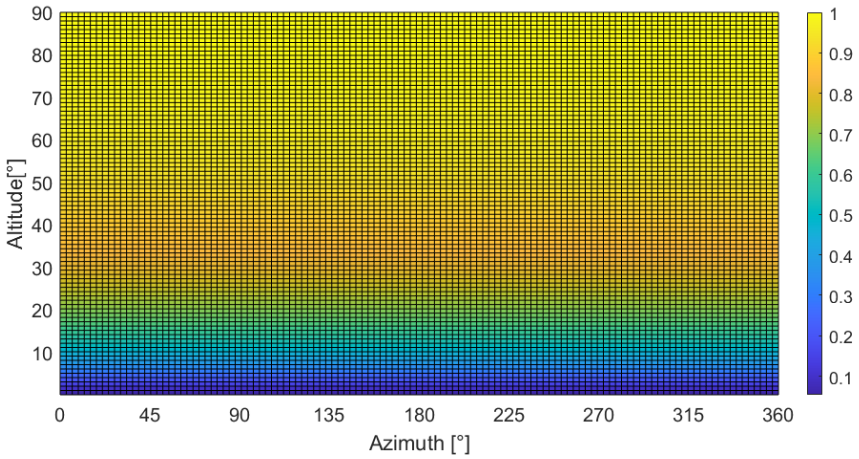

Figure 4.2: AM correction factor

4.1.2. AoI correction factor for flat surfaces

As introduced in subsection 2.4.1, the direct irradiance on the POA is directly proportional to the cosine of the AoI. This is known as the "cosine law". It considers that the direct beams that reach the PV panels are reduced proportionally to the misalignment angle (AoI) that the normal to the POA of the modules makes with the altitude of the Sun. Equation 4.4 represents the correction factor f_{AoI}, which is obtained with the cosine of the AoI:

$$f_{AoI} = \cos(\theta_M) \cdot \cos(\theta_Z) + \sin(\theta_M) \cdot \sin(\theta_z) \cdot \cos(A_S - A_M) \tag{4.4}$$

Where θ_Z is the zenith angle (90°-a_S), a_S is the altitude of the Sun, A_S is the azimuth of the Sun and A_M is the module azimuth.

Figure 4.3 shows the effect of the AoI mismatch for a PV placed flat on the surface. And Figure 4.4 shows the analemma after applying both correction factors (AM & AoI).

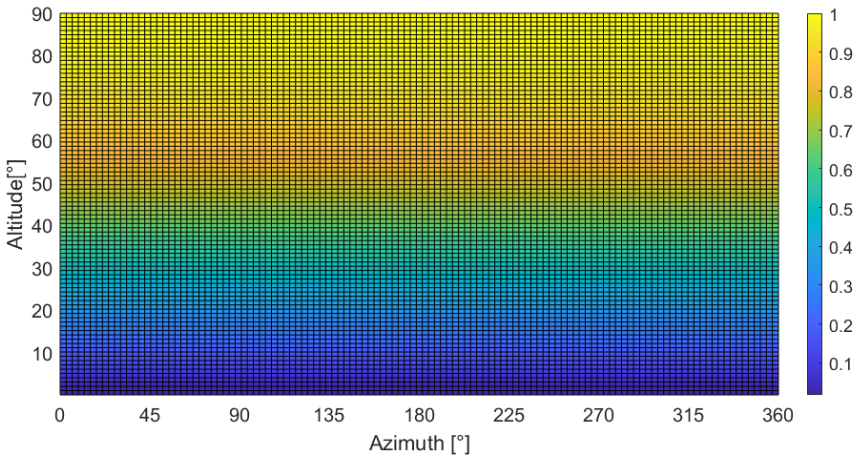

Figure 4.3: AoI correction factor, adapted from [20].

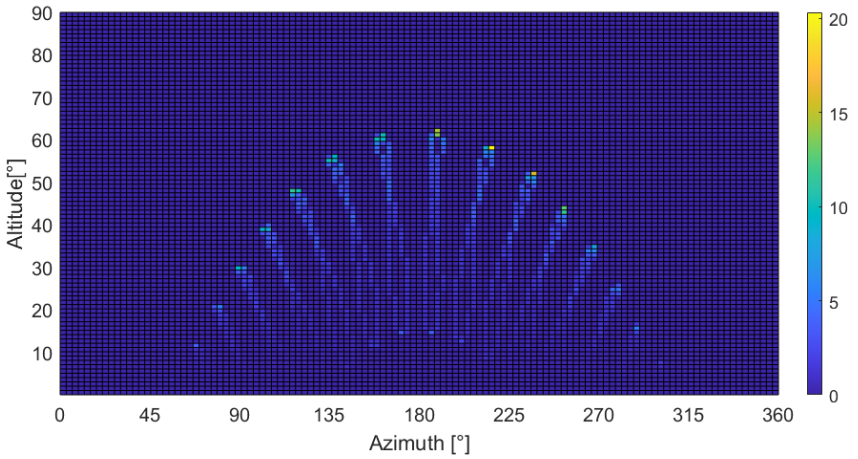

Figure 4.4: Analemma weighted by the AoI and AM correction factors for a flat surface, adapted from [20].

Regarding the SCF definition, Ferri used this formula in her work [20].

$$SCF = 1 - \frac{\sum(Sun_{Mat}(lat,long) \cdot Skyline_{Mat} \cdot f_{AoI}(0°) \cdot f_{AM})}{\sum Sun_{Mat}(lat,long)} \tag{4.5}$$

Where Sun_{Mat}(lat,long), $Skyline_{Mat}$, $f_{AoI}(0°)$ and f_{AM} are 90 x 360 matrices. Sun_{Mat}(lat,long) is plotted in Figure 4.1 and describes how many hours the Sun spends in each degree of altitude and azimuth throughout the year, it is dependant on the location. Secondly, $Skyline_{Mat}$ describes the skyline, it is equal to 0 when there is built environment or any kind of obstacle at that altitude and azimuth and 1 when it is free horizon. Therefore, the multiplication with Sun_{Mat} equals 0 when the Sun is behind the skyline. Finally, $f_{AoI}(0°)$ and f_{AM} weight the total amount of hours in free horizon.

4.1.3. AoI correction factor for all tilts and orientations

In this thesis project the algorithm has been adapted to allow the AoI correction factor to work for any surface. Furthermore, the Sun Coverage Factor has been redefined to make a stronger correlation with the irradiance at any tilt or orientation.

After taking into account the AM and AoI correction factors, the maximum amount of Sun hours received at a surface will no longer be the total amount of Sun hours, as considered by Ferri in Equation 4.5. Now the maximum amount of hours will be weighted by the two correction factors, which is shown in the denominator of Equation 4.6. Also, now the numerator will consider the tilt and orientation of the panel with f_{AoI} thanks to the changes made in the algorithm script.

$$SCF = 1 - \frac{\sum(Sun_{Mat}(lat,long) \cdot Skyline_{Mat} \cdot f_{AoI}(\theta_M) \cdot f_{AM})}{\sum(Sun_{Mat}(lat,long) \cdot f_{AoI}(0°) \cdot f_{AM})} \tag{4.6}$$

Two examples have been plotted to visualise how the tilt and orientation affect the analemma. The first one is a PV panel facing the East (90° azimuth) and tilted 30°. As it can be seen in Figure 4.5a the correction factor is equal to 1 when the sun is aligned with the orientation and at an altitude of 60° (as described in Equation 4.4). However, when the sun is behind the module (azimuth in between 180 and 360°) the factor equals 0. This is reflected in the analemma illustrated in Figure 4.5b, where the AM correction factor is also applied but has a negligible influence.

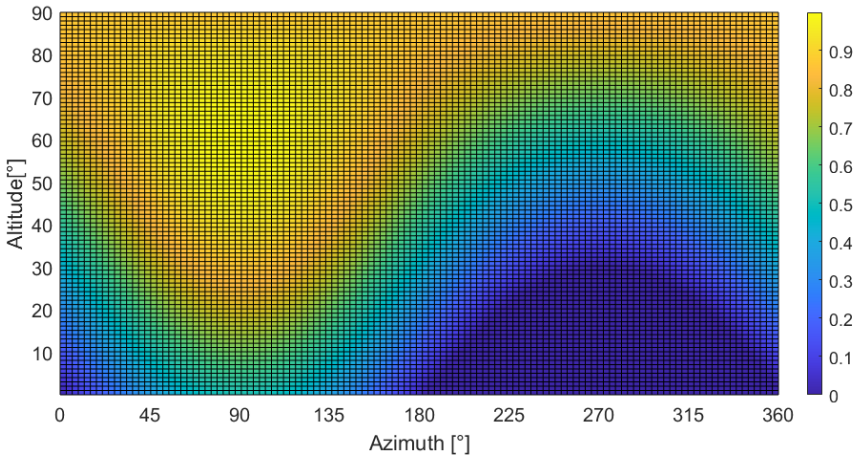

(a) AoI correction factor for a surface facing East and tilted 30°.

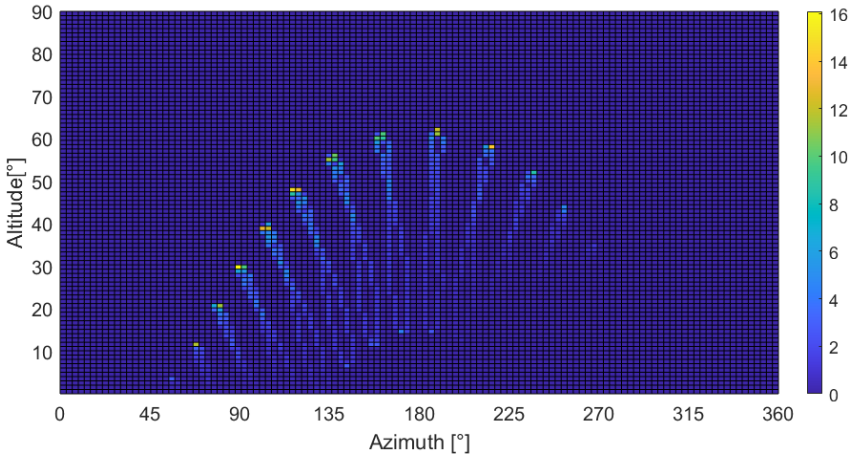

(b) Analemma seen from a surface facing East and tilted 30°.

Figure 4.5: The influences of the optical air mass and the Angle of incidence mismatch for a surface facing East and tilted 30°.

The second example could represent a facade of a building, since the surface considered is facing South and is tilted 90°. Again here, Figure 4.6a shows that the correction factor for Sun position in between 270° and 90° is equal to 0 since the sunlight will not be visible for the surface. Figure 4.6b represents the analemma weighted with both correction factors.

4.2. Calculation of irradiation and yield

This section dives into the steps followed in order to calculate the irradiation and yield of the rooftops in the municipality of Delft. Once the improvements to the skyline-based method have been applied, the coefficients are generated. Then, the LiDAR data and the roof segment information are imported. However, to ensure the model is as computationally efficient as possible certain considerations must be made, such as what radius should be considered to calculate the skyline profile or how many points of a plane should be calculated and how many could be interpolated. These are introduced in the upcoming subsections, where sensitivity analysis' reveal the reasoning behind the chosen values, which do not compromise accuracy of the calculation.

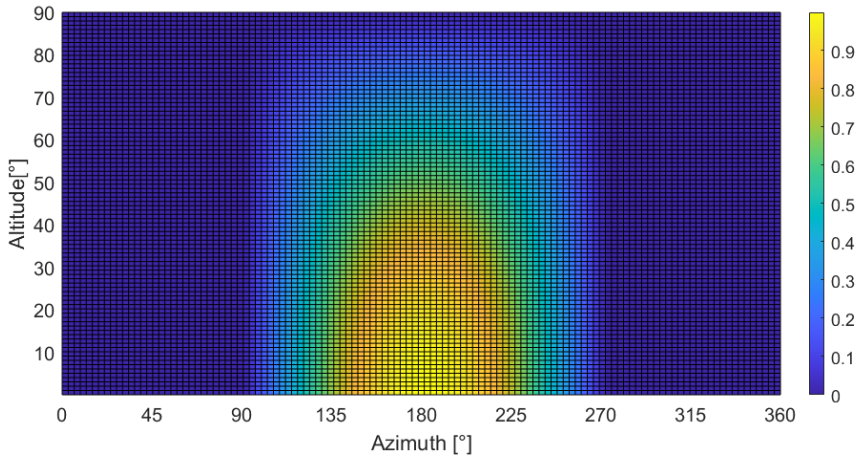

(a) AoI correction factor for a surface facing South and tilted 90°.

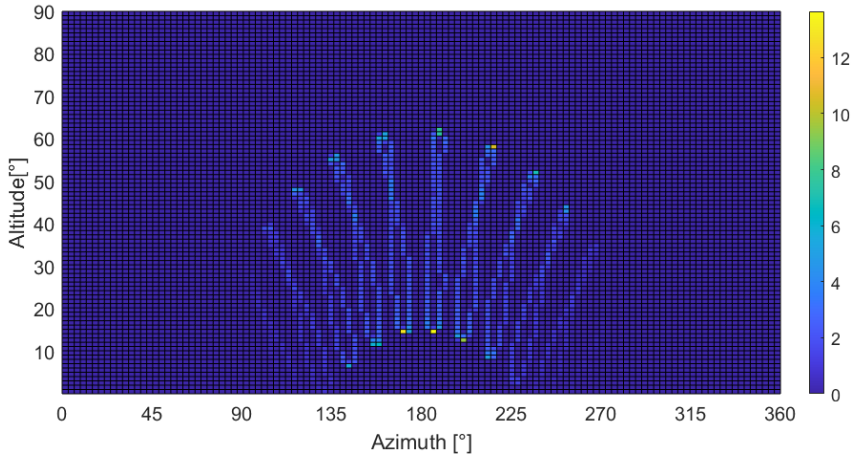

(b) Analemma seen from a surface facing South and tilted 90°.

Figure 4.6: The influences of the optical air mass and the Angle of incidence mismatch for a surface facing South and tilted 90°.

4.2.1. Generation of coefficients

The generation of the coefficients is the first step. As introduced in subsection 2.4.2, five coefficients are generated that account for the different components of irradiance. These coefficients are calculated only once and are location dependant. Climate data is used as an input, which is the average of weather data of the past 20 years. Among others, it includes the direct, diffuse and global irradiance and the temperature of both the surface and ambient every hour.

In order to estimate the yield coefficients a PV panel must be chosen. In this project the SunPOWER MAXEON 3 400 W module was selected to estimate the PV potential of Delft, due to the fact that it is one of the most efficient in the market. The main characteristics of this PV module are shown in Table 4.1, the datasheet can be found in Appendix C.

However, in order to carry out the yield estimation validation, showed in subsection 5.2.2, the JA Solar JAM6-60-270/BK was used. Since this was the PV module the systems were using. The main characteristics are displayed in Table 4.2 and the datasheet can be found in Appendix C.

Table 4.1: Main characteristics: SunPOWER MAXEON 3 | 400 W

Nominal Power (P_{nom})	400 W
Panel Efficiency	22.6%
Panel Width	1046 mm
Panel Height	1690 mm
Power Temp. Coef.	-0.29%/°C

Table 4.2: Main characteristics: JA Solar JAM6-60-270/BK

Nominal Power (P_{nom})	270 W
Panel Efficiency	16.51%
Panel Width	991 mm
Panel Height	1650 mm
Power Temp. Coef.	-0.41%/°C

4.2.2. Radius for skyline profile calculation

The tool developed in this thesis project is a quick scan irradiation and yield potential calculator, which will be used to map the solar potential in large areas. Therefore, one of the main requirements is that it must be computationally fast and if possible, use as little memory as possible. Nevertheless, the accuracy of the estimations must also be as high as possible. In that scenario, a suitable radius to calculate the skyline profile of the studied points has to be chosen. One that does not compromise accuracy for speed or the other way around. For calculating such a value, a sensitivity analysis has been done. Over 100 points laying in different rooftops have been studied, resulting in an average case, shown in Figure 4.7.

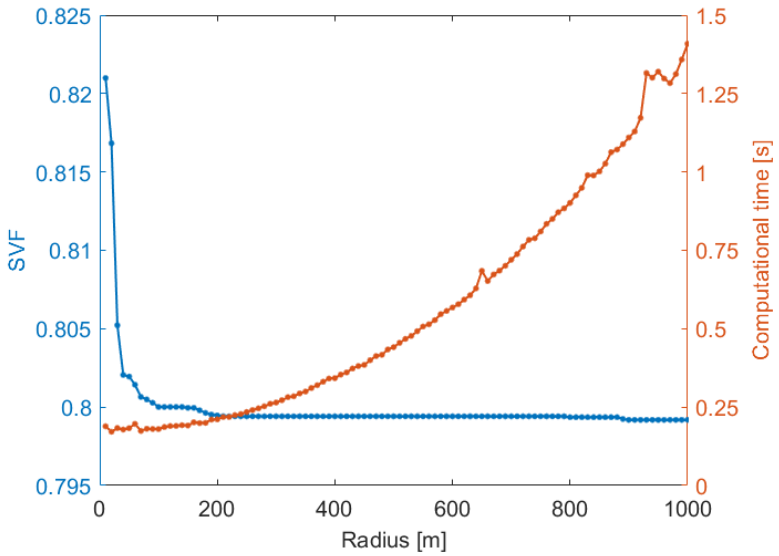

Figure 4.7: Radius sensitivity analysis of an average case over 100 studied points

In order to choose the appropriate radius the Sky View Factor has been studied, it has been calculated at different radius values. From Figure 4.7 it can be observed that the SVF decreases for increasing radius. The bigger the radius, the more of the actual horizon will become visible for the observer. However, once the SVF stabilises it can be concluded that a bigger radius would not add

accuracy and would make the algorithm slower. In the average case, a radius of 200 m shows to be enough to estimate the SVF accurately and is over 5 times computationally quicker than estimating the SVF based on a 1000 m radius. Thus, in this project a radius of 200 m has been selected to estimate the skyline as fast and precisely as possible.

4.2.3. Interpolation of calculated points

In this project, the used height point cloud has a high density of points, more specifically, it contains one point every 0.5 m in the x and y axes. Thus, at first sight calculating the skyline profile of every single point on a roof seems to add up unnecessary computational burden while not contributing highly to accuracy, since most of the times the skyline will not change much in a few meters. However, as in the previous subsection a sensitivity analysis has been carried out to estimate what percentage of points can be calculated and what percentage can be interpolated without impacting too much the accuracy of the calculation.

Two types of roofs have been analysed, big building roofs (over 300 m^2 of flat area) and average household roofs (20-30 m^2 of tilted area). Again, as in the radius sensitivity analysis average cases have been chosen to show the relative error obtained by calculating different percentage of points. The minimum percentage of points calculated has been 10% since under this value the interpolation of many roof segments was not possible due to lack of points for triangulation.

Figure 4.8 shows an average big flat building in Delft (52.004094, 4.368994). As it can be seen, the relative error increases when the percentage of calculated points decreases. The computational time, however, decreases with a lower percentage on calculated points. A 5% relative error of yield was considered admissible in an effort to optimise the calculation time as much as possible. Therefore, 10% of the points evenly distributed on each roof segment would be calculated and the rest would be interpolated for big buildings.

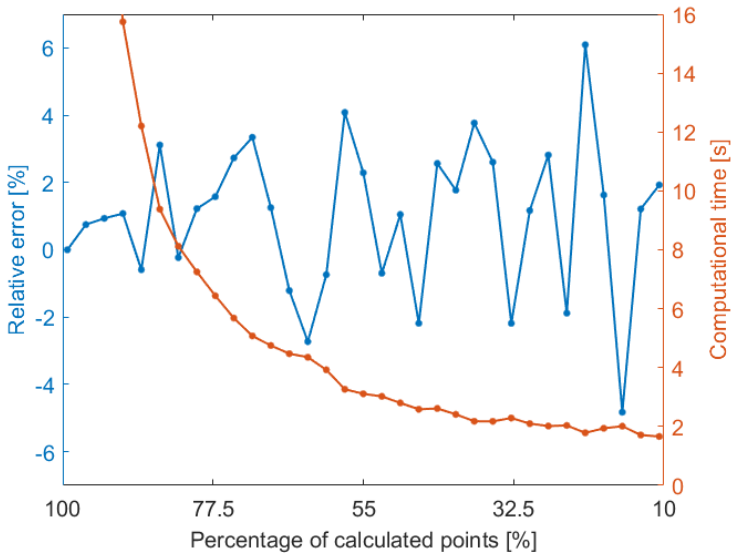

Figure 4.8: Big building sensitivity analysis

Figure 4.9 represents an average household in Delft (51.988557, 4.349148), which shows a similar trend to Figure 4.8 regarding relative error and computational time. In this case, again, the minimum possible percentage of calculated points was proved to be enough to estimate the potential of the whole roof accurately, under 1% error. Thus, for smaller roof segments also 10% of the points

would be calculated and the rest would be interpolated.

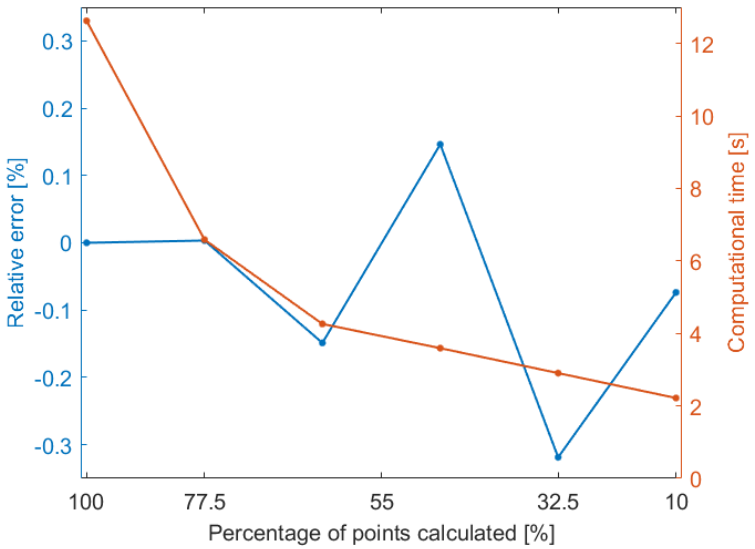

Figure 4.9: Average household sensitivity analysis

Comparing both study cases it can be seen that the smaller roof segments experience a lower relative error with a smaller percentage of calculated points, this could be concluded as being due to the fact that the skyline profile can change more drastically in big building than in small ones. Also remarkable is the fact that the difference in computational time is not as large as expected, this happens because the algorithm works faster per point the more points it studies.

4.3. Summary

This chapter has explained the improvements made to the Simplified skyline-based method. It has further analysed the changes proposed by [20] and described the latest to estimate irradiance for surfaces with any tilt or orientation. In section 4.2, the steps followed before being able to calculate the irradiation and yield have been introduced, reasoning the value chosen for radius of skyline profile and the percentage of points per plane. The full methodology is illustrated in Figure 4.10. Having the accuracy improved, the values of irradiation and yield for the municipality of Delft and the validation of the calculation tool are shown in Chapter 5.

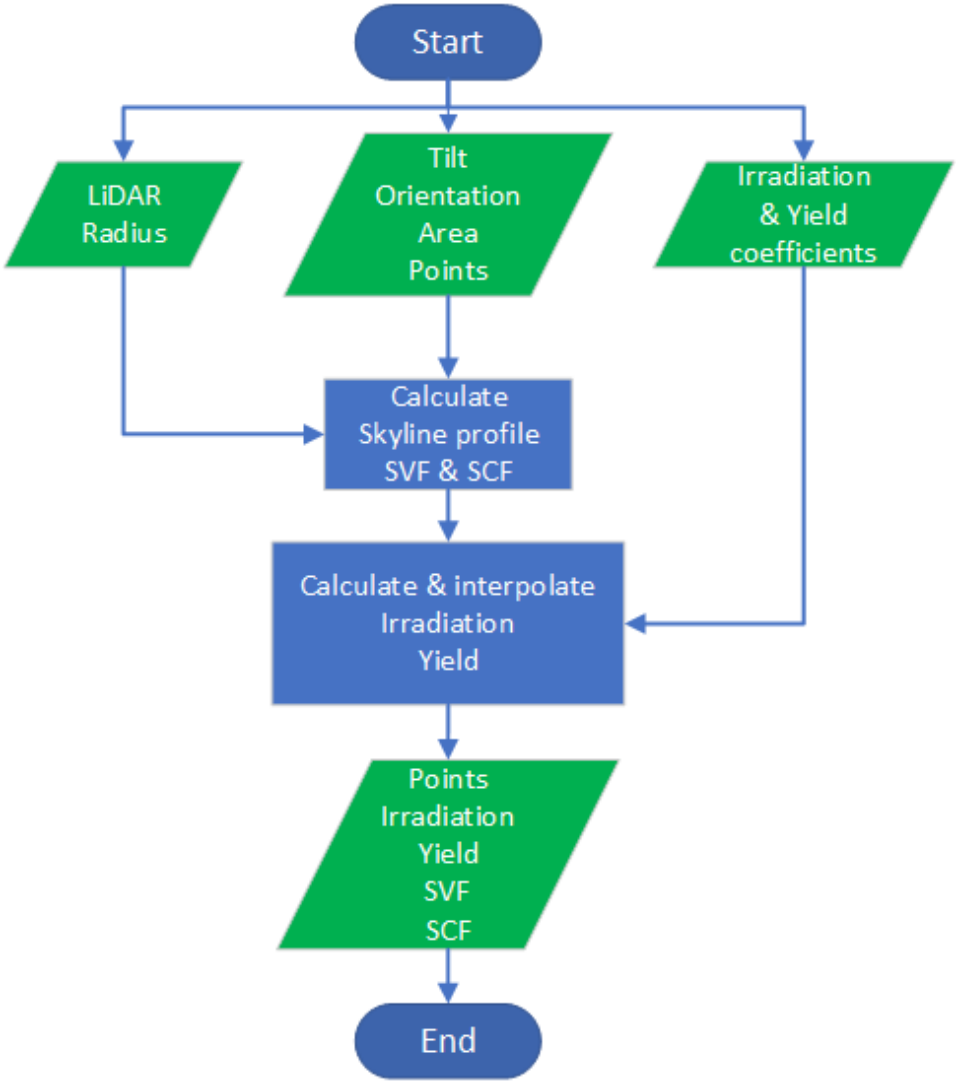

Figure 4.10: Irradiation and yield calculation methodology flowchart.

5

Results and discussion

In this chapter the results obtained in this thesis are discussed. Firstly, the validation of tilt, orientation and area for the Roof extraction model are shown. Secondly, a comparison between the accuracy and deviation of the improved Simplified skyline-based method and the old version is done. The yield calculation is also validated with generation values of real PV systems. Finally, the irradiation and PV yield results for the municipality of Delft are illustrated with maps and compared with the total electricity demand.

5.1. Validation of roof segment extraction model

This section aims to show the validation of the roof segment extraction tool. More specifically, a validation of the tilt and orientation calculation accuracy. For doing so, real data of a set of 100 PV systems in the municipality of Delft has been obtained from a trusted source. This data set contains the location of the buildings and the tilt and orientation of rooftop PV systems, which are fully aligned with the roof surfaces. Furthermore, the accuracy of the roof area calculation has also been done comparing the obtained values with the roof segment extraction model and the surface values provided by BAG data. This study has been done for the 22321 studied buildings in Delft. Subsection 5.1.4 introduces the computational time of this tool.

5.1.1. Accuracy of tilt estimation

In order to make an accurate yield prediction for tilted roofs an accurate tilt calculation must be done. Thus, being able to estimate the slope of the roof surfaces becomes crucial for the success of the PV potential calculation tool.

As introduced previously, the data set used to validate the calculation contains 100 different roof segments that have a PV system. No roof segment in the data set has a tilt smaller than 20° since these were discarded due to the fact that most of them were systems placed on flat roofs and, therefore, were not aligned with the roof surface, making them useless for this study. Moreover, the data set does not include roof surfaces with a tilt over 60° because they have no PV systems tilted in the 60-90° range.

Figure 5.1 represents the results of the validation, the plotted points are the calculated tilts while the line describes the real tilt values.

The results show an average absolute error of -0.02° and a maximum deviation of 3.7°. The biggest

deviations were found in the city center of Delft, where buildings are oldest and have more irregular roof surfaces and more dormers and windows, which make the calculation more difficult.

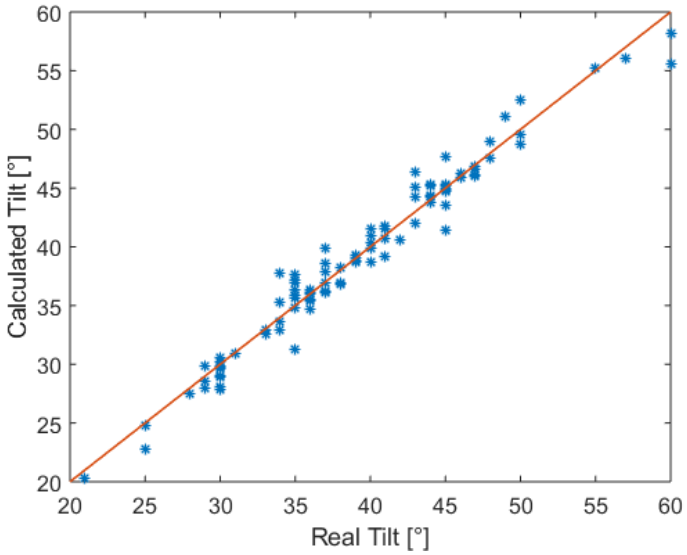

Figure 5.1: Tilt validation: the plotted line describes 100% accuracy and the points show the calculated values.

5.1.2. Accuracy of orientation estimation

The roof surface orientation calculation accuracy study was done in the same way as the tilt validation. Also, similar to the tilt validation, a certain range of values are not studied in the orientation validation. Orientations in between 350° and 50° are not included, since there were no PV systems placed in such azimuth angle. It is worth mentioning that this range of orientations represent the least favourable for solar energy applications in the Northern hemisphere.

Figure 5.2 shows the results. Again here, the plotted points are the calculated values, which aim to be as close as possible to the plotted line, which represent the real values.

The average absolute error is equal to 0.66° and the maximum deviation found among the 100 roof segments is of 4.53°.

5.1.3. Accuracy of area estimation

The area calculation accuracy study was done differently to the previous studies. The validation was done with the 2D surface values provided by BAG for each building polygon and the calculated area by the roof segment extraction model, the methodology of calculation is explained in section 3.4.

In this study, the percentage of the total roof area that has been estimated by the in-house developed model is analysed.

For flat buildings the comparison was straight-forward because the calculated area by the tool is already in 2D. Nevertheless, for tilted roofs the calculated area had to be transformed into a 2D value. Therefore, the area of the tilted surfaces was multiplied by the cosine of the tilt angle. It is worth mentioning that, this tilt angle is calculated by the roof segment extraction model introduced

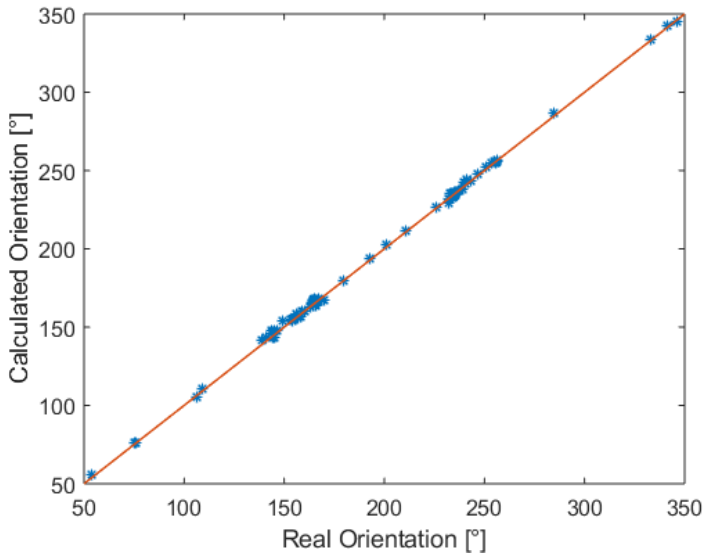

Figure 5.2: Orientation Validation: The plotted line describes 100% accuracy and the points show the calculated values.

in Chapter 3 and not the real value (not available). However, the estimation is considered accurate enough as demonstrated in subsection 5.1.1.

The results show that the average percentage of area extraction out of the 22321 buildings in Delft is 80.42%. In most of the cases the lost area has been due to the lack of roof edge detection, which is a limitation of LiDAR itself as introduced in subsection 3.2.1. However, as explained in [38], "for reasons concerning aesthetics, ballast, safety and ease of installation there is a minimum distance PV modules should be away from the edge of a roof. For pitched roofs this is about 30 centimetres, mostly determined by the regulations for the installation of mounting systems. For flat roofs, common distances from the edge are 50 to 100 centimetres. Mounting systems generally require a minimum of about 60 centimetres from the roof edge of flat roofs for product warranty.". Therefore, losing points on the edges of the building is luckily not that impactful in the rooftop PV potential estimation.

Figure 5.3a and Figure 5.3b show two examples of an average flat and tilted building, represented in 2D. As mentioned previously, most of the lost area is close to the edges.

5.1.4. Computational time

The roof segment extraction model takes on average 5 seconds per building. For the whole Delft this means a computational time of 31 hours. The calculations were made with a computer with the following specifications: 128 GB RAM and 2 x 6-core Intel® Xeon® (3.47 GHz) CPU.

5.2. Validation of the improved Simplified skyline-based method

The second objective of this thesis was to further develop the Simplified skyline-based method for calculating irradiation and yield more accurately. For doing so, the correlation between the SCF and the irradiance has been improved by enabling the AoI correction factor to work for any surface. This can be seen in subsection 5.2.1 by comparing the coefficient accuracy and deviation of the improved method with the old one. In subsection 5.2.1, a yield calculation validation with 25 real PV systems

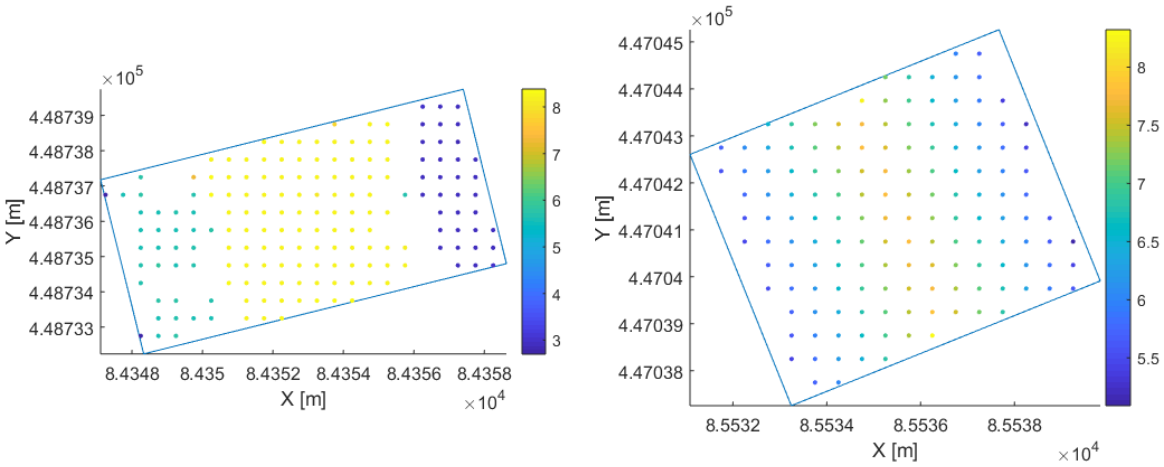

(a) An average flat building, 19.5% of the area is lost close to the edges.

(b) An average tilted building, 19.5% of the area is lost close to the edges.

Figure 5.3: 2D representation of average flat and tilted buildings, both with a calculated area of 80.5% of the total surface, the colour bar represents the height of the points.

is shown. Finally, subsection 5.1.4 introduces the computational time of the tool.

5.2.1. Coefficient accuracy and deviation improvement

The improved Simplified skyline-based method applies the optical airmass and the AoI correction factors to the Sun matrix. Thus, the direct irradiance received by the POA is weighted and becomes more accurate and so does the SCF. Consequently, the calculation of irradiation and yield, dependant on SCF, also becomes more accurate.

In this section the cross validation results of the Perez irradiance model and the Simplified skyline-based method are shown for both the old and improved versions. This is shown for the tilts of 0°, 30°, 45°, 60°and 90° and compared in Figure 5.4.

An improvement in both accuracy and deviation is accomplished in every single tilt, however, smaller tilts show a greater improvement, specially for the deviation. This is due to the fact that the SCF is directly influenced by the DNI. The larger the tilt angle, the least direct irradiation and the more diffuse share it will receive, since the Sun will spend more time behind the POA of the module. This means that the fitting for SCF will become worse at higher tilt angles (greater deviation from Perez model), this is seen in the deviation of both old and improved versions after 60°. Despite the influence of the AoI is smaller at high tilts, the improved Simplified skyline based method still yields better deviation results than the old method, since there are still a few direct irradiance hours to weight and correct.

The detailed comparisons of accuracy and deviation of the most representative cases, 0°, 45° and 90° are also shown individually in Figure 5.5, Figure 5.6 and Figure 5.7.

5.2.2. Yield calculation accuracy study

After receiving the yield data of a set of 25 PV systems from a trusted source, a yield calculation accuracy study has been carried out to validate the improved Simplified skyline-based method. All the PV systems are located in Eindhoven, the Netherlands, and use JA Solar JAM6-60-270/BK PV

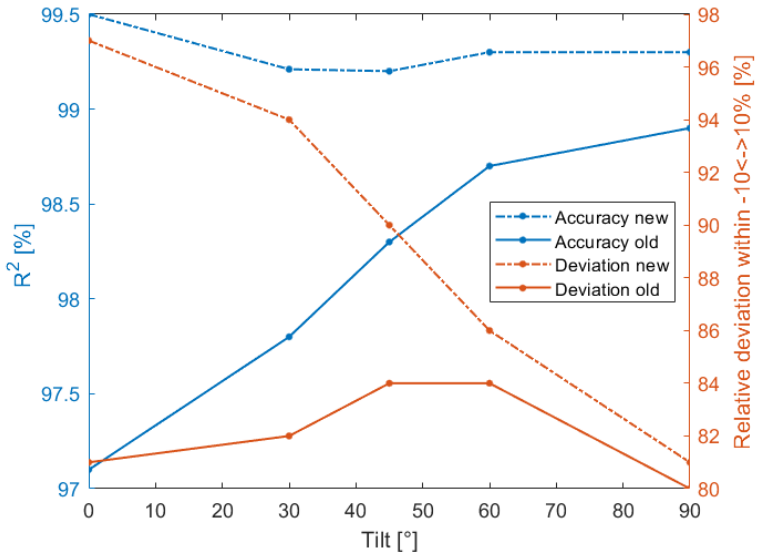

Figure 5.4: Summary of the comparison of the accuracy and deviation from the Perez model simulation for 0°, 30°, 45°, 60° and 90°, with both the old and improved Simplified skyline-based method.

modules, as introduced in subsection 4.2.1.

The thermal model used in the Simplified skyline-based method is the one proposed in [39]. Moreover, the DC-AC conversion efficiency for PV systems has been assumed to be 93% taking into account the European efficiency of SE3000-SE3500-SE4000 solar inverter (97.5%) from [40] and the following system losses: maximum power point tracking (MPPT) losses (accounting for 1% absolute efficiency loss at system level), module mismatch losses (1% absolute), Ohmic losses (1.5% absolute) and soiling losses (1% absolute).

Regarding the results, the average relative error of calculation is underestimating the real yield value by 6.64% and the biggest registered deviation has been -14.18%. Figure 5.8 illustrates the comparison between the calculated yield and the measured one. The plotted line represents 100% accuracy.

The calculation tendency is clearly to underestimate the real annual yield, the yield estimation of 17 out of the 25 has been lower than the actual one. One possible reasoning is the fact that the input data for generating the coefficients which are later used for calculating the yield are based on climate data, which is the average of the weather data of the last 20 years. The validation has been done with the yield value of PV systems of a certain year, this year could have received a higher annual irradiation than the average.

5.2.3. Computational time

The irradiation and yield calculation tool takes on average 2.7 seconds per building. This adds up to 16.74 hours of computational time for the 22321 studied buildings in Delft. Together with extracting the roof segments, the tool takes 7.7 seconds per building and, therefore, 47.74 hours to calculate the potential of all the roof surfaces in Delft. This calculations were also done with a computer with the following specifications: 128 GB RAM and 2 x 6-core Intel® Xeon® (3.47 GHz) CPU.

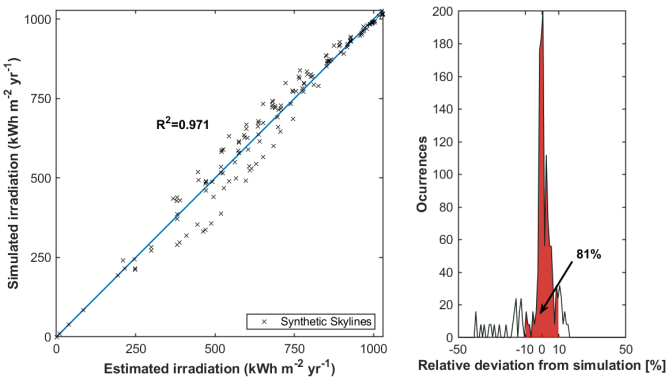

(a) Accuracy and deviation of the old method vs Perez irradiance method.

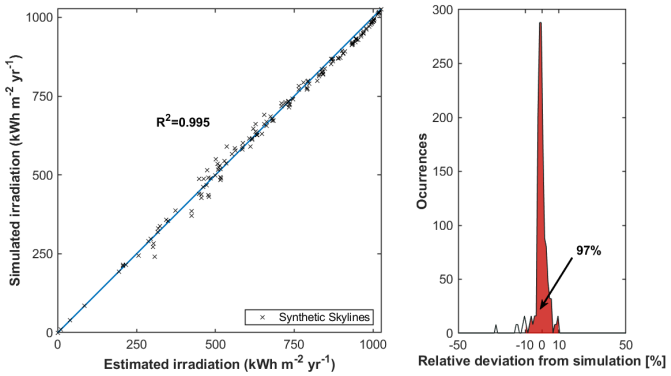

(b) Accuracy and deviation of the improved method vs Perez irradiance method.

Figure 5.5: Cross validation results of the old and improved versions of the Simplified skyline-based methods for a tilt of 0°.

5.3. Rooftop PV potential in the municipality of Delft

This section analyses the potential of rooftop PV in the municipality of Delft. It shows how the data extracted from the roof segment extraction model combined with the improved Simplified skyline-based method can be used to map the irradiation and PV yield potential of urban areas. subsection 5.3.1 and subsection 5.3.2 focus on the detailed visualisation of the potential (per roof segment), while subsection 5.3.3 illustrates the potential annual yield per building. Finally, subsection 5.3.4 compares the total rooftop PV potential with the current total electricity consumption in Delft. All the PV yield calculations have been carried out using SunPOWER MAXEON 3 | 400 W PV module, which is introduced in subsection 4.2.1.

5.3.1. Visualisation of the irradiation in Delft

The tool developed in this thesis is able to produce detailed maps, showing for instance, the potential irradiation received at every surface of each roof of the city. This has been done by using the 3D analyst toolbox of ArcGIS, where Natural Neighbor interpolation has been used to make a smooth map out of the imported points (learn more about the procedure in Appendix A).

Figure 5.9 shows the irradiation potential of Molenbuurt in Delft, the maximum estimated irradiation is equal to 1236.2 kWh/m^2/y for an optimally tilted and oriented roof while the lowest is equal to 6 kWh/m^2/y, a point almost completely shadowed.

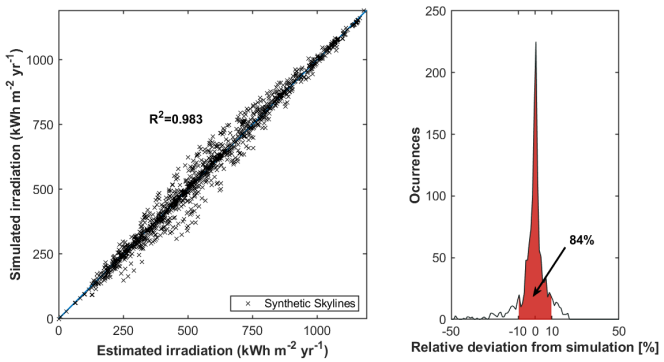

(a) Accuracy and deviation of the old method vs Perez irradiance method.

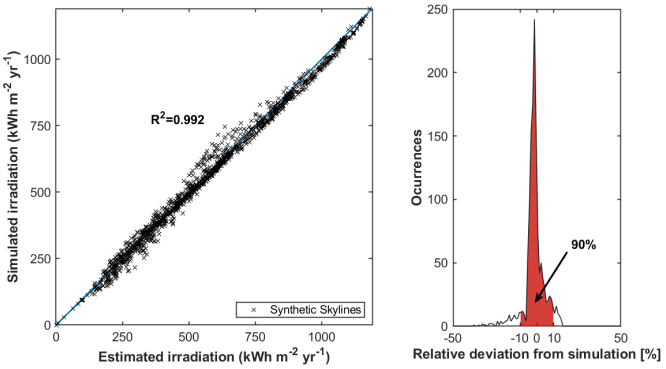

(b) Accuracy and deviation of the improved method vs Perez irradiance method.

Figure 5.6: Cross validation results of the old and improved versions of the Simplified skyline-based methods for a tilt of 45°.

5.3.2. Visualisation of the PV yield in Delft

The detailed visualisation of the PV yield looks identical to the one of irradiation, since the yield is fully dependant on the irradiation and the map is obtained following the same procedure in ArcGIS.

The values are also in the same range. However, this is by chance. The yield units are kWh/kW/y, while the irradiation ones are kWh/m^2/y. As introduced in subsection 4.2.1 the panel used for the yield calculation is a 400 W SunPOWER MAXEON 3 (see Appendix C).

Figure 5.10 illustrates the potential yield generation of the different roof surfaces in the neighbourhood located in between Rotterdamseweg and Proosdijpad, just above the TU Delft campus. The maximum obtained yield is equal to 1206.38 kWh/kW/y while the lowest is just 24 kWh/kW/y.

5.3.3. Visualisation of the yield per building in Delft

This visualisation shows the potential annual yield in a simpler way. It colours each building in one colour, depending on the amount of energy they can generate. The represented value is the sum of the potential energy generation of every roof surface in the building. It is assumed that PV panels can fully cover the roof area. Figure 5.11 shows the total potential PV generation of the buildings located in the city centre in Delft.

The steps followed to draw this map are also explained in Appendix A. Furthermore, a zoomed out

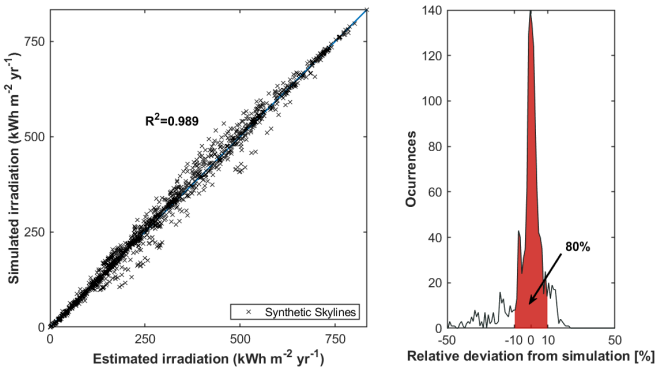

(a) Accuracy and deviation of the old method vs Perez irradiance method.

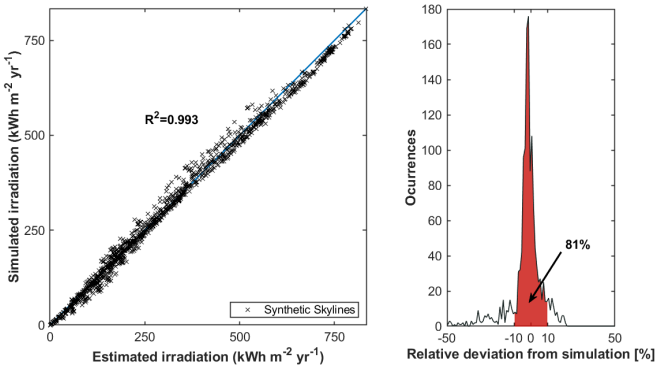

(b) Accuracy and deviation of the improved method vs Perez irradiance method.

Figure 5.7: Cross validation results of the old and improved versions of the Simplified skyline-based methods for a tilt of 90°.

version of this map, which shows a bigger part of Delft is included in Appendix B.

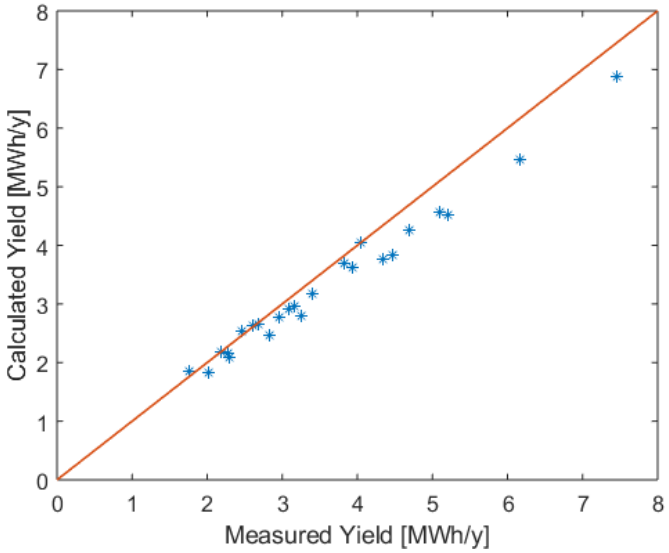

Figure 5.8: PV yield estimation validation, the plotted line represents 100% accuracy of estimation.

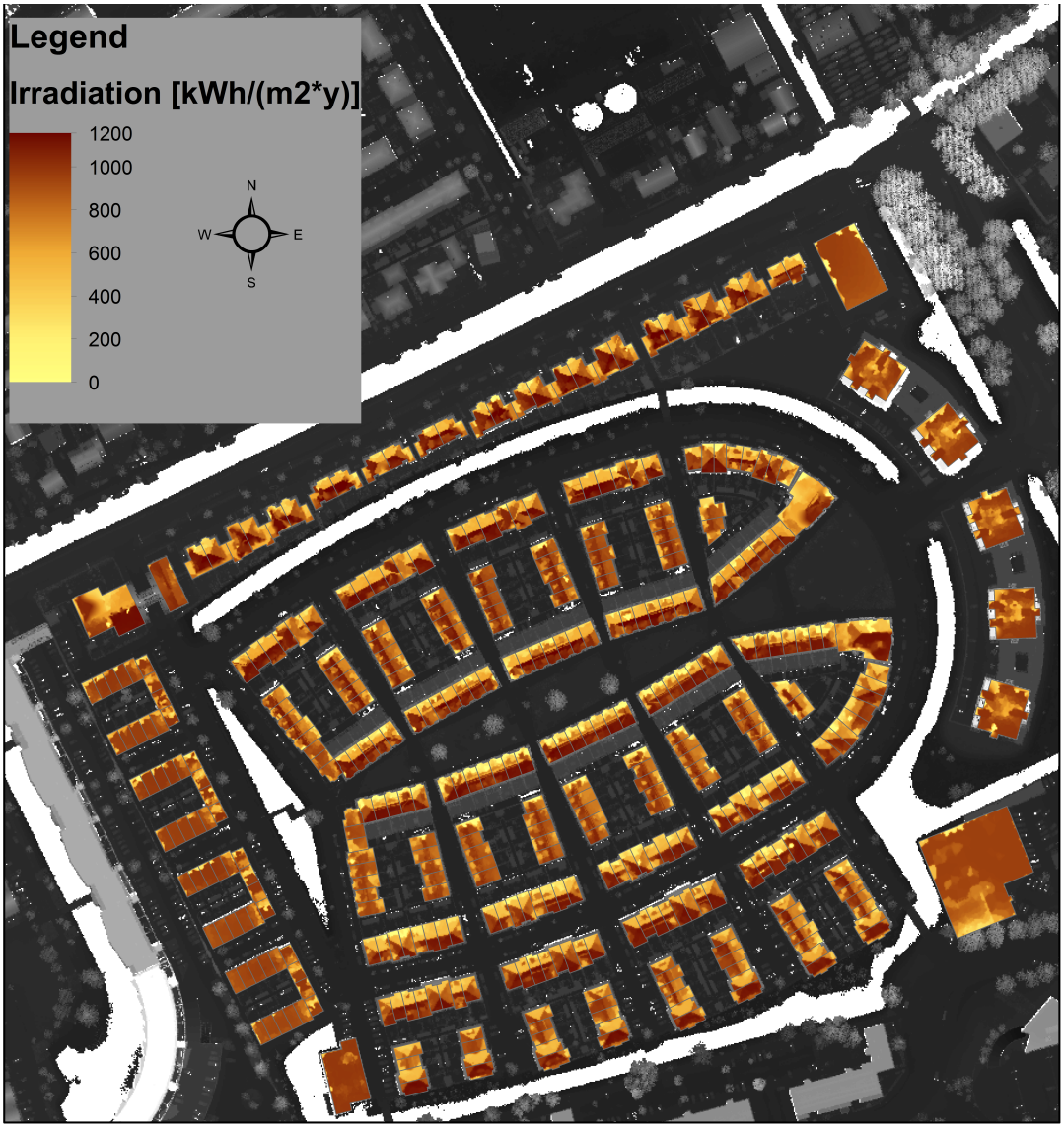

Figure 5.9: Irradiation potential of Molenbuurt, located west in the municipality of Delft.

Figure 5.10: Detailed yield potential in the neighbourhood located in between Rotterdamseweg and Proosdijpad, north from the TU Delft Campus.

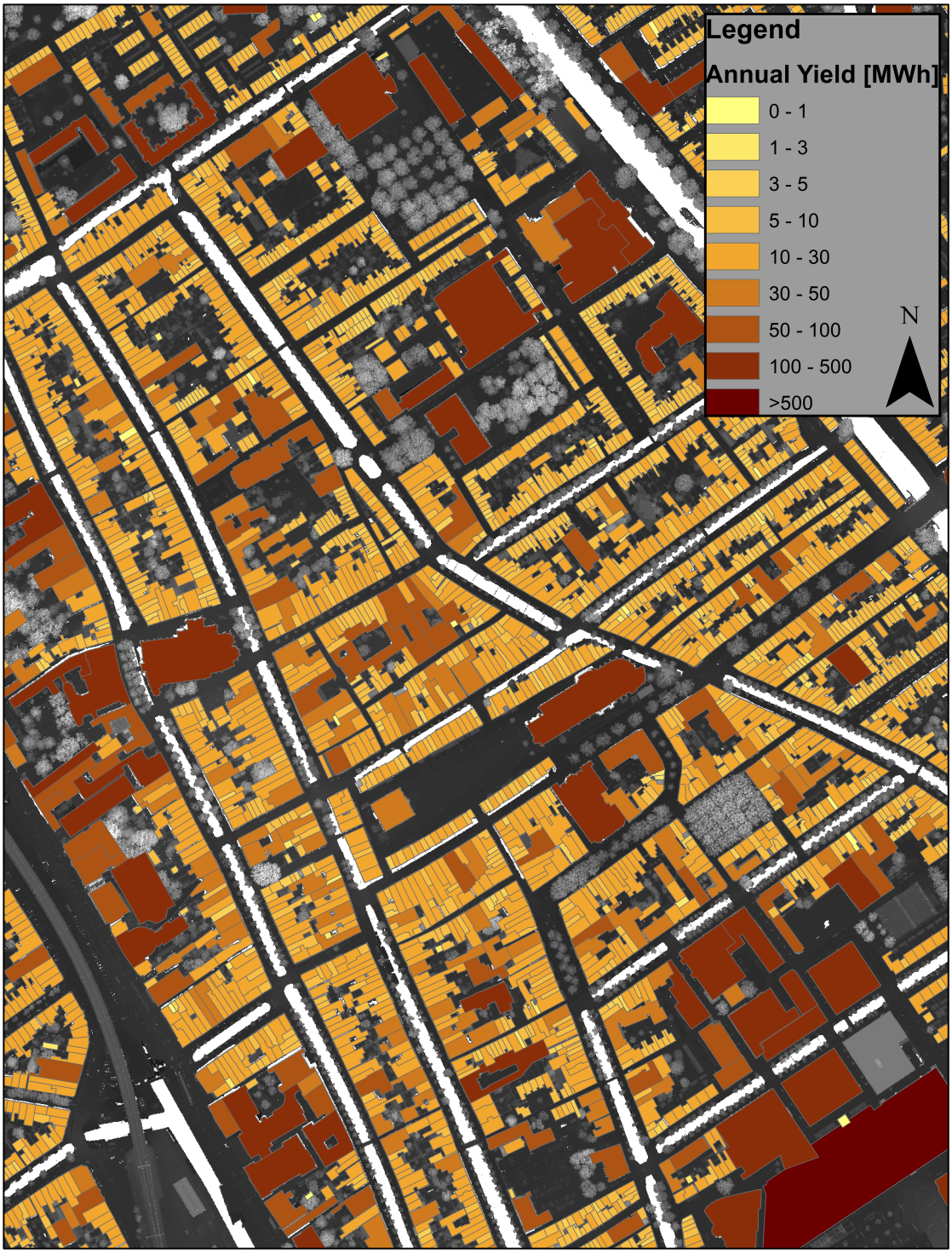

Figure 5.11: Potential yield generation per building, Delft city centre.

5.3.4. Comparison of the potential PV generation and total electricity consumption

As introduced in Chapter 1 the Netherlands has an electricity mix mostly dependant on fossil fuels, with only about 13% of the electricity coming from renewable energy sources. However, this is far from the targets set for 2030, which account that 70% of the electricity consumption will come from renewables. According to Planbureau voor de Leefomgeving (PBL) in [41],the consumed electricity carbon intensity in 2017 in the Netherlands was 0.59 kg CO_2/kWh which would be reduced to 0 kg CO_2/kWh if solar energy would generate the consumed electricity.

One of the goals of this thesis is to analyse the potential of PV generation in the built environment of Delft. However, in order to understand the magnitude of the energy amount presented it is helpful to compare it with the actual electricity consumption, therefore, giving more context.

Figure 5.12a and Figure 5.12b represent the electricity consumption by the households and by the industry & institutions in the 8 years. In 2018, the annual electricity consumption accounted to households reduced to 115 GWh, while the industry and institutions increased their consumption to 421.34 GWh. Both together accounted for 536.34 GWh of electricity consumed last year.

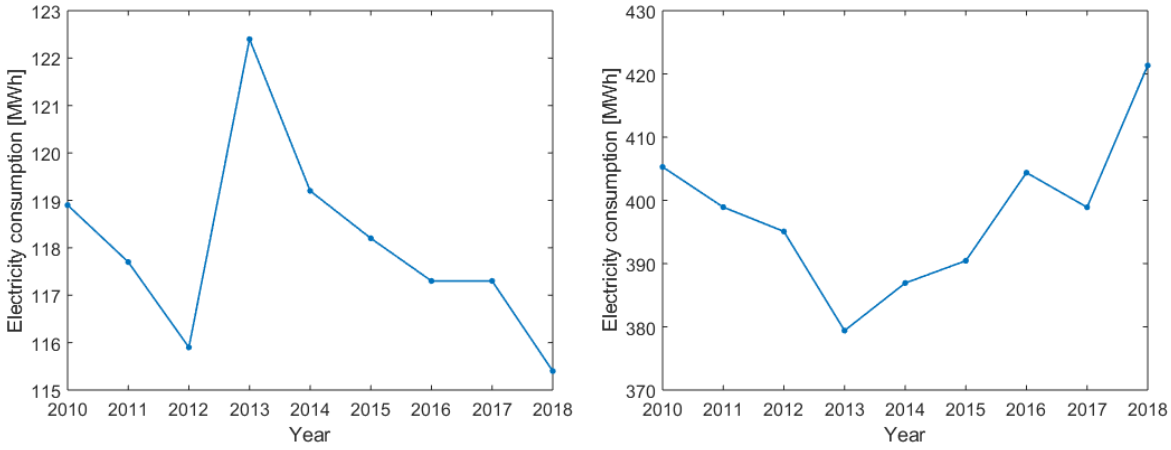

(a) Households.

(b) Industry and institutions.

Figure 5.12: Annual electricity consumption of households and industry and institutions in Delft [42].

Regarding the potential PV generation, two scenarios have been studied: full coverage of roofs for PV applications and coverage of only suitable roofs, which are the ones with a yield prediction of over 650 kWh/kW/y, which will pay back the investment in 10 years according to the calculations made in [38]. It is important to highlight that the full coverage scenario would cover up to around 80.5% of the total area of the roofs since that is on average the percentage of the total area extracted from buildings with the roof segment extraction model, as explained in subsection 5.1.3. As introduced previously it is assumed that PV modules could cover the complete extracted roof area.

The full coverage scenario estimates a PV potential generation of 437.38 GWh, which would need a surface of 2.6 km^2. This would account for a 81.55% of the total electricity consumption in 2018, reducing up to 258 kt of CO_2 in a year.

On the other hand, the suitable roof scenario estimates a PV potential generation of 384.81 GWh, which would need a surface of 2.08 km^2. This would account for a 71.74% of the total electricity consumption in 2018, reducing up to 227 kt of CO_2 in a year.

Both scenarios show optimistic predictions for solar energy in urban environments. However, unfortunately electricity only accounts for 29.81% of the total energy consumption in Delft (excluding roads/highways), which was 1798.61 GWh in 2017 [42]. Thus, the full roof coverage scenario would cover up to 24.32% of the total demand and the suitable roof scenario up to 21.4%. It is clear that the energy transition should also focus in energy efficiency and sustainable heating mechanisms.

6

Conclusions

This chapter aims to provide the reader with a summary of the findings of this MSc thesis. Firstly, the conclusions drawn for each research question are analysed individually in sections 6.1, 6.2 and 6.3. Finally, the general conclusion and added value of the developed tool are discussed in 6.4.

6.1. Extraction of the PV potential surface information from open source data

The first challenge in this thesis was to find the way to extract the information of the surfaces where potentially PV could be installed. Since this would be the input for later estimating the irradiation impinging on the plane and calculating the potential energy generation.

After doing extensive research it was found that there was no immediately available data set that included information of the built environment, such as tilt, orientation and area of the roofs. Therefore, it was decided to calculate them in-house. Reading through literature it was discovered that combining height point cloud data with cadastral data there were ways to segment the roofs and extract those parameters.

The algorithm to extract roof segments and their information was successfully developed in MATLAB, which is the commonly used software in the research group and directly compatible with the skyline generation code introduced in section 2.3. Chapter 3 describes the followed methodology in detail. In order to ensure that the data extraction from the height point cloud and cadastral data was done accurately a validation was done in Chapter 5. This validation study calculated the estimation accuracy of tilt and orientation of 100 roof surfaces in the municipality of Delft.

For the tilt accuracy estimation, an average absolute error of -0.02° and a maximum deviation of 3.7° were obtained. Showing a high tilt calculation accuracy of the developed tool. The biggest deviations were found in the city center of Delft, where buildings are older and have more irregular roof surfaces and more dormers and windows.

On the other hand, the roof orientation estimation resulted the following: an average absolute estimation error of 0.66° and a maximum deviation of 4.53° among the 100 studied roof surfaces.

The third studied parameter was the accuracy of the area estimation. This could not be done by roof segment since there is no open data set that provides such information. Thus, it was done by comparing the sum of the areas of the extracted surfaces with the 2D building polygon area provided by BAG data.

The results showed that on average 80.42% of the total building area is extracted successfully, among the 22321 studied buildings in Delft. In most of the cases the lost area has been due to the lack of roof edge detection, which is a limitation that LiDAR itself faces. It is important to highlight that PV panels are usually not installed close to the edges of the roofs due to security and ballast reasons. Therefore, losing points on the edges of the building is luckily not that impactful in the rooftop PV potential estimation.

Finally, the roof segment extraction model takes on average 5 seconds per building. For the municipality of Delft this means a computational time of 31 hours. The calculations were made with a computer with the following specifications: 128 GB RAM and 2 x 6-core Intel® Xeon® (3.47 GHz) CPU.

6.2. Evolution of the existing tool to calculate a high resolution PV yield in large scale urban areas

As introduced in section 2.4 the conventional method of PV modelling is the so-called irradiance based approach, which estimates the POA irradiation and yield every hour and then integrates it to obtain the annual PV generation of a surface. In the same section, an alternative method is described, the Simplified skyline-based method, which avoids the hourly calculations to minimise the computational time. This is the method used in this project since only the annual PV potential is of interest and low computational time is a priority to estimate large scale areas.

The Simplified skyline-based method is based on two solar irradiation indicators, SVF and SCF, which quantify the landscape and are correlated with the diffuse isotropic and ground reflected irradiation and with the direct and circumsolar irradiation, respectively.

However, as described in [19] the SCF is not an irradiance-weighted parameter. Hence, making a stronger correlation between SCF and the irradiance would improve the method. In an effort to do so, [20] came up with two correction factors for the SCF, the air mass and angle of incidence correction factors. Thus, the irradiation and yield estimations would become more accurate. Nevertheless, the correction factors were limited, since the AoI factor only worked for the case of a 0° tilted module, which is not suitable for the built environment, where roofs with different tilts and orientations are found.

The work developed in this thesis project has enabled to use the AoI factor for any surface, no matter the tilt or orientation. Furthermore, the SCF has been redefined to make a stronger correlation with the irradiance, which was explained in section 4.1.

These changes in the method show a positive impact on the accuracy and deviation of the coefficients when cross-validated with the Perez model. For 0°, 45° and 90° tilted roofs, respectively 97%, 90% and 81% of the obtained POA yearly irradiation values deviated within ±10% from Perez irradiance model, whereas the old Simplified skyline-based method resulted higher deviation (respectively 81%, 84% and 80% of the obtained POA yearly irradiation values deviated within ±10%).

Accuracy and deviation estimations are improved for every single tilt, however, smaller tilts show a greater improvement. This is related to the fact that SCF is direcly influenced by the DNI. The larger the tilt angle, the least direct irradiation and the more diffuse irradiation share it will receive, since the Sun will spend more time behind the POA of the module. Consequently, the fitting for SCF will become worse at higher tilt angles (greater deviation from Perez model), this is seen in the deviation of both old and improved method after 60°. The improved Simplified skyline based method still yields better deviation results than the old method for large tilts, since there are still a few direct irradiance hours to weight and correct.

After receiving the yield data of a set of 25 PV systems from a trusted source, a yield calculation accuracy study was done to validate the improved Simplified skyline-based method. All the studied PV systems are located in Eindhoven, the Netherlands. The results show that on average the relative error of calculation is underestimating the real yield value by 6.64%. The biggest registered deviation has been -14.18%.

The yield estimation of 17 out of the 25 has been lower than the actual one, which shows a clear trend to underestimate the real annual yield. The possible interpretation of this can be that the year in which this yield data was measured could have received a higher annual irradiation than the average. The coefficients which are later used for estimating the yield are based on climate data, which is the average of the available weather data from the past 20 years. Therefore, when the annual irradiation received in a certain year deviates from the average, the estimation of annual irradiation will also show a deviation.

In any case, further validation should be done to see if the tendency continues to be to consistently underestimate the real value. If that would be the case, applying a correction factor could be a solution in the long term.

Regarding the computational time of the irradiation and yield calculation tool, it takes on average 2.7 seconds per building, which adds up to 16.74 hours of computational time for the 22321 studied buildings in Delft. As for the roof segment extraction model, this calculations were done with a computer with 128 GB RAM and 2 x 6-core Intel® Xeon® (3.47 GHz) CPU.

6.3. Proof of application of the developed model

The main goal of this thesis project was to develop a tool able to assess the PV potential of rooftops in large scale. As introduced in Chapter 1, this tool could be relevant for urban planners (municipalities) and DSOs (Distributed System Operators) that will increasingly require to keep track of the potential PV generation in the built environment. Furthermore, by facilitating yield prediction in a quick and user-friendly manner green energy generation could be incentivised among citizens.

It is therefore essential to demonstrate the application of the tool to prove its potential. For doing so, a rooftop PV potential assessment was carried out for the municipality of Delft.

Two scenarios for the PV potential generation were studied: full coverage of roofs and coverage of only suitable roofs, which are the ones with a yield prediction of over 650 kWh/kW/y, which will pay back the investment in 10 years according to the calculations made in [38]. It is important to highlight that the full coverage scenario would cover up to around 80.5% of the total area of the roofs since that is on average the percentage of the total area extracted from buildings with the roof segment extraction model, as explained in subsection 5.1.3. As introduced previously, it was assumed that PV modules could cover the complete extracted roof area and that the DC-AC conversion efficiency for PV systems is 93%.

In 2018, the annual electricity consumption of households in Delft was 115 GWh, while the industry and institutions consumed 421.34 GWh. Both together accounted for 536.34 GWh of electricity consumed, which is the reference value for the comparisons with the potential PV generation.

Regarding the PV potential scenarios, the full coverage one estimates a PV potential generation of 437.38 GWh, which would need a surface of 2.6 km^2. This would account for a 81.55% of the total electricity consumption in 2018, reducing up to 258 kt of CO_2 in a year.

On the other hand, the suitable roof scenario estimates a PV potential generation of 384.81 GWh,

which would need a surface of 2.08 km^2. This would account for a 71.74% of the total electricity consumption in 2018, reducing up to 227 kt of CO_2 in a year.

Both scenarios showed optimistic predictions for solar energy in urban environments. However, unfortunately electricity only accounts for 29.81% of the total energy consumption in Delft (excluding roads/highways), which was 1798.61 GWh in 2017 [42]. Thus, the full roof coverage scenario would cover up to 24.32% of the total demand and the suitable roof scenario up to 21.4%. It is clear that the energy transition should also focus on energy efficiency and sustainable heating mechanisms.

Finally, to represent the calculated PV potential generation values in a visual way PV potential maps were generated, which show both roof segment and building resolution. They can be found in section 5.3 and Appendix B.

6.4. General conclusion and added value

As previously introduced in Chapter 1, the main goal of the research project was the following:

Development and proof of application of a large scale rooftop PV potential assessment tool with roof segment resolution.

The developed tool is capable of assessing the PV potential of large urban areas with roof segment resolution, as proved in the municipality of Delft, with an average error of -6.64% on average. Only by using openly available height point cloud, cadastral and climate data. Furthermore, it can be used for any area in the World that has the above-mentioned data sets available. Regarding computational time, the tool takes on average 7.7 seconds per building to extract its roof surfaces and calculation the PV potential of each of them.

Compared to the existing online yield prediction platforms (Zonatlas and PicoGeodan), the developed tool is clear about its yield calculation methodology and shows specific values of potential energy generation per roof surface in the created maps.

In contrast to the solar irradiation tool from ArcGIS, it is able to estimate the irradiation and yield accurately, as validated with real systems and cross validated with the Perez model, which is considered to be the 2^{nd} most accurate irradiance model in terms of clear-sky irradiation estimation according to [14].

Finally, in comparison with r.sun from GRASSGIS it is more user friendly and enables further research and development on how to estimate the irradiation and yield better within the PVMD research group.

7

Recommendations

This chapter focuses on discussing the possible improvements to the existing rooftop PV potential assessment tool and proposes future steps to make a more impactful tool.

7.1. Possible improvements for the developed tool

In this first section, the possible upgrades to the model are suggested. These recommendations are divided into three groups: roof segment extraction model, irradiation and yield calculation tool and mapping.

7.1.1. Roof segment extraction model

Despite the results showing high accuracy of estimation, a few improvements to the model are recommended:

LiDAR normalisation
In this project, as introduced in previous chapters, height point cloud data is used to extract the roof segments of buildings and to estimate the obstacle view from the roofs, also known as skyline profile.

In order to extract the roof segment heights correctly, a so-called height point cloud normalisation must be done. This consists of the subtraction of the Digital Surface Model (DSM, considers built environment and bare Earth elevation) by the Digital Terrain Model (DTM, only considers bare Earth elevation). The result will be a height point cloud where every point will have a height over the same reference: a zero height level surface.

This has not been done in this project since in the Netherlands most of the land is at 0 meter height. However, it is crucial to do it at any other location where there are height differences within the landscape. Figure 7.1 illustrates the explanation.

BAG data
The roof segment extraction model also makes use of cadastral data (also known as BAG) to extract the information of the roofs of the buildings. In this project the cadastral data has been extracted

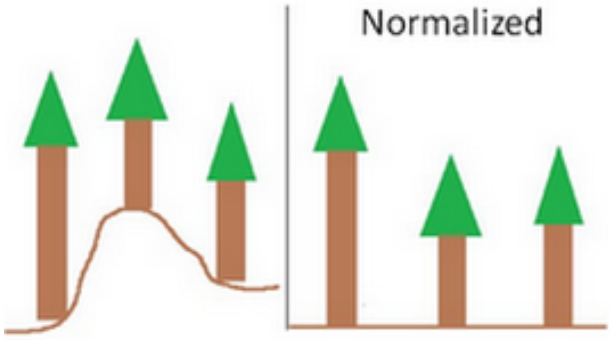

Figure 7.1: Normalisation of a point cloud, from [43].

from [34], where they use the official BAG data and combine it with height point cloud data to convert it to 3D BAG. It was the most straightforward way to obtain BAG data. However, the 3D BAG used missed two useful attributes:

- **Verblijsobject ID**: Is an identification number linked to the property rather than to the building. For instance, small storage hut has a building ID but not a verblijsobject ID. The versblijsobject ID can be useful to know the postcode of the property or to be linked to the electricity consumption point, which is described with this identification number.
- **Building classification**: The 3D BAG data set did not include the building classification that the official BAG does, which describes the use of the buildings as household, historical, industrial etc. This is interesting information for making a more realistic PV potential assessment, where for example, churches would be discarded as a suitable PV area.

In order to have the official BAG data, it should be downloaded as a WFS geoservice from pdok.nl.

7.1.2. Irradiation and yield calculation model

The evolved irradiation and yield calculation tool has shown consistent results and clear improvements compared to its previous version. Nevertheless, there are a few areas where more research could be done. The first one is the interpolation method of the calculated points and the second one is a further validation.

Interpolation

The irradiation and yield calculation model calculates 10% of the points in a roof segment and interpolates the values of the remaining ones (as introduced in subsection 4.2.3). The interpolation method used in the model is the nearest neighbour interpolation method. It was found empirically that the results obtained with that method yielded better accuracy and computational results than linear or natural neighbour interpolation methods. However, this was only proved for a few cases. Therefore, a better study of the interpolation methods is advisable.

Moreover, further research should be done to know what points should be calculated (position of them) and which should be interpolated to yield the best results, so far it was found to be extremely case dependant.

Further validation

The yield calculation model has been validated for 25 PV systems in the Netherlands. The results

showed a clear tendency to underestimate the yield by around 6%. In order to withdraw better conclusions and see if this is a general trend, it is advisable to validate it with more systems and also in more climates. Although, big variations in the results are not expected, since the old model was already validated in different climates [19]. Furthermore, validation for high tilt angles would also be interesting, since this has not been done until now. All the studied PV systems were placed in rooftops that were not steeper than 60°.

7.1.3. Mapping

In this project, the irradiation and yield data has been imported from MATLAB and the maps have been made in ArcGIS, as explained in Appendix A. Once in ArcGIS, natural neighbour interpolation method was used to make the maps out of the imported points. As introduced previously, further research should be done to conclude which interpolation method is the most appropriate for this application.

Moreover, ArcGIS was used due to the availability of the software and the previous work carried out in the research group. No market analysis was made to explore if other softwares could perform better for this application. Hence, it is recommended to investigate if alternative softwares (open source if possible) could work as well or better.

7.2. Future work

The developed tool in this project is a strong base for large scale rooftop PV potential assessments. However, its applications could be expanded if further steps would be made. This section focuses on proposing those steps to make the tool even more impactful.

7.2.1. Impact of PV in the low voltage grid

As introduced in Chapter 1, future energy systems will be more sustainable but also more complex. The massive penetration of urban solar energy together with the EV charging will bring some challenges, such as keeping the LV grid within its voltage and frequency limits. PV potential studies combined with grid infrastructure could play an important role by enabling decision makers to see if the hosting capacity of the grid could allow further PV installations or if the grid might require upgrades.

There are already some projects that have started studying the impact of PV in the low voltage network hosting capacity, like [44]. In this paper the authors simplify the LV grid voltage constraints to the distance to the nearest electrical substation and to the minimum consumption (installed PV power higher than minimum power consumption on the same substation will lead to major voltage constraints). With these two considerations they categorise buildings into: no potential, no hosting capacity constraint, distance constraint and minimum consumption constraint. Consequently, what percentage of the existing PV potential could be installed without constraining the grid is shown.

A similar approach could be followed using the developed tool and grid data, which is openly provided by the DSO, in the case of Delft, Stedin. In this thesis project some work has already been done towards obtaining a LV grid PV impact map, however, time constraints limited the progress. Figure 7.2 shows the LV lines and substations in a neighbourhood in Delft.

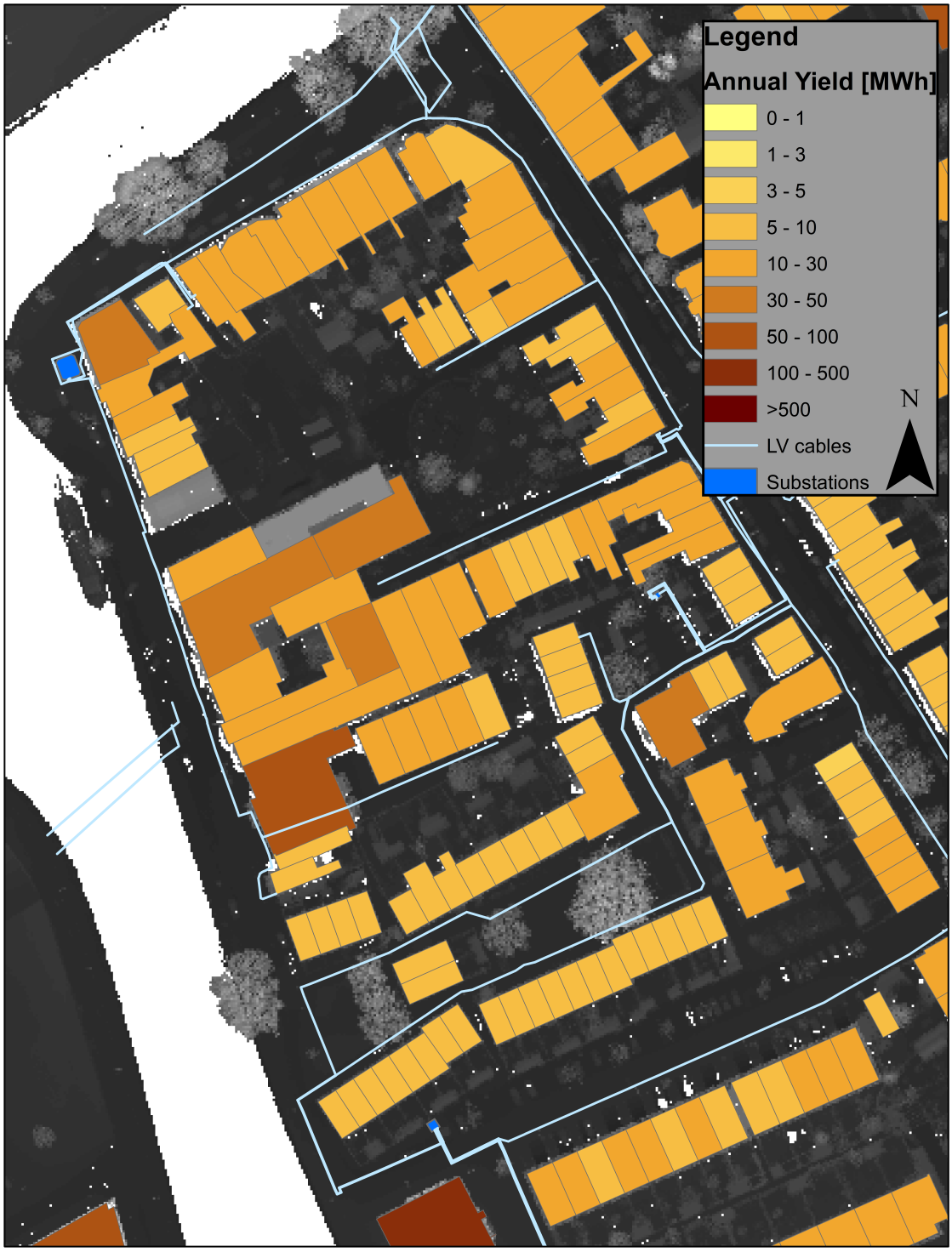

Figure 7.2: LV grid lines and substations in the neighbourhood located in between Rotterdamseweg and Proosdijpad, north from the TU Delft Campus.

Although this study could not be fully completed in this thesis project some of the steps needed to succeed in such study have been spotted. They are introduced in the following bullet points:

- **Verify that voltage constraints can be simplified to distance and power mismatch**: Further research should be made to see if simplifying the voltage constraints in the LV grid to only distance from connection point to substation and power mismatch would be enough.
- **Distance calculation**: Finding a methodology to estimate the distance from the connection point to the nearest substation will be one of the challenges. It could either be done with GIS solutions from the library or by developing an in-house algorithm (as done in [44]).
- **Conversion of annual energy values to power values**: The tool developed in this thesis calculates the potential annual PV generation of surfaces. Nevertheless, for a grid impact study instantaneous power values are needed. For doing so, a conversion step is needed. This could be done following an AI approach, which would require a large amount of data of power and energy values of different tilts and orientations, or with a model based approach, where correlation formulas are used.
- **Electricity consumption**: The electricity consumption is a very privacy sensitive information. Therefore, DSOs are not allowed to share it. However, they do provide average building consumption data for every postcode of the city as seen in [45], which could be a starting point to estimate the power consumption profile.

Such a study would be a preliminary diagnosis of the capacity of the network to host PV and would be of great value for municipalities and DSOs. Thus, it is highly advisable to continue working on it.

7.2.2. 3D mapping

So far, in spite of having calculated the irradiation and yield for 3D points, all the maps made in this project have been in 2D. These maps show the potential of PV in a clear way but it would certainly be an upgrade to generate this maps in 3D. 3D maps could have been already been generated in this project by using ArcScene, however, only the roofs would have been shown in such a map. This is because the used height point cloud data format, TIF, does not have enough point density to detect building facades.

In the future, LAS height point cloud format could be used for 3D mapping, this data format has a higher point density than TIF and is able to detect facades. Further steps need to be taken to convert the LAS point cloud into smooth buildings, which are discussed in [46] and [47].

7.2.3. Addition to the Dutch PV portal

An interesting application for the data calculated with the developed tool would be to compliment the PVMD developed Dutch PV Portal 3.0. More specifically, the roof surface data extracted from the roof segment extraction model could compliment the Rooftop Scan functionality.

Figure 7.3 shows the interface of the Rooftop Scan tool, where the following parameters need to be filled out: location (Address), electricity use and roof characteristics (technology, tilt and azimuth).

Many users might face the challenge of not knowing the tilt and/or azimuth of their roof segments. There, is where the data calculated with the developed tool could be helpful. Once the user fills in their address, a look up table could be used to know the roof segment characteristics of that building

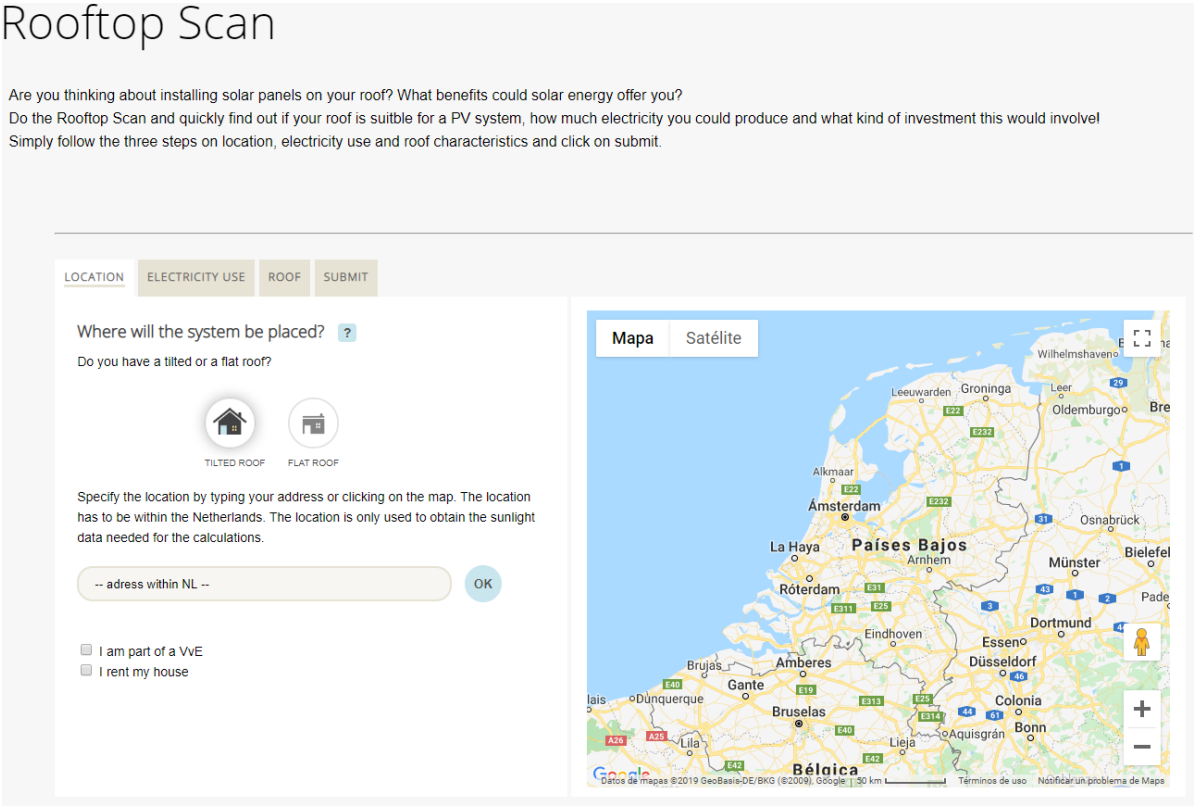

Figure 7.3: PV system design functionality in the Dutch PV portal [48]

(tilt, azimuth, area, SVF). Then, when the user needs to complete the tilt and/or azimuth fields, the values of his/her roof surfaces could be displayed. Thus, facilitating the use of the tool.

Furthermore, the SVF of the chosen roof segment could also be displayed. Hence, warning the user if high shading can be expected for the chosen roof surface.

A

Manual for ArcGIS

A.1. Conversion from geopackage to shapefile

In order to import the BAG data to MATLAB, the 3DBAG file downloaded from [34] needs to be converted from geopackage (.gpkg) to shapefile (.shp). These are the followed steps:

1. Import the .gpkg file to ArcMap.
2. Go to the "Selection" tab, click "select by attributes".
3. Firstly, specify the "Gemeentecode" of your area of interest, in this project the Gemeentecode of Delft was utilised (0503). Secondly, 'bouwjaar' should be older than 01-01-2014, which is the day the plane flew over Delft to get the LiDAR data. Thirdly, only polygons with an "Area" bigger than 25 m^2 should be chosen to avoid small storage buildings.
4. Once the buildings are selected, click "export selected layer" and save it as a shapefile.
5. Then, go to ArcToolbox > Conversion Tools > To Shapefile > Feature Class To Shapefile (multiple). Click on the 'Environments...' button at the bottom of the dialog box. To the right of the 'OK' button. There, the fields 'Output has Z Values' and 'Output has M Values' should be set to 'Disabled'.
6. Click 'OK', and the shapefile is ready to be imported to MATLAB.

A.2. Procedure to create irradiation and PV yield maps

The maps shown in the report of this thesis project are done following the methodology explained below:

1. Import shapefile with the building polygons.
2. Import the shapefile with the points and corresponding Irradiation adn PV yield values.
3. Go to ArcToolbox/3D Analyst/Raster interpolation/Natural neighbor. There add your point shapefile and in 'Environments/Raster analysis/Mask add the polygon shapefile.
4. Click OK and the interpolation map is ready.
5. The LiDAR TIF file was added as background and a Legend can be added in "Inset" tab.

B

PV yield maps

The detailed PV yield maps of the city centre of Delft and the campus of the TU Delft and the PV yield per building for the central part of the city of Delft are illustrated below:

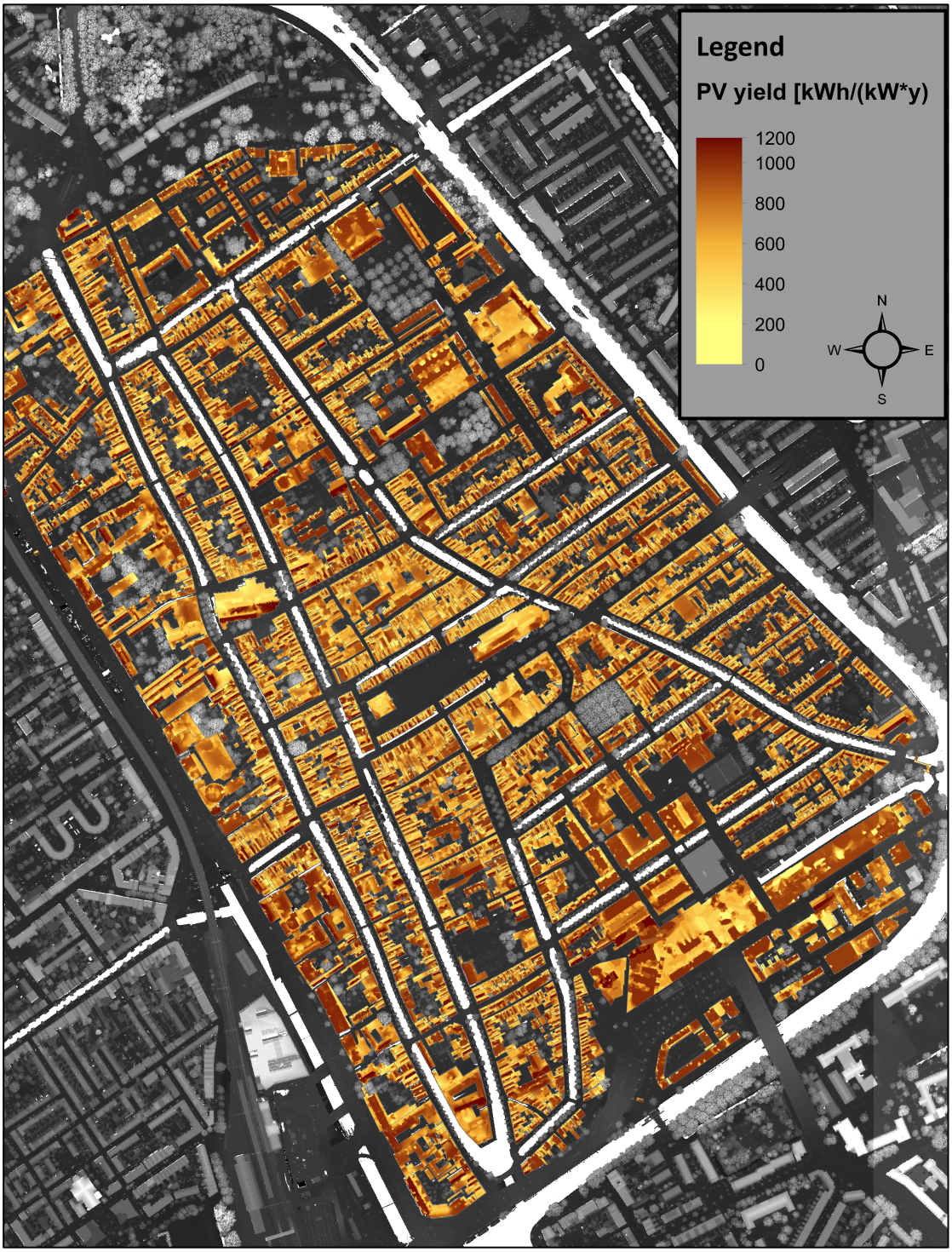

Figure B.1: Detailed yield potential of the city centre of the municipality of Delft.

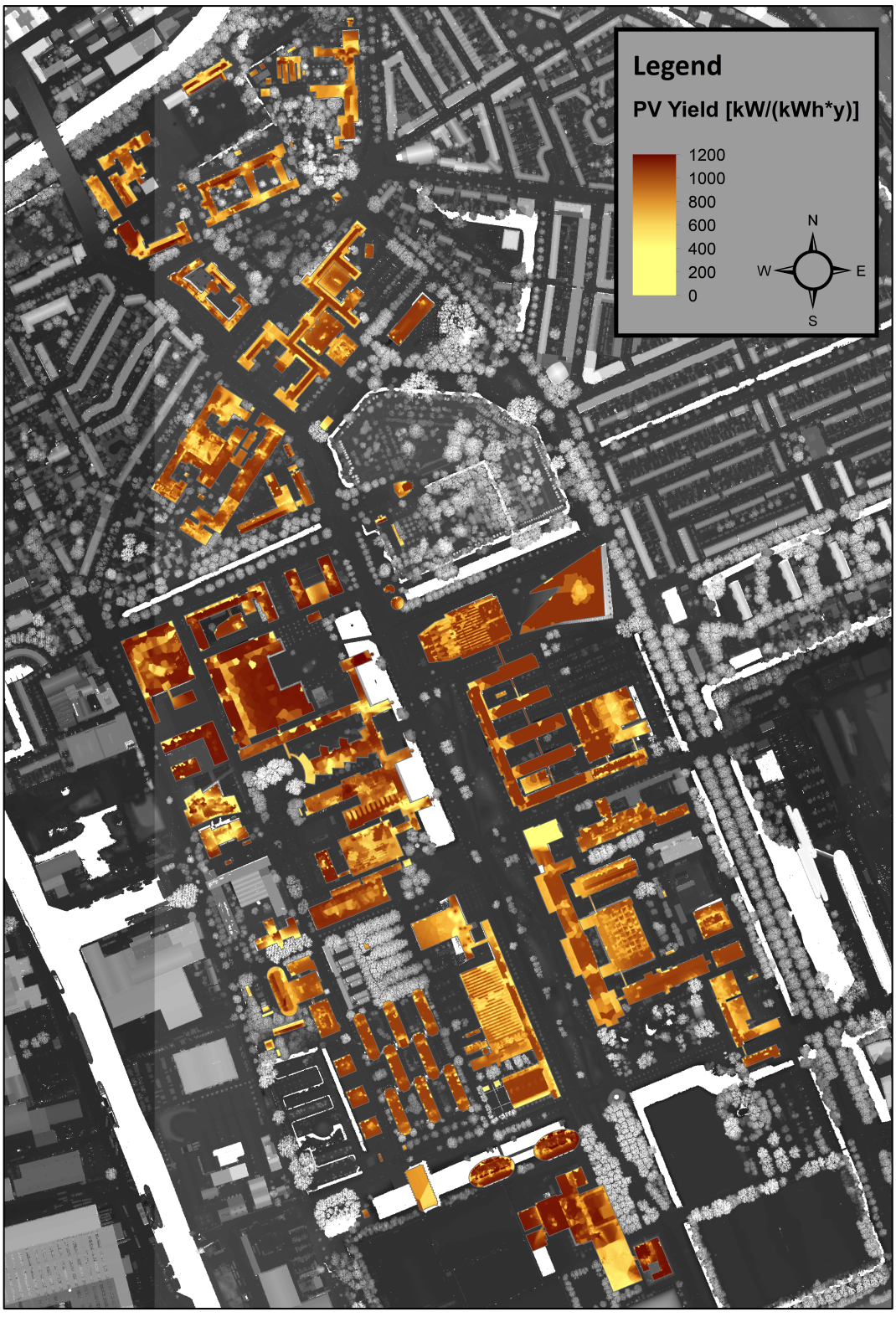

Figure B.2: Detailed yield potential of the TU Delft Campus.

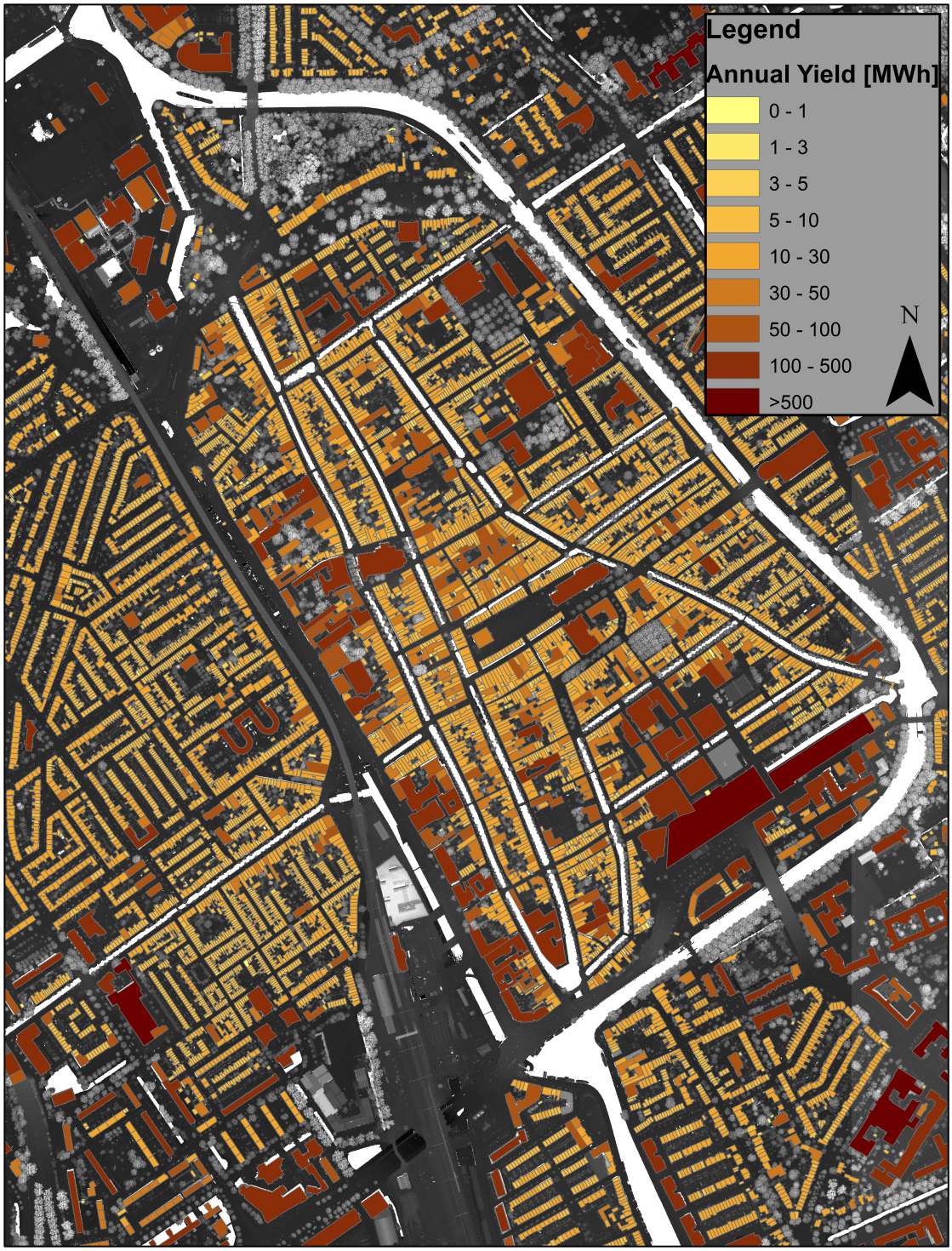

Figure B.3: PV yield potential per building of the central part of the city of Delft.

C

PV module datasheets

JA SOLAR

FULL SQUARE MONO

JAM6(R)(BK)

60/260-280

FULL SQUARE MONOCRYSTALLINE SILICON MODULE

Key Features

- Full Square Monocrystalline modules designed for residential and utility applications, rooftop or ground mount
- High power output of more than 275W and module efficiency up to 16.82% which has been verified by TÜV Rheinland
- Anti-reflective and self-cleaning surface reduces power loss from dirt and dust
- Outstanding performance in low-light irradiance environments
- Excellent mechanical load resistance: Certified to withstand high wind loads (2400Pa) and snow loads (5400Pa)
- High salt and ammonia resistance certified by TÜV NORD

Reliable Quality

- Positive power tolerance: 0~+5W
- 100% EL double-inspection ensures modules are defects free
- Modules binned by current to improve system performance
- Potential Induced Degradation (PID) Resistant

Comprehensive Certificates

- IEC 61215, IEC 61730, UL1703, CEC Listed, MCS and CE
- ISO 9001: 2008: Quality management systems
- ISO 14001: 2004: Environmental management systems
- BS OHSAS 18001: 2007: Occupational health and safety management systems
- Environmental policy: The first solar company in China to complete Intertek's carbon footprint evaluation program and receive green leaf mark verification for our products

Specifications subject to technical changes and tests. JA Solar reserves the right of final interpretation.

JA Solar Holdings Co., Ltd.

JA Solar Holdings Co., Ltd. is a world-leading manufacturer of high-performance photovoltaic products that convert sunlight into electricity for residential, commercial, and utility-scale power generation. The company was founded on May 18, 2005, and was publicly listed on NASDAQ on February 7, 2007. JA Solar is one of the world's largest producers of solar cells and modules. Its standard and high-efficiency product offerings are among the most powerful and cost-effective in the industry.

Add: NO.36, Jiang Chang San Road, Zhabei, Shanghai 200436, China
Tel: +86 21 6095 5888 / +86 21 6095 5999
Fax: +86 21 6095 5858 / +86 21 6095 5959
Email: sales@jasolar.com market@jasolar.com

Superior Warranty

- 10-year product warranty
- 25-year linear power output warranty

www.jasolar.com

JAM6(R)(BK) 60/260-280

JA SOLAR

Engineering Drawings

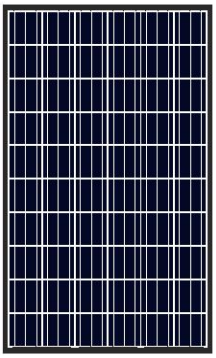

■ Standard J-BOX design

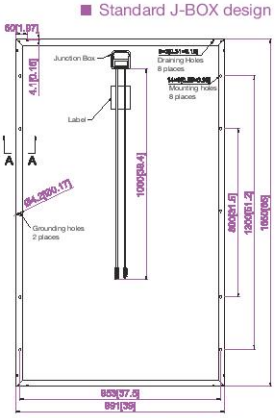

■ Split J-BOX design

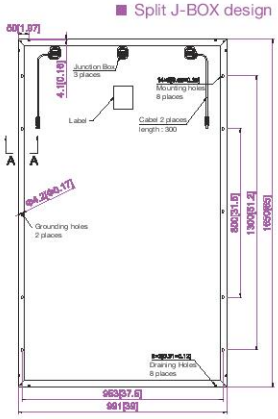

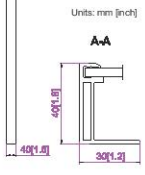

■ customized cable length available upon request

MECHANICAL PARAMETERS

Cell (mm)	Full Square Mono 156x156
Weight (kg)	18.2 (approx)
Dimensions (L×W×H) (mm)	1650x991×40
Cable Cross Section Size (mm^2)	4
No. of Cells and Connections	60 (6×10)
Junction Box	IP67, 3 diodes
Connector	MC4 Compatible
Packaging Configuration	26 Per Pallet

WORKING CONDITIONS

Maximum System Voltage	DC 1000V(TÜV)
Operating Temperature	-40℃~+85℃
Maximum Series Fuse	15A
Maximum Static Load, Front (e.g., snow and wind) Maximum Static Load, Back (e.g., wind)	5400Pa (112 lb/ft^2) 2400Pa (50 lb/ft^2)
NOCT	45±2℃
Application Class	Class A

ELECTRICAL PARAMETERS

TYPE	JAM6(R)(BK) 60-260	JAM6(R)(BK) 60-265	JAM6(R)(BK) 60-270	JAM6(R)(BK) 60-275	JAM6(R)(BK) 60-280
Rated Maximum Power at STC (W)	260	265	270	275	280
Open Circuit Voltage (Voc/V)	38.32	38.52	38.71	38.89	39.07
Maximum Power Voltage (Vmp/V)	30.49	30.78	31.08	31.36	31.64
Short Circuit Current (Isc/A)	9.04	9.13	9.21	9.30	9.39
Maximum Power Current (Imp/A)	8.53	8.61	8.69	8.77	8.85
Module Efficiency [%]	15.90	16.21	16.51	16.82	17.12
Power Tolerance (W)	-0~+5W				
Temperature Coefficient of Isc (αIsc)	+0.049%/℃				
Temperature Coefficient of Voc (βVoc)	-0.340%/℃				
Temperature Coefficient of Pmax (γPmp)	-0.410%/℃				
STC	Irradiance 1000W/m^2, Module Temperature 25℃, Air Mass 1.5				

I-V CURVE

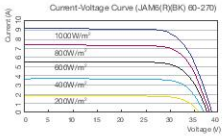

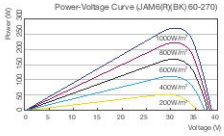

NOCT

TYPE	JAM6(R)(BK) 60-260	JAM6(R)(BK) 60-265	JAM6(R)(BK) 60-270	JAM6(R)(BK) 60-275	JAM6(R)(BK) 60-280
Max Power at STC (Pmax) [W]	190.06	193.72	197.37	201.03	204.68
Open Circuit Voltage (Voc) [V]	34.83	34.97	35.09	35.21	35.46
Max Power Voltage (Vmp) [V]	27.91	28.28	28.56	28.88	28.99
Short Circuit Current (Isc) [A]	7.36	7.39	7.42	7.46	7.47
Max Power Current (Imp) [A]	6.81	6.85	6.91	6.96	7.06
Condition	Under Normal Operating Cell Temperature, Irradiance of 800 W/m^2, spectrum AM 1.5, ambient temperature 20℃, wind speed 1 m/s				

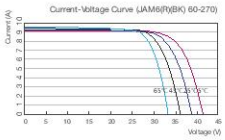

Electrical data in this catalog do not refer to a single module and they are not part of the offer. They only serve for comparison among different module types.

SUNPOWER®

MAXEON®

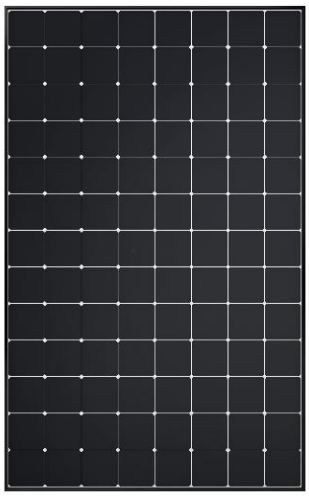

MAXEON® 3 | 400 W

Residential Solar Panel

SunPower Maxeon panels combine the top efficiency, durability and warranty available in the market today, resulting in more long-term energy and savings. [1,2]

Maximum Power. Minimalist Design.

Industry-leading efficiency means more power and savings per available space. With fewer panels required, less is truly more.

Highest Lifetime Energy and Savings

Designed to deliver 60% more energy in the same space over 25 years in real-world conditions like partial shade and high temperatures. [2]

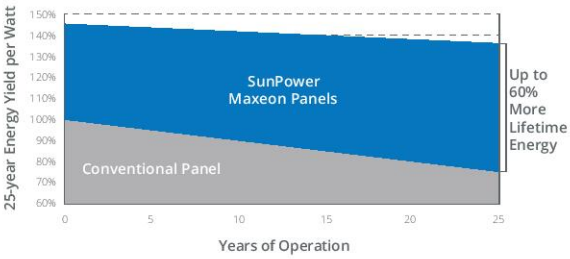

Better Reliability, Better Warranty

With more than 25 million panels deployed around the world, SunPower technology is proven to last. That's why we stand behind our panel with an exceptional 25-year Combined Power and Product Warranty, including the highest Power Warranty in solar.

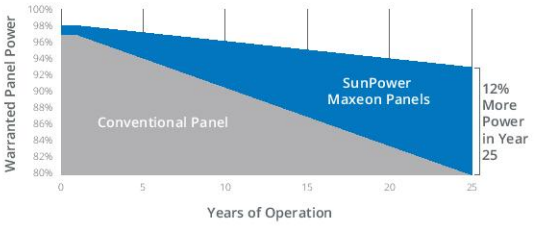

Fundamentally Different. And Better.

The SunPower Maxeon® Solar Cell

- Enables highest efficiency panels available [2]
- Unmatched reliability [3]
- Patented solid metal foundation prevents breakage and corrosion

As Sustainable As Its Energy

- Ranked #1 in Silicon Valley Toxics Coalition Solar Scorecard [4]
- First solar panels to achieve Cradle to Cradle Certified™ Silver recognition [5] *(pending)*
- Contributes to more LEED categories than conventional panels [6]

MAXEON® 3 | 400 W Residential Solar Panel

Electrical Data			
	SPR-MAX3-400	SPR-MAX3-395	SPR-MAX3-390
Nominal Power (Pnom) [7]	400 W	395 W	390 W
Power Tolerance	+5/0%	+5/0%	+5/0%
Panel Efficiency	22.6%	22.3%	22.1%
Rated Voltage (Vmpp)	65.8 V	65.1 V	64.5 V
Rated Current (Impp)	6.08 A	6.07 A	6.05 A
Open-Circuit Voltage (Voc)	75.6 V	75.4 V	75.3 V
Short-Circuit Current (Isc)	6.58 A	6.56 A	6.55 A
Max. System Voltage	1000 V IEC		
Maximum Series Fuse	20 A		
Power Temp Coef.	−0.29% / ° C		
Voltage Temp Coef.	−176.8 mV / ° C		
Current Temp Coef.	2.9 mA / ° C		

Operating Condition And Mechanical Data	
Temperature	−40°C to +85°C
Impact Resistance	25 mm diameter hail at 23 m/s
Solar Cells	104 Monocrystalline Maxeon Gen III
Tempered Glass	High-transmission tempered anti-reflective
Junction Box	IP-68, Stäubli (MC4), 3 bypass diodes
Weight	19 kg
Design Load	Wind: 2660 Pa, 274 kg/m² front & back Snow: 4000 Pa, 408 kg/m² front
Max. Load [9]	Wind: 4000 Pa, 408 kg/m² front & back Snow: 6000 Pa, 611 kg/m² front
Frame	Class 1 black anodized (highest AAMA rating)

Tests And Certifications	
Standard Tests [8]	IEC 61215, IEC 61730
Quality Management Certs	ISO 9001:2015, ISO 14001:2015
EHS Compliance	RoHS (Pending), OHSAS 18001:2007, lead free, REACH SVHC-163 (Pending)
Sustainability	Cradle to Cradle Certified™ (Pending)
Ammonia Test	IEC 62716
Desert Test	MIL-STD-810G
Salt Spray Test	IEC 61701 (maximum severity)
PID Test	1000 V: IEC 62804
Available Listings	TUV

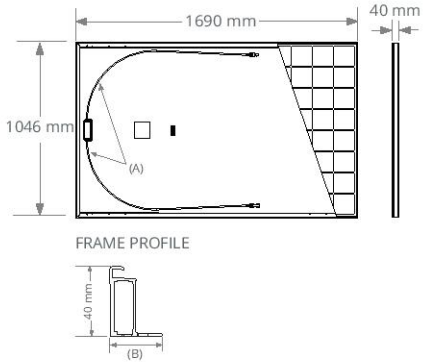

A. Cable Length: 1200 mm +/-10 mm
B. LONG SIDE: 32 mm
SHORT SIDE: 24 mm

Please read the safety and installation guide.

1 SunPower 400 W, 22.6% efficient, compared to a Conventional Panel on same-sized arrays (310 W, 16% efficient, approx. 2 m²), 8% more energy per watt (based on PVSyst pan files for avg EU climate), 0.5%/yr slower degradation rate (Jordan, et. al. "Robust PV Degradation Methodology and Application." PVSC 2018).
2 DNV "SunPower Shading Study," 2013. Compared to a conventional front contact panel.
3 #1 rank in "Fraunhofer PV Durability Initiative for Solar Modules: Part 3". PVTech Power Magazine, 2015.
4 SunPower is rated #1 on Silicon Valley Toxics Coalition's Solar Scorecard.
5 Cradle to Cradle Certified is a multi-attribute certification program that assesses products and materials for safety to human and environmental health, design for future use cycles, and sustainable manufacturing.
6 Maxeon2 and Maxeon3 panels additionally contribute to LEED Materials and Resources credit categories.
7 Standard Test Conditions (1000 W/m² irradiance, AM 1.5, 25° C). NREL calibration Standard: SOMS current, LACCS FF and Voltage.
8 Class C fire rating per IEC 61730.
9 Calculated with a 1.5 Safety Factor.

Designed in USA
Made in Philippines (Cells)
Modules Assembled in Mexico

Visit www.sunpowercorp.co.uk for more information.
Specifications included in this datasheet are subject to change without notice.

SUNPOWER®
MAXEON®

Bibliography

[1] United Nations. The paris agreement. , 2015.

[2] Het ministerie van Economische Zaken en Klimaat. Klimaatakkord, 2019. Retrieved from: https://www.klimaatakkoord.nl/klimaatakkoord.

[3] EBN. Energie in nederland 2019, 2019. Retrieved from: https://www.ebn.nl/wp-content/uploads/2019/01/EBN_Infographic2019_14JAN19.pdf.

[4] Eurostat. Eu population in 2019, 2019. Retrieved from: https://ec.europa.eu/eurostat/tgm/table.do?tab=table&language=en&pcode=tps00001&tableSelection=1&footnotes=yes&labeling=labels&plugin=1.

[5] Rijksdienst voor Ondernemend. Offshore wind energy roadmap, 2018. Retrieved from: https://english.rvo.nl/subsidies-programmes/offshore-wind-energy.

[6] Government of the Netherlands. Stimulating the growth of solar energy, 2019. Retrieved from: https://www.government.nl/topics/renewable-energy/stimulating-the-growth-of-solar-energy.

[7] McKinsey. Energy perspective 2019, 2019. Retrieved from: https://www.mckinsey.com/industries/oil-and-gas/our-insights/global-energy-perspective-2019.

[8] United Nations. World urbanization prospects 2018, 2018. Retrieved from: https://population.un.org/wup/Country-Profiles/.

[9] Zonatlas. About zonatlas, 2018. Retrieved from: https://www.zonatlas.nl/start/over-ons/.

[10] Pico Geodan. About zonatlas, 2018. Retrieved from: https://pico.geodan.nl/pico/data/energieopwekking_zonpv.html.

[11] István Szemán. Comparison of the most popular open-source gis software in the field of landscape ecology. *Acta Geographica Debrecina Landscape & Environment*, 6(2):76–92, 2012.

[12] J Hofierka, M Suri, and T Huld. r. sun-solar irradiance and irradiation model, 2007. Retrieved from: https://grass.osgeo.org/grass76/manuals/r.sun.html.

[13] CT Committee et al. Spatial distribution of daylight-luminance distributions of various reference skies. Technical report, CIE, International Commission on Illumination, 1994.

[14] Christian A Gueymard. Clear-sky irradiance predictions for solar resource mapping and large-scale applications: Improved validation methodology and detailed performance analysis of 18 broadband radiative models. *Solar Energy*, 86(8):2145–2169, 2012.

[15] Esri. Modelling solar radiation, 2019. Retrieved from: http://desktop.arcgis.com/en/arcmap/10.3/tools/spatial-analyst-toolbox/modeling-solar-radiation.htm.

[16] P Rich, RC Dubayah, W Hetrick, and S Saving. Using viewshed models to calculate intercepted solar radiation: applications in ecology. american society for photogrammetry and remote sensing technical papers. In *American Society of Photogrammetry and Remote Sensing*, 524–529, 1994.

[17] Pinde Fu and Paul M Rich. A geometric solar radiation model with applications in agriculture and forestry. *Computers and electronics in agriculture*, 37(1-3):25–35, 2002.

[18] Esri. How solar radiation is calculated, 2019. Retrieved from: `http://desktop.arcgis.com/en/arcmap/10.3/tools/spatial-analyst-toolbox/how-solar-radiation-is-calculated.htm`.

[19] A. Calcabrini; Hesan Ziar; Miro Zeman; Olindo Isabella. A simplified skyline-based method for estimating the annual solar energy potential in urban environments. *Nature*, , 2019.

[20] Carlotta Ferri. Irradiation and dc yield potential of solar highways in the netherlands. Master's thesis, Delft University of Technology, 2019.

[21] O.Isabella R. van Swaaij A. Smets, K.Jager and M. Zeman. *Solar Energy: The physics and engineering of photovoltaic conversion technologies and systems*. UIT Cambridge, 2016.

[22] Laserliner. Digital level meter, 2018. Retrieved from: `https://www.laser-liner.co.uk/product/digilevel-pro-120-cm/`.

[23] Recta. Digital compass, 2019. Retrieved from: `http://www.recta.ch/en/dt-120`.

[24] Meteonorm. Horicatcher, 2019. Retrieved from: `https://meteonorm.com/en/product/horicatcher`.

[25] Furkan Sonmez. An albedo irradiance model usable for bifacial pv modules based on lidar data and ray casting. Master's thesis, Delft University of Technology, 2017.

[26] Martijn Keijzer. A multi-surface reflected irradiance model for pyranometer corrections and pv yield calculations in complex urban geometries. Master's thesis, Delft University of Technology, 2019.

[27] Richard Perez, Pierre Ineichen, Robert Seals, Joseph Michalsky, and Ronald Stewart. Modeling daylight availability and irradiance components from direct and global irradiance. *Solar energy*, 44(5):271–289, 1990.

[28] U.S. Geological Survey. Airborne lidar system components, 2010. Retrieved from: `https://www.ngs.noaa.gov/corbin/class_description/Nayegandhi_green_lidar.pdf`.

[29] ArcGIS desktop. What is lidar data?, 2018. Retrieved from: `http://desktop.arcgis.com/en/arcmap/10.5/manage-data/las-dataset/what-is-lidar-data-.htm`.

[30] GIS Stack Exchange. Difference between dsm and dtm, 2010. Retrieved from: `https://gis.stackexchange.com/questions/5701/differences-between-dem-dsm-and-dtm`.

[31] PDOK-Downloads page. Actueel hoogtebestand nederland (ahn3), 2018. Retrieved from: `https://downloads.pdok.nl/ahn3-downloadpage/`.

[32] PDOK. Actueel hoogtebestand nederland (ahn3), 2018. Retrieved from: `https://www.pdok.nl/attenderingsservice-rss/-/asset_publisher/mvZkjafth739/content/actueel-hoogtebestand-nederland-ahn3-`.

[33] TU Delft 3D Geoinformation group. About - 3d geoinformation, 2019. Retrieved from: https://3d.bk.tudelft.nl/about/.

[34] TU Delft 3D Geoinformation group. 3d basisregistratie adressen en gebouwen (bag), 2019. Retrieved from: http://3dbag.bk.tudelft.nl/documentation.

[35] MathWorld-A Wolfram Web Resource Eric W. Normal vector of a plane, 2019. Retrieved from: http://mathworld.wolfram.com/Plane.html.

[36] Christian A Gueymard. Direct solar transmittance and irradiance predictions with broadband models. part i: detailed theoretical performance assessment. *Solar Energy*, 74(5):355–379, 2003.

[37] Aden B Meinel and Marjorie P Meinel. Applied solar energy: an introduction. *NASA STI/Recon Technical Report A*, 77, 1977.

[38] Tim de Vries. Development and validation of a quick-scan algorithm for evaluation of rooftop pv potential. Master's thesis, Delft University of Technology, 2018.

[39] Martin K Fuentes. A simplified thermal model for flat-plate photovoltaic arrays. Technical report, Sandia National Labs., Albuquerque, NM (USA), 1987.

[40] SolarEdge. Solaredge single phase inverters, 2019. Retrieved from: https://www.solaredge.com/sites/default/files/se-single-phase-16a-inverter-datasheet.pdf.

[41] Planbureau voor de Leefomgeving (PBL). Klimaat- en energieverkenning 2019, 2019. Retrieved from: https://www.pbl.nl/sites/default/files/downloads/pbl-2019-klimaat-en-energieverkenning-2019-3508.pdf.

[42] Rijkswaterstaat. Climate monitor, 2018. Retrieved from: https://klimaatmonitor.databank.nl/dashboard/dashboard/energiegebruik/.

[43] GIS stackexchange. Normalising point cloud data, 2014. Retrieved from: https://gis.stackexchange.com/questions/112587/normalizing-point-cloud-data.

[44] M Joos, N Lebert, B Gaiddon, E Séguin, and PE Gautreau. Spatial representation of low-voltage network hosting capacity for photovoltaic roof-top installations using an open-source tool. , 2018.

[45] Stedin. Electricity and gas consumption data, 2019. Retrieved from: https://www.stedin.net/zakelijk/open-data/verbruiksgegevens.

[46] Hans-Gerd Maas and George Vosselman. Two algorithms for extracting building models from raw laser altimetry data. *ISPRS Journal of photogrammetry and remote sensing*, 54(2-3):153–163, 1999.

[47] J Lesparre and BGH Gorte. Simplified 3d city models from lidar. In *XXII ISPRS Congress, Commission II, Melbourne, Australia, 25 August-1 September 2012; IAPRS XXXIX-B2, 2012*. International Society for Photogrammetry and Remote Sensing (ISPRS), 2012.

[48] TU Delft Dutch PV Portal 3.0. Rooftop scan, 2019. Retrieved from: https://pvportal-3.ewi.tudelft.nl/RooftopScan.php.

List of Acronyms

AoI	Angle of incidence
BIPV	Building integrated photovoltaics
DHI	Direct Horizontal Irradiance
DNI	Direct Normal Irradiance
EV	Electric Vehicle
LAS	LIDAR Data Exchange File
LiDAR	Light Detection And Ranging
POA	Plane of array
PV	Photo Voltaic
PVMD	Photovolatic material devices
SCF	Sun Coverage Factor
SF	Shading Factor
SVF	Sky View Factor
TIF	Tagged Image File Format